2019

Temporal coding in the hippocampus

BOSTON UNIVERSITY

GRADUATE SCHOOL OF ARTS AND SCIENCES

Dissertation

TEMPORAL CODING IN THE HIPPOCAMPUS

by

DANIEL M. SALZ

B.A., State University of New York – Buffalo, 2005

Submitted in partial fulfillment of the

requirements for the degree of

Doctor of Philosophy

2019

Approved by

First Reader

Marc W. Howard, Ph.D.
Professor of Psychological and Brain Sciences

Second Reader

Michael E. Hasselmo, D. Phil.
Professor of Psychological and Brain Sciences
Professor of Biomedical Engineering

Third Reader

Steve Ramirez, Ph.D.
Assistant Professor of Psychological and Brain Sciences

Additional Reader

Uri Eden, Ph.D.
Professor of Mathematics and Statistics

DEDICATION

I would like to dedicate this work to my wonderful wife Jessie.

ACKNOWLEDGMENTS

I would like to thank my advisor Howard Eichenbaum, and my fellow and past lab members who engendered a supportive and friendly atmosphere excited about talking science and problem solving projects. I especially would like to thank Norbert Fortin, who trained me, Ben Kraus and Jon Ruekemann for going above and beyond to help me when I was stuck. I also want to thank Marc Howard for his time and thoughtful support helping guide me after Howard's passing. I also want to thank Shelley Russek and Sandi Grasso for going above and beyond to ensure that I could cross the finish line. I went through a difficult time when I was writing this thesis and there are countless supportive people to thank for helping get me back on my feet and across the finish line. In particular I want to thank Loren Devito for taking time to sit with me and advise me on writing, Lucy Krivitsky for pep talking me through the whole process, and Kayle Sawyer for taking so much time to help my thesis in a myriad ways. Finally I want to thank my family for being so loving and supportive of me: thank you mom for helping me edit and Wendy for encouraging me by working beside me. Every person is in part made from the community that surrounds them, and I feel endlessly lucky to have such a wonderful community surrounding me.

TEMPORAL CODING

IN THE HIPPOCAMPUS

DANIEL SALZ

Boston University Graduate School of Arts and Sciences, 2019

Major Professor: Marc Howard, Ph.D., Professor of Psychological & Brain Sciences

ABSTRACT

There is a large body of evidence that the hippocampus is involved in temporal aspects of memory. It remains unclear what neural processes within the hippocampus contribute to this ability. The following experiments aim to quantify and qualify these neural processes while rats perform temporal memory tasks. First we examined the firing of neurons in the hippocampus while rats compared a current series of odors to a learned sequence of odors. We found evidence of neural correlates which might represent whether a stimulus odor was in the correct ordinal sequence or not. Next we examined the delay intervals in between learned sequences of events with the goal of identifying the origin of "time cells" in the hippocampus. We used a delayed alternating T-maze task that our lab has used before to record time cells in area CA1 of the hippocampus. We found time cells in CA3, one of the major inputs to CA1 and demonstrated that they behave in many ways like place cells previously observed in these two regions. Time cells had previously been reported to occur only when an animal is engaged in a task with memory load. We demonstrated that memory load isn't necessary to observe time cells. Our observations of the similarities between place and time cells led us to conjecture that the hippocampus might process space and time similarly. In a final study I examined time

cell firing properties with an aim at constraining models of time cells. We defined time cells in several ways including a new methodology that is promising as a future unbiased selection criteria. All of our findings help further elucidate several different ways that neural coding in the hippocampus contributes to temporal processing.

TABLE OF CONTENTS

LIST OF TABLES

LIST OF FIGURES

LIST OF ABBREVIATIONS

ANOVA ..... Analysis of Variance

CA1 ..... Cornu Ammonis subfield 1 (region of the hippocampus)

CA2 ..... Cornu Ammonis subfield 3 (region of the hippocampus)

CA3 ..... Cornu Ammonis subfield 4 (region of the hippocampus)

fMRI ..... Functional Magnetic Resonance Imaging

InSeq ..... In Sequence (odor in correct ordinal location)

LEC ..... Lateral Entorhinal Cortex

LFP ..... Local Field Potential

LL ..... Log Likelihood

MAP ..... Multichannel Acquisition Processor

MEC ..... Medial Entorhinal Cortex

OutSeq ..... Out of Sequence (odor in different ordinal location)

PBS ..... Phosphate Buffered Saline

PESG ..... Perievent Spectrogram

SMI ..... Sequence Memory Index

SUA ..... Single Unit Activity

CHAPTER ONE

Introduction

How does the brain process the temporal aspect of memory? There is a rich history of research on this question. In 1972, Tulving originally defined episodic memory, later operationalizing it as 'remembering what happened where and when' (Tulving, 2001). In order to do this, the brain must take in information about its environment, the events that are occurring in that environment, and the order of those events. As part of this process of forming episodic memories, the brain must take events that occurred far apart in time, and bind them together in the proper sequence. We have known since patient HM developed profound amnesia after receiving a bilateral anterior temporal lobectomy which removed two thirds of his hippocampi were removed along with his amygdale, and entorhinal, prirform and parahipoocampal cortrices, that these portions of the temporal lobe are necessary for forming new long term and episodic memories. Additional studies on patients with more localized hippocampal lesions, have shown that hippocampus is particularly important for episodic memory and remembering the temporal order of events (Mayes et al., 2010; Spiers, Burgess, Hartley, Vargha-Khadem, & O'Keefe, 2001).

There continues to be mounting evidence that the hippocampus in particular is important for temporal aspects of memory. fMRI studies have demonstrated increased activation of the hippocampus during learning and recall of sequences of events (Lehn et al., 2009; Ross, Brown, & Stern, 2009). Fortin et al. (2002) extended this finding to rats with hippocampal lesions who could not remember the order of a trial unique sequence of

odors, but could remember the odor identities. In some tasks when a rat has to hold onto information across a gap in time a task becomes hippocampal-dependent, even when a rat can perform the task without a hippocampus if there is no delay. Examples of this include the alternating T maze which is hippocampal-dependent only after a delay between turns, eyeblink conditioning which can occur without a hippocampus if the conditioned and unconditioned stimulus overlap, the Object-Trace-Odor Paired Associate Task (Kesner, Hunsaker, & Gilbert, 2005), and tone fear conditioning which is not hippocampal-dependent but becomes hippocampal-dependent only after a delay between the tone and shock is introduced in trace fear conditioning (McEchron, Tseng, & Disterhoft, 2003). A similar finding in humans using functional magnetic resonance imaging (fMRI) found high hippocampal activation when a subject had to bind color and item judgements across a delay compared to when there was no delay (Staresina & Davachi, 2009).

The hippocampus is a complicated structure with three main pathways. There are two trisynaptic pathways that originate in the entorhinal cortex through the dentate gyrus, to either area cornu ammonis subfield 3 or 2 (CA3 or CA2) and end in cornu ammonis subfield 1 (CA1). There is also a direct pathway from entorhinal cortex to CA1 called the temporamonic pathway. Precise lesion work with animals has further dissociated how the different subregions of the hippocampus process temporal aspects of memory. Hoge & Kesner (2007) found that a temporal object task where rats were exposed to a series of objects, and then spent more time exploring the less recent object, was disrupted by CA1 lesions but not CA3 lesions. Neither lesion affected a recognition/novel object task. Kesner et al. (2005) performed an object trace odor paired associate task, where the

animals were exposed to an object, and after a delay of 10 seconds an odor. If this odor was the associated pair with the object, the rat was to dig for reward, and to withhold response if the object and odor were not paired. Once again only rats with CA1 lesions were impaired, while CA3 rats were unimpaired. Farovik, Dupont, & Eichenbaum, (2010) had rats learn two odor sequences that were separated by a delay of 3 or 10 seconds and were later tested on the order of the sequence. Rats with CA3 lesions were unable to perform the task at either delay period, but rats with CA1 lesions were impaired only at 10 seconds. All of this evidence lends strong support to Kesner's theory that CA1 seems to be especially important for bridging intermediate length delays, and the temporal pattern separation involved in remembering sequences across time (Kesner & Hunsaker, 2010). Of the three pathways to CA1, there is only direct evidence of the temporammonic pathway being involved in temporal aspects of memory. Researchers optogenetically controlled direct inputs to CA1 from entorhinal cortex layer III and layer II island cells (a subset of layer II cells) which affected the memory performance of rats on a trace fear conditioning task to be increased or decreased (Kitamura et al., 2014).

Another example of temporal memory is seen with interval timing tasks in which a subject is not just making an association across time, but needs to explicitly time a certain delay period in order to do a behavior to get rewarded or avoid aversive stimuli. Examples of this type of task that have a delay on the order of hundreds of milliseconds are delay and trace eyeblink conditioning task. The cerebellum, thalamus, and brain stem are important for good performance on both tasks, but hippocampus, prefrontal cortex, caudate, and primary sensory cortex are only needed in trace conditioning when there is a

break between the conditioned and unconditioned stimulus and not in delay conditioning where the delay overlaps with the stimulus (Weiss & Disterhoft, 2011; Woodruff-Pak & Disterhoft, 2008; Yang et al., 2014). The hippocampus is vital for learning trace eyeblink conditioning, but after learning and consolidation of this memory hippocampus is no longer necessary for good performance (Weiss & Disterhoft, 2011). Evidence suggests that some part of the forebrain is bridging this temporal gap during sustained performance on this task (Woodruff-Pak & Disterhoft, 2008), this might be performed by cells in prefrontal cortex that increase and maintain firing during the trace (Gilmartin & Helmstetter, 2010). In this theory hippocampus initially captures the conditioned association across the trace, and then imparts that information to the cortex in such a way that the prefrontal cells are trained to sustain firing to particular downstream cells in the Pontine nuclei for the appropriate period of time. Alternatively, the temporal gap might be bridged by a sequence of prefrontal cells that each fire for a short period that together fully span the delay. These cell firing patterns during the delay look similar to "time cells" in the hippocampus (Bolkan et al., 2017; Tiganj, Jung, Kim, & Howard, 2016).
Even though it has been demonstrated that hippocampus is only necessary in its contribution to the initial learning of the tone eye puff temporal association, hippocampal cells continue to be active in this task in overtrained rats (Hattori, Chen, Weiss, & Disterhoft, 2015).

There are many other tasks with interval timing on longer time scales such as a peak interval procedure where after a conditioned stimulus, a subject may respond after a certain fixed delay for a reward. During probe trials when there is no reward given,

animals tend to increase their responses leading up to and decreasing after the fixed reward interval in a Gaussian with a mean close to the fixed interval time and a standard deviation that increases as the length of the fixed interval increases. This scalar property in these timing tasks is found in animals and humans and is a good example of Weber's law in a non-sensory paradigm (Gibbon, 1977; Rakitin et al., 1998). It is currently unknown exactly how the brain times these delays, but there are several classes of models that have been suggested.

One historically popular type of model is called a pacemaker accumulator model which involve a clock like pacemaker that regularly emits pulses that a different accumulator neural system counts. One variant of a pacemaker accumulator model is Scalar Expectancy Theory, which ascribes interval timing to cells that fire at a Poisson rate after an onset stimulus. These cells synapse onto a downstream reader which sums the input in a linear way until the reinforcing stimulus causes the system to save the overall accumulated input. A system could use this saved input to time future expected events (Staddon & Higa, 1999). One of the main criticisms aimed at this model is it predicts relative accuracy in measuring time intervals should increase as the time interval increases which is inconsistent with experimental findings and the Weber Law (Staddon & Higa, 1999). Another category of model uses a very different mechanism to time an interval. These models can be broadly classified as oscillator based models. The models use oscillators of different frequencies that combine in a beat pattern which will consistently reach a peak of activation ranging from hundreds of milliseconds to tens of seconds (Miall, 1989). An example of this model used to accurately simulate a peak

interval timing procedure is the Striatal Beat Frequency model. In this model neurons in cortex are forced to synchronize when exposed to dopamine from inputs from the ventral tegmental area. These dopamine inputs are triggered by the conditioned stimulus starting the interval. Different neurons in cortex fire at different frequencies and all synapse on striatal spiny neurons. When a set of neurons all coincidentally fire on synapses of the same cell, they cause it to fire. With a particular set of cortex neurons with sufficient synaptic strength on the same neuron this will always happen at the least common multiple of all the input firing frequencies. In this way, very short to much longer time periods can be encoded accurately (Meck, Penney, & Pouthas, 2008).

There is also evidence that the hippocampus is necessary for time period estimation of longer time periods. Rats with hippocampal lesions were able to discriminate between delays of one three and twelve minutes, but were unable to discriminate between delays of eight and twelve minutes. Additionally, these hippocampal rats showed performance enhancement on discriminating delays of one and one and half minutes (Jacobs, Allen, Nguyen, & Fortin, 2013). Similar findings were found in human patients with hippocampal lesions, who could accurately estimate the length of shorter but not longer movie clips.(Palombo, Keane, & Verfaellie, 2015). These examples support the idea that hippocampus possibly acts in competition with cortico-striatal systems for time interval estimation on short time scales, but hippocampus seems to be essential for distinguishing time intervals on longer time periods. This ability to temporally distinguish longer intervals is likely linked to hippocampus's role of linking sequences of events on these longer time scales. This also demonstrates that in all the

behavioral paradigms that are hippocampal-dependent for performing a task on shorter time scales, hippocampus is not contributing timing information about the length of a temporal interval. Instead the hippocampus is likely to be contributing to the binding of associations across time.

It wasn't until recently that the first evidence of a potential mechanism for how cells in CA1 could be contributing to this temporal processing was discovered. Researchers have identified two main correlates of temporal processing. One study had rats run on a running wheel during a delay on the alternating T maze task (Pastalkova, Itskov, Amarasingham, & Buzsáki, 2008). This alternating T maze task is made hippocampal-dependent by addition of a delay. Pastalkova discovered cells in CA1 that fire at certain times during a delay in a similar way and with many similar features to how place cells fire in a location in space.

We have called these neurons "time cells," and they appear to emerge from the same pyramidal cell population in CA1 as place cells. This means that cells in CA1 can be both place cells on a maze and time cells during a delay. These time cells also have similar firing characteristics to place cells including field width firing rate and theta phase precession (Pastalkova et al., 2008). MacDonald, Lepage, Eden, & Eichenbaum (2011) also found these time cells in a nonspatial Object-Trace-Odor Paired Associate Task similar to a task found to be hippocampal-dependent(MacDonald et al., 2011). He found that these cells conjunctively coded for space and time by firing in one portion of the delay box but only at a specific time during the delay. There was still some question about whether the cells were firing because of a path integrated distance, or the amount of

time that has passed. Kraus, Robinson II, White, Eichenbaum, & Hasselmo, (2013) were able to separate out these two possible drivers of cell firing. This was accomplished by having the rats run on a treadmill on the stem of an alternating T-maze and varying the speed while holding the time or distance constant. In this way a rat could run 10 meters, either very slowly in a long amount of time, or quickly in a short amount of time. Alternatively, the rat could run for 20 seconds which is a short distance or long distance based on the speed of the treadmill. Kraus was able to show that CA1 time cells seem to code time and distance conjunctively. Cells that look like time cells have also been found in primates. Although delays in primate tasks tend to be too short to have extended time cell sequences, there are cells that ramp up and down across the delay (Sakon, Naya, Wirth, & Suzuki, 2014). Time cell sequences have also been shown on a shorter time scale. Groups of CA1 cells were shown to fire at set times after the stimulus onset during trace eyeblink conditioning (Modi, Dhawale, & Bhalla, 2014).

Time cells

Time cells in the hippocampus have been shown to exist when there is a memory load during a delay (Pastalkova et al., 2008). Pastalkova argued that these cells required memory load using a control task which involved two rats running on a wheel for 10 and 20 seconds respectively, similar to the experimental rats who ran on a running wheel during the delay in her alternation task. The control rats were rewarded for their run on the opposite side of a box, and then began running again for the next trial. Cells fired randomly throughout the wheel run, unlike the temporal firing during the wheel run in the delay of the memory task. This finding was corroborated by Gill, Mizumori, & Smith

(2011) who demonstrated that time cells developed and sharpened their temporal tuning curves as a rat learned a memory task, but did not change during a random control task. This dependence on memory load is clearly contrasted with place cells, which fire in a spatially tuned manner whenever there is a fixed spatial environment regardless of whether the rat is engaged in a memory task. Considering how similar spatial and temporal firing attributes are in CA1 by other measures, it was interesting that time cells had this unusual property.

Another correlate of temporal processing has been recently found in the hippocampus. Manns, Howard, & Eichenbaum (2007) describe a task where rats learn a trial unique sequence of odors. They reported that the population of CA1 cells slowly changed their representation over time. Through a combination of cells ceasing to fire, new cells starting to fire, and other cells changing their firing rates, the population of cells look more similar when a rat sampled an odor closer in time, and grew more different the more time went by. In a single trial the more the population coding changed over that trial the more likely the rat when tested would make a correct judgement about which odor came first in the sequence. This phenomenon was further described by Mankin et al. (2015). This experiment compared the spatial representation of rats placed in the same context multiple times across days, or rats placed in two different contexts. In this study CA1 cells showed the same pattern as Manns demonstrated, a slow gradual change in the representation over time of the same context. CA3 cells on the other hand stayed consistent in their representation of a context across time. Interestingly, CA2 cells showed the opposite pattern, changing its representation across time, regardless what

context the rat was in. In primates Naya & Suzuki (2011) showed a similar effect in hippocampus. During a delay between two sequential cues the hippocampal population slowly changed its representation from the first cue to the second cue. A similar finding in human studies showed that humans watching repeated clips of movies quickly developed a predictable changing representation of the sequence over time (Paz et al., 2010). The Naya and Paz experiments give us a tantalizing hint that the population changes seen by Mankin and Manns, may not be random drift of a population, but predictable population changes that relate to salient changes in the environment. Through this lens, the phenomena of time cells on a short time scale and population change over short and long time scales may be able to be connected.

Connectivity and context

There are several models that account for the origin of time cells. Itskov, Curto, Pastalkova, & Buzsáki, (2011) postulated that when the CA3 recurrent network stops receiving external input, CA3 continues to fire with the attractor state that was firing when external input stopped. Then slowly over time the network activity flows in a specific repeatable neural trajectory, with new cells starting to fire based on strength of connectivity, and longer firing cells becoming quiet because of adaptation. CA3 then projects to CA1 driving similar sequences of time cells. Cells in this model fire at specific times because the network when placed in the same initial state will flow in the same neural trajectory and at the same rate leading to a consistent temporal sequence of time cells. In this view hippocampus can use these sequences of cell firing to map out experiences that are happening across time. A similar process might be happening in

spatial coding where sequences of cells might be employed during initial navigation to represent an environment in space. There is some evidence for this process in preplay, a phenomenon where sequences of cells fire during high frequency oscillations in sleep before a rat explores a new context. When a rat explores the novel environment after sleep, these same sequences of cells are found as the rat moves through space in the new environment. It is possible that the hippocampus is mapping these preexisting sequences of cells to new experiences in space or time. In this case the sequences of stimuli are applied during a new exploration of a spatial context (Buhry, Azizi, & Cheng, 2011; Dragoi, 2013). Time cells might have similar origins encoding sequences across temporal events. Rats sleeping after learning new contexts also have cells that fire in quick succession during high frequency oscillations in a phenomenon called replay. During replay, these cells fire in the same sequences as fired when the rat ran through a series of place fields in the environment. Similar replay sequences where found during sleep after rats performed a task with time cells, implying that the hippocampus is processing space and time in a similar way (Wang, Roth, & Pastalkova, 2016).

Oscillatory interference and temporal context models

Oscillatory interference models can be used to model a wide variety of phenomena including time cells. The necessary ingredients are at least two oscillators which can be internal to a cell like oscillating membrane potentials, or external rhythmic inputs like cells with persistent firing rates or local field potentials and their rhythmic inhibitory inputs. Grid cells have been modeled this way using speed modulated head direction cells that drive cells that persistently fire at different phases across the maze

based on this input. When enough of these persistent cells that synapse on the same grid cell fire at the same time (their oscillatory lowest common denominator) they drive the cell to fire, and these oscillatory synchronous firings happen in a grid field across space. A group of grid cells modeled in this way that synapse onto pyramidal cells can naturally drive place cell behavior when grid fields from multiple grid cells with different sized spacing conjointly fire in the same location (Hasselmo, 2008). This oscillatory interference model can also accommodate when a rat is running on a running wheel or a treadmill. The way that the head direction cells are speed modulated means that the interval of time passed until constructive interference occurs is a reliable output for the distance traveled. Time cells have been shown to be influenced by both distance traveled and time elapsed (Kraus et al., 2013). The oscillatory interference model can nicely account for the distance input of these results. In a similar experiment, cells were recorded in the medial entorhinal cortex (MEC) that showed a spatial firing pattern that leads to them being designated as grid cells. These cells were recorded during a delayed alternation task with a treadmill run during the delay and were shown to fire differently in space than they did on the treadmill. This difference was not predicted by the oscillatory interference model. This means that something about the input that results from moving around in space is necessary for driving or perhaps correcting grid cells to fire with a specific field width and field spacing (Kraus et al., 2015). Without the reliable regularly spaced firing fields in time of grid cells during a delay, the oscillatory interference between grid cells can't be directly responsible for the generation of time cells as

formulated in this particular model. The oscillatory interference mechanism may still play a role in time cell generation.

Another interesting model of the origin of time cells is the temporal context model (Howard & Eichenbaum, 2013). The foundation of this model is designed to account for episodic memories coding across time of a sequence of inputs while accounting for a broad array of behavioral findings including that memories are scale invariant across time and the temporal contiguity effect (where you are more likely to remember the next word in a memorized list of words then other words in the list, and are more likely to remember words from adjacent learned lists, Sederberg, Miller, Howard, & Kahana, 2010). This model postulates a series of leaky integrator neurons that fire in reaction to stimuli and stop firing after different periods of time depending on the properties of the leak current. At any instance of time there is a set of these cells that encode for the history of stimuli up to that moment, with more recent stimuli represented more strongly. This population of cells through a specific set of connectivity with the hippocampus could result in time cells when there is an initial reliable sequence of inputs followed by a period of no drivers to the system, hippocampus coding would be dominated by cells that fire at set periods after the last salient input. The temporal context model also accounts for the findings that there is a drift of the population code across time. A set of inputs from being in the same location receiving the same stimulus would not result in a identical population representation because of the changing ensemble of cell read outs due to the history of inputs into the system. The more time has passed the more different the stimuli history of the system is, resulting in increasingly different

population coding. The temporal context model also accounts for the fact that time cells get wider as the delay increases, and predicts that this widening should follow a log normal distribution. This aspect of the temporal context model is strongly influenced by the Weber Fechner law which has a long history of describing neural and behavioral phenomena. One strength of the temporal context model and the Weber Fechner law is the testable hypothesis that time cells would widen across time in a predictable distribution.

Experiments

The following series of experiments were designed to more closely examine temporal processing in the hippocampus. First, I identified nonspatial sequential firing properties in CA1 in a hippocampal-dependent sequence task. Most of this chapter have been published (Allen, Salz, McKenzie, & Fortin, 2016). I then aimed to help identify how and in which brain structures "time cells" originate, and gain hints at how this information percolates through and is processed by the hippocampal system. This was accomplished by recording from area CA3, one of the major inputs into CA1, using a task in which we have previously demonstrated time cells in CA1. By recording from each of these input areas we attempted to piece together how they participate in the temporal processing in area CA1. This chapter is an earlier version of a publication. In the published paper, time cells were defined using a more unbiased method described in the final chapter (Salz et al., 2016). In a final project I closely examined time cell properties to see if they fit the predictions of the Weber Fechner law.

CHAPTER TWO

There is a confluence of evidence from human and animal lesion work that the hippocampus plays an important role in the ability to remember a sequence of events, a necessary component of episodic memory. Many studies have also shown that hippocampal pyramidal cells represent sequences of locations in space. The connection between the behavioral evidence that hippocampus is necessary to encode sequences of nonspatial events at the same location and the electrophysiological evidence demonstrating that hippocampus represents sequences of locations has been conjectured but never explicitly demonstrated. We attempted to find neural representation of nonspatial sequences by electrophysiologically recording from cells as rats performed in two separate hippocampal-dependent nonspatial paradigms. Both tasks involve paying attention to the current sequence of odors and appropriately responding if odors were match or nonmatch in one task, or in sequence or out of sequence in the other task. We will demonstrate that despite the animals being behaviorally 'fixed' there are cells in both tasks which represent whether an odor was a match or nonmatch (a simple example of a sequence) or if the odor was in the appropriate position in a larger sequence. These findings give strong support to the idea that the hippocampus is involved with memory of sequences of events, whether those events are sequences of locations or odors delivered in the same location.

This chapter was organized to contain a synthesis of the publication (Allen et al. 2016) and unpublished data with some overlapping sequential findings presented at the Society for Neuroscience annual meeting in 2012. It this chapters final form, only data

from the 2016 paper was included with a rewritten introduction and conclusion to better tie the work with the rest of the thesis.

Allen, T. A., Salz, D. M., McKenzie, S., & Fortin, N. J. (2016). Nonspatial Sequence Coding in CA1 Neurons. *The Journal of Neuroscience*, *36*(5), 1547–1563.

Introduction

Temporal processing is intricately involved in a variety of behaviors, from physical activities, and speech, to memory allowing for associations to be made between events (Allen & Fortin, 2013; Merchant, Harrington, & Meck, 2013). This temporal structure of memory is necessary for episodic memory which along with who what and where information contains a sequence of events including the temporal relationship between those events (Allen & Fortin, 2013; Davachi & DuBrow, 2015; Eichenbaum & Fortin, 2005; Eichenbaum, MacDonald, & Kraus, 2014; Ranganath & Ritchey, 2012). There is a large body of evidence that hippocampus is necessary for episodic memory (Burgess, Maguire, & O'Keefe, 2002; Fortin, Wright, & Eichenbaum, 2004; Tulving & Markowitsch, 1998). Neurophysiological evidence has focused in particular on the hippocampus's ability to encode sequences of spatial locations experienced over time. (Burgess et al., 2002; Dragoi & Buzsáki, 2006; Foster & Wilson, 2006; Gupta, Meer, Touretzky, & Redish, 2012; Karlsson & Frank, 2009; Mehta, 2015; Skaggs & McNaughton, 1996). There is evidence that these place cell sequences are important for memory including sequence replays in sleep (Jadhav & Frank, 2014), and theta sequences that read forward and backwards at choice points and rewards (Gupta et al., 2012). All of this research depends on analyzing data when rats are learning in different locations as they move around an environment, but many memories can exist in the same location. Since we know that hippocampus is necessary for forming new memories, there must be a neural mechanism for learning sequences of events that occur in the same location. It has already been demonstrated that hippocampal neurons can fire differentially in the

same location based on the behavioral context at the moment including trial type and planned trajectory (Dudchenko & Wood, 2014; Frank, Brown, & Wilson, 2000; Smith & Mizumori, 2006). We believe that hippocampal neurons will encode events that occur in the same location differently, and furthermore when a sequence of events regularly repeats itself, the neurons will encode the sequence position of an event.

We tested this hypothesis using a hippocampal-dependent task (Quirk, Allen, & Fortin, 2013) in which rats learned a sequence of odors all sampled from the same odor port. During the task, odors were typically presented in the correct ordinal location of the sequence (InSeq). There were also probes in which an odor from the sequence was presented in a different ordinal location in the sequence (OutSeq). Initially we tested rats on a session with a highly familiar sequence of odors (Well-Trained), and then recorded sessions in which the rats were learning a new sequence (Novel1, Novel2) in order to compare different levels of performance as rats learn a sequence of odors. While rats performed this task, we recorded from area CA1 of the hippocampus and found cells that fired differentially based on whether an odor was presented InSeq or OutSeq, and this representation within hippocampus strengthened with improved performance on the task. This is evidence of a mechanism that might contribute to the hippocampus ability to learn episodic sequences and help to disambiguate those sequences of events from other similar sequences.

Materials and methods

Subjects

Five male Long-Evans rats, weighing approximately 350 g at the beginning of the experiment, served as subjects. Rats were individually housed and maintained on a 12 hour light/dark cycle. Rats had free access to food, but access to water was limited to 2-10 min each day depending on how much water they received as reward during behavioral training (3-6 mL). On weekends, rats received full access to water for at least 12 hours to ensure adequate overall hydration. Hydration levels were monitored daily. All procedures were conducted in accordance with the Institutional Animal Care and Use Committee.

Equipment and stimuli

Subjects were tested in a quiet experimental room with automated equipment capable of repeated deliveries of multiple distinct odors in a single odor port (Fig 1A). The apparatus consisted of a linear track (length = 150 cm, width = 9 cm), with walls angled outward (30 degrees from vertical, height = 40 cm). The odor port, located on one end of the track, was equipped with photobeam sensors to precisely detect nose entries and was connected to an odor delivery system (www.med-associates.com). Two water ports were used for reward delivery: one located under the odor port, the other at the opposite end of the track. Timing boards (www.plexon.com) and digital I/O devices (www.ni.com) were used to measure response times and control the hardware. All aspects of the task were automated using custom MATLAB scripts

(www.mathworks.com). A 96-channel Multichannel Acquisition Processor (MAP; www.plexon.com) was used to interface with the hardware in real-time, and record the behavioral and electrophysiological data.

Odors consisted of synthetic food extracts contained in glass jars (A: Lemon; B: Rum; C: Anise; D: Vanilla; E: Banana; V: Almond; W: Cinnamon; X: Coconut; Y: Peppermint; Z: Strawberry) that were volatilized with desiccated, charcoal-filtered air (flow rate = 2 L/min). To prevent cross-contamination, separate Teflon tubing lines were used for each odor, which converged in a single channel at the bottom of the odor port. In addition, an air vacuum located at the top of the odor port provided constant negative pressure to quickly evacuate odor traces. Readings from a volatile organic compound detector confirmed that odors were cleared from the port 500–750 ms after odor delivery (inter-odor intervals were limited by software to a minimum of 800 ms).

Behavior

The sequence task (Fig 1A; Allen et al., 2014) involves repeated presentations of sequences of non-spatial items (odors) and requires subjects to determine whether each item is presented "in sequence" (InSeq; by holding the nose-poke response until the signal) or "out of sequence" (OutSeq; by withdrawing the response before the signal). In the present study, we used five-item sequences and focused on two types of OutSeq probe trials (Repeats and Skips; see below). In each session, a given odor sequence (e.g., Seq1: ABCDE) was presented 30-50 times, with approximately half the presentations including all items InSeq (ABCDE) and half including one item OutSeq (e.g., ABDDE). Each odor presentation was initiated by a nose poke (provided 800 ms had elapsed since

the previous odor) and was terminated after the rat either held for 1.2 s (signaled by a beep) or pulled its nose out. Water rewards were delivered below the odor port after correct responses (10 μL) and at the opposite end of the track following correct completion of a full sequence (20 μL). Following an incorrect response, a buzzing sound was emitted and the sequence was terminated. To enhance the segmentation between each odor sequence (completed correctly or not), rats were required to run to the end of the track opposite the odor port before the next sequence could be presented.

Naïve rats were initially trained in a series of incremental stages over approximately 6-8 weeks. First, rats were trained to nose-poke and hold their nose in the odor port for a water reward. The minimum required nose-poke duration started at 50 ms and was gradually increased (in 15 ms steps) until rats held reliably for 1.2 s and reached a criterion of 80% correct nose-pokes over three sessions (100-200 nose-pokes per session). Rats were then habituated to odor presentations in the port (odor A, then odors AB) and required to maintain their nose-poke response for 1.2 s to receive a reward (~3 sessions). Second, rats were trained to identify InSeq and OutSeq items. Rats were initially trained on a 2-item sequence in which they were presented with "AB" and "AA" sequences in equal proportions. While the correct response on the first odor was to hold for >1.2 s (Odor A was always the first item), the second response required rats to determine whether the second item was InSeq (AB; hold for >1.2 s to receive reward) or OutSeq (AA; withdraw before 1.2 s to receive reward). After reaching criterion on the 2-item sequence, the number of items per sequence was increased to 3, 4 and 5 in successive stages (criterion: >80% correct across all individual odor presentations over 3

sessions). After reaching criterion performance on the 5-item sequence (>80% correct on both InSeq and OutSeq items), rats underwent surgery for microdrive implantation.

OutSeq probe trials. Our previous work included a detailed analysis of performance across different types of OutSeq items in rats and humans, which suggested that similar cognitive processes and sequence representations support task performance across species (Allen et al., 2014). However, to maximize sampling, the present study included only two types of OutSeq items: Repeats, in which an earlier item was presented a second time in the sequence (e.g., ABA) and Skips, in which an item was presented too early in the sequence (e.g., ABD, which skipped over item C). Note that OutSeq items could be presented in any sequence position except the first (i.e., sequences always began with an InSeq item).

Surgery

Rats received a preoperative injection of the analgesic buprenorphine (0.5 mg/kg, 0.2 mg/ml, i.p.) approximately 10 min prior to induction of anesthesia. General anesthesia was induced using isoflurane (induction: 4%; maintenance: 1–2%) mixed with oxygen (800 mL/min). After being placed in the stereotaxic apparatus, rats were administered glycopyrrulate (0.2 mg/mL, 0.5 mg/kg, s.c.) to help prevent respiratory difficulties. A protective ophthalmic ointment was then applied to their eyes and their scalp was locally anesthetized with marcaine (7.5 mg/mL, 0.5 mL, s.c.). Body temperature was monitored and maintained throughout surgery and a Ringer's solution with 5% dextrose was periodically administered to maintain hydration (total volume of 5 mL, s.c.). The skull was exposed following a midline incision and adjustments were

made to ensure the skull was level. Six support screws (4 titanium, 2 stainless steel) and a ground screw (stainless steel; positioned over the cerebellum) were anchored to the skull. A piece of skull approximately 3 mm in diameter (centered on coordinates: -4.0 mm AP, 3.5 mm ML) was removed over the left hippocampus. Quickly after the dura was carefully removed, the base of the microdrive was lowered onto the exposed cortex, the cavity was filled with Kwik-Sil (www.wpiinc.com), the ground wire was connected and the microdrive was secured to the support skull screws with dental cement. Each tetrode was then advanced ~900 μm into the brain. Finally, the incision was sutured and dressed with Neosporin and rats were returned to a clean cage where they were monitored until they awoke from anesthesia. One day following surgery, rats were given an analgesic (Flunixin, 50 mg/ml, 2.5 mg/kg, s.c.) and Neosporin was re-applied to the incision site.

Electrophysiological recordings

Spiking activity and local field potentials (LFP) were recorded from the CA1 pyramidal layer of the dorsal hippocampus as rats performed the task (Fig 2). Each chronically-implanted microdrive contained 20 independently-drivable tetrodes, with each tetrode consisting of 4 twisted nichrome wires (13 μm diameter; www.calfinewire.com) gold-plated to achieve a final tip impedance of ~250 kΩ (measured at 1 kHz). Following the surgical recovery period, tetrodes were slowly advanced over a period of ~3 weeks while monitoring established electrophysiological signatures of the CA1 pyramidal cell layer (e.g., sharp waves, ripples and theta amplitude). Recording sessions began when sufficiently large ensembles of neurons (>50) could be recorded simultaneously.

Voltage signals recorded from the tetrode tips were referenced to a common skull screw positioned over the cerebellum, and differentially filtered for single-unit activity (SUA; 154 Hz to 8.8 kHz) and local field potentials (LFP; 1.5-400 Hz). The neural signals were then amplified (SUA: 10,000-32,000X; LFP: 1,000X), digitized (SUA: 40 kHz; LFP: 1 kHz), and recorded to disk with the data acquisition system (MAP; www.plexon.com). Action potentials from individual neurons were manually isolated offline using a combination of standard waveform features across the four channels of each tetrode (Offline Sorter; www.plexon.com). Proper isolation was verified using inter-spike interval distributions for each isolated unit (assuming a minimum refractory period of 1 ms) and cross-correlograms for each pair of simultaneously recorded units on the same tetrode. Putative pyramidal neurons and interneurons were identified by previously identified characteristic firing rates and peak-to-peak spike widths (Csicsvari et al., 1998; 1999; Mizuseki & Buzsáki, 2013) and sorted through a minimum variance algorithm using multivariate Euclidean distances (linkage and cluster functions in MATLAB2013a; Fig 2B). Both types of neurons were included in our analyses. To confirm recording sites, current was passed through the electrodes prior to perfusion (0.9% phosphate-buffered saline followed by 4% paraformaldehyde) to produce small marking lesions, which were subsequently localized on Nissl-stained tissue slices (Fig 2D).

Sequence memory performance analyses

Performance on the task can be analyzed using a number of measures (see Allen et al., 2014). In the present study, within-session performance was analyzed using continuous (nose-poke duration) and categorical (expected vs observed frequencies)

measures (see Fig 1B). Nose-poke duration analyses used paired t-tests to determine whether the rat held its response significantly longer on InSeq than OutSeq trials. G-tests were used to determine whether the observed frequency of InSeq and OutSeq responses for a given session (or trial type) was significantly different than the frequency expected by chance. Note that the G-test provides a measure of performance that controls for response bias and is a robust alternative to the Chi-Squared test, especially for datasets including cells with smaller frequencies (Sokal & Rohlf, 1995).

To compare performance across sessions or animals, we calculated a Sequence Memory Index (SMI; Allen et al., 2014; Eq 1). In essence, the SMI normalizes the proportion of InSeq and OutSeq items presented during a session and reduces sequence memory performance to a single value ranging from -1 to 1. A score of 1 represents perfect sequence memory, in which a subject would have correctly held its nose-poke response on all InSeq items and correctly withdrawn on all OutSeq items. A score of 0 indicates chance performance, such as if subjects responded to InSeq and OutSeq items with the same response pattern (e.g., holding until the signal 80% of the time regardless of the trial type). Negative SMI scores represent performance levels below that expected by chance. We have previously found that SMI is a normally distributed measure (Allen et al., 2014; 2015) and used Q-Q plots to confirm that the present data also closely followed a normal distribution, and thus used traditional (parametric) t-tests and ANOVAs for these statistical comparisons. One-sample t-tests were used to perform comparisons with chance levels, repeated-measures ANOVAs to compare performance across sessions (Well-Trained, Novel1 and Novel2) and quadratic regression analyses

were used to test parallels between neural activity and performance levels across sessions. Tests were considered significant at $p < 0.05$ and trends were noted when $p < 0.10$.

$$SMI = \frac{(0.9*\mathrm{IN}_{cor})(0.1*\mathrm{OUT}_{cor})-(0.9*\mathrm{IN}_{inc})(0.1*\mathrm{OUT}_{inc})}{\sqrt{(0.9*IN_{cor}+0.9*IN_{inc})(0.1*OUT_{cor}+0.1*OUT_{inc})(0.9*IN_{cor}+0.1*OUT_{inc})(0.9*IN_{inc}+0.1*OUT_{cor})}} \quad (1)$$

Single-cell analyses

Single-cell activity was analyzed using resampling, non-parametric statistics (1000 permutations; e.g., Sokal & Rohlf, 1994; McKenzie et al., 2013; Neunuebel & Knierim, 2014), as spiking activity often violates the assumptions of normality and homogeneity of variance required for traditional (parametric) statistics. To capture the bursting firing properties of hippocampal neurons while limiting the number of statistical comparisons performed, we first binned the firing rate of each neuron over 50 ms and then segmented this activity into 250-ms windows to perform the statistical analyses (each 250-ms window contained five firing rate values for that neuron). For each comparison of interest (e.g., InSeq trials vs OutSeq trials), we calculated the t or F ratio for each 250-ms activity window separately (e.g., the two 250-ms windows preceding port withdrawal) and then determined the probability of obtaining a ratio this large (or larger) by random sampling. This probability distribution was created by randomly permuting trials within the same 250-ms activity window and calculating the associated t or F ratio, a process that was repeated 1000 times. A comparison was considered statistically significant if this probability was < 0.05 (Bonferroni corrected for the number of 250-ms activity windows included in the comparison). Our primary analyses compared

activity across temporal context (InSeq vs OutSeq), but the same approach was used for secondary analyses comparing activity across odors, sequence positions, or probe types (Repeats vs Skips).

For each neuron that reached statistical significance, we visually inspected the pattern of activity across trials using perievent rasters and histograms (e.g., Fig 3A,B). The number of statistically significant cells was then compiled in each session. Note that the neural activity of each session was analyzed independently and that no attempts were made to track the same neurons across sessions for a given rat. As neurons could have been resampled between sessions, for each cell category we report cell counts and the corresponding percentage (in relation to the total number of neurons active during task performance). Since we focused on periods of neural activity during which the animals' location and behavior was constant (500 ms window preceding port withdrawal, unless specified otherwise), the spatial distribution (X-Y coordinates) of spikes was not different across trial types and thus not described in further details here.

To help quantify the amount of information provided by individual cells about the InSeq/OutSeq status of odors, we adapted previous measures of information content used in spatial (Skaggs et al. 1993) and temporal processing (MacDonald et al., 2013). The sequential information content of each cell was calculated with the following equation:

$$Sequential\ Information\ Content = P_{IN}\left(\frac{\lambda_{IN}}{\hat{\lambda}}\right) log_2\left(\frac{\lambda_{IN}}{\hat{\lambda}}\right) + P_{OUT}\left(\frac{\lambda_{OUT}}{\hat{\lambda}}\right) log_2\left(\frac{\lambda_{OUT}}{\hat{\lambda}}\right) \quad (2)$$

Where P_{IN} is the probability of an InSeq trial, P_{OUT} is the probability of an OutSeq trial, λ_{IN} is the firing rate of the cell during InSeq trials, λ_{OUT} is the firing rate of the cell during OutSeq trials, and $\hat{\lambda}$ is the overall mean firing rate of the cell during odor sampling

periods. A value of 0 bit indicates that the activity of a given cell provides no information about the InSeq/OutSeq status of trials, while a value of 1 bit indicates that it can be fully determined by the activity of that cell.

Ensemble analyses

To analyze the pattern of ensemble activity across InSeq and OutSeq trials, we created an N x M ensemble activity matrix for each animal and session (N, number of simultaneously recorded neurons; M, number of trials). For each trial (M: trial-1 to trial-m), the raw firing rate of each neuron during the 500 ms odor sampling period preceding port withdrawal was calculated (N: neuron-1 to neuron-n). Note that the firing rate was averaged over the full 500 ms period, instead of being binned over 50 ms and analyzed as two separate 250-ms activity windows as in the single-cell analyses. Therefore, for each trial, the raw firing rate of all simultaneously recorded neurons produced a population activity vector in N-dimensional space (where N is the number of simultaneously recorded neurons). Neurons with a firing rate below 1 Hz across all trials were excluded from the analysis. As in our single-cell analyses, the activity of each session was analyzed independently and no attempts were made to track the same neurons across sessions for any of the rats. Ensemble analyses were first performed using raw firing rates and repeated using z-normalized firing rates. Raw and normalized data produced the same pattern of results.

We first used standard correlational methods to quantify the similarity of population activity vectors across trials (e.g., Mankin et al., 2012; MacDonald et al., 2013). While this approach provides a simple and intuitive quantification of the overlap

across population vectors, it may not be particularly suited for our experimental design as we expect all vectors to be highly correlated because the location and behavior of the animal is held constant across trials. Therefore, we then used hierarchical agglomerative clustering algorithms (linkage and cluster functions in MATLAB2013 using Ward's method as a minimum variance algorithm) to determine whether the InSeq/OutSeq status of each trial could be accurately decoded from the activity of simultaneously recorded neurons (e.g., Manns & Eichenbaum, 2009; McKenzie et al., 2014). More specifically, the population activity vectors of each trial from an ensemble activity matrix were sorted into a hierarchy of binary clusters that minimized the within-cluster variance (sum of squares) between constituent population vectors and the cluster centroids. Classification accuracy was evaluated by determining the degree to which the top two clusters corresponded to InSeq and OutSeq trials (using percent of trials correctly classified). Next, we performed a leave-one-out, cross-validated k-means analysis in which the population activity vector of each trial is categorized using the activity from all other trials. Statistical significance for decoding accuracy was established using a resampling approach similar to that used in our single-cell analyses. Specifically, the trial labels for the ensemble matrix were permuted 1000 times and, for each permutation, the classifier algorithm was re-run and classification accuracy re-calculated to compute the probability of obtaining an accuracy value this large (or larger) by this random shuffling of the ensemble activity. Decoding accuracy was considered statistically significant if this probability was less than 0.05.

Local field potential analyses

Perievent spectrograms were used to visualize local field potential (LFP) activity during task performance (NeuroExplorer v5.0; www.neuroexplorer.com). To capture odor- and sequence-related shifts in the power of oscillations at different frequencies throughout entire sequences, seven separate 4 s perievent spectrograms were produced for each rat and session (five centered on each port entry, one immediately before and after the sequence; see Fig 6A) using tetrodes with confirmed sequence cell activity. To compare LFP activity across InSeq and OutSeq items, separate spectrograms were produced for InSeq and OutSeq trials, and these spectrograms were then subtracted from each other to produce a difference spectrogram for each rat and session.

We focused our analyses on theta (4-12 Hz) and slow gamma/beta (20-40 Hz; see Igarashi et al., 2014) frequency bands, as our spectrograms showed high power in those bands at the level of individual sequence presentations, individual rats, and group. We will refer to 20-40 Hz as slow gamma/beta because it is currently disputed where to define these respective bands. Our analyses where done from 20-40 Hz to mirror Igarashi et al. but most likely 20-40 Hz contains the high range of beta and the low range of slow gamma. To explore differences in the amplitude of these frequency bands, LFPs were band-pass filtered (Butterworth) and phase determined with a Hilbert transform (e.g., Brandon et al., 2013). For each session and animal, the mean waveform for each frequency band was then obtained by aligning snippets of the filtered LFP signals in 250 ms windows (centered on the trough, or 0 degree phase) and averaging all z-score normalized waveforms together (Csicsvari et al., 1998; 1999; Patel et al., 2012). To

quantify task-related effects, averaging was restricted to the relevant time periods (PreSeq: 500 ms period preceding the first port entry; InSeq or OutSeq: 500 ms preceding port withdrawal; see Fig 6C and Fig 6E) and the mean absolute amplitude (average of amplitude values at 0 degree and 180 degree; trough and peak, respectively) was calculated for each average waveform. The mean absolute amplitude was compared across conditions using difference scores. Paired sample t-tests were used to test for significant differences.

Results

Strong, weak and intermediate levels of sequence memory performance across sessions

Our analyses focused on three sessions across animals (Well-Trained, Novel1, Novel2; Fig 1B,C), which differed by the amount of training associated with the sequence presented. In the Well-Trained session, rats were tested on the sequence they learned before surgery (Seq1: ABCDE) and continued to correctly identify items as InSeq or OutSeq at a high rate. In fact, according to a previously established sequence memory index (SMI; Allen et al., 2014), rats showed strong sequence memory in that session (SMIWell-Trained = 0.51 ± 0.05; mean ± SEM; SMIWell-Trained vs. Chance: $t(4) = 9.57$, $p < 0.001$; Fig 1C), a performance level comparable to that previously reported in unoperated rats (SMI = 0.47; Allen et al., 2014). In addition, single-subject analyses showed that each rat significantly differentiated between InSeq and OutSeq items (all G-tests P's < 0.001) and that each rat demonstrated memory for the full sequence, as this effect was observed at each ordinal position in the sequence (all positional G-tests P's < 0.05; e.g., Fig 1B, left panel).

Subsequently, rats were tested on a novel sequence (Seq2: VWXYZ) for two daily sessions and demonstrated weak (Novel1) and intermediate (Novel2) levels of performance. As expected, sequence memory was weakest in the Novel1 session (SMINovel1 = 0.09 ± 0.05) with none of the rats individually performing above chance levels (all G-tests P's > 0.10). However, some learning had occurred by the end of the session (second half of trials), as suggested by a trend toward significance for SMI comparisons with chance levels (SMINovel1 vs. Chance: $t(3) = 1.76$, $p = 0.089$) and the fact that the more powerful G-test combining accuracy data from all rats reached significance ($GNovel1(1) = 4.74$, $p < 0.01$). In the Novel2 session, rats showed significant levels of sequence memory (SMINovel2 = 0.28 ± 0.05; SMINovel2 vs. Chance: $t(3) = 5.17$, $p < 0.001$) with each rat individually performing above chance levels (G-tests P's < 0.05). SMI analyses across sessions confirmed that sequence memory performance was associated with the amount of training ($F(2,12) = 17.57$, $p < 0.001$; quadratic fit: $F(2,12) = 8.053$, $p < 0.01$; Fig 1C), a pattern captured by the representative rat shown in Fig 1B. Overall, these findings indicate that rats exhibited strong, weak, and intermediate levels of sequence memory across the three sessions of interest.

Ensemble characteristics were similar across sessions

Spiking and local-field potential (LFP) activity was recorded from the CA1 region during task performance (Fig 2). A few marking lesions were observed near the CA2 border (<10% of tetrodes) raising the possibility that a small proportion of the CA1 cells reported here were from CA2. While this proportion is too small for examining potential subfield differences, it is important to note that the patterns of activity we observed were

well distributed across tetrode locations. One rat was excluded from the Novel1 and Novel2 sessions because of damage to his microdrive. We isolated a total of 713 single-units from 13 sessions (5 rats in Well-Trained, 4 in Novel1, 4 in Novel2) using conventional multi-dimensional cluster sorting techniques. Neurons were then classified as putative principal neurons or interneurons according to previously established firing rate and waveform characteristics (Csicsvari et al. 1998; 1999; Mizuseki & Buzsáki, 2013) using an algorithm that minimizes variance based on Euclidean distances. The clustering algorithm classified 84% (599/713) of units as principal neurons and 16% (114/713) as interneurons (Fig 2B). Principal neurons had a mean session firing rate of 0.87 ± 0.05 Hz (mean ± SEM) and a mean peak-to-peak spike width of 470 ± 2 μs. In contrast, interneurons had higher firing rates (8.32 ± 0.93 Hz) and thinner peak-to-peak spike widths (198 ± 3 μs). The observed firing rates and waveform characteristics are comparable to previous reports (e.g., Csicsvari et al., 1998; 1999; Mizuseki & Buzsáki, 2013).

Ensemble characteristics were comparable across the three sessions of interest. There were no significant differences in the number of neurons per ensemble across sessions ($F(2,12) = 0.08$, $p = 0.93$) or rats ($F(4,12) = 2.36$, $p = 0.14$), with an overall mean of 55 neurons per ensemble. More specifically, we isolated 274 neurons in the Well-Trained session from five rats (ensemble sizes: 47, 66, 62, 55 and 44), 234 neurons from four rats in the Novel1 session (ensemble sizes: 79, 55, 67 and 33), and 205 neurons from four rats in Novel2 (ensemble sizes: 47, 69, 50 and 39). Moreover, no significant

differences were observed in the ratio of principal neurons to interneurons recorded across sessions (5.25:1; $F(2,12) = 0.47$, $p = 0.64$).

Hippocampal neurons exhibited sequence coding in the form of differential activity to InSeq and OutSeq items (sequence cells)

The main goal of the study was to determine whether, while the animals' location and behavior remained constant, hippocampal neurons differentially coded for individual items depending on their temporal context (InSeq or OutSeq). Note that this analysis excludes the first item of each sequence, as they were only presented InSeq. We began by collapsing this analysis across sessions to maximize statistical power in quantifying cell proportions (see below). Of 713 neurons recorded, we found that 187 neurons (26.2%) exhibited such sequence coding (hereafter referred to as "sequence cells" for clarity; e.g., Fig 3A,B), in that they showed significant differences in firing rates on InSeq and OutSeq trials (resampling t-tests p's < 0.05; see methods). This proportion is much higher than expected by chance as determined by the Type I error rate ($G(1) = 419.49$, $p < 0.001$), especially considering the fact that all isolated neurons were included in the analysis, regardless of overall firing rate. Even under highly conservative conditions, such as when we maximized the available odor sampling window by focusing only on trials with odor sampling periods of at least 500 ms (which excluded many correct OutSeq trials) and subsequently downsampled the number of InSeq trials to match the remaining OutSeq trials (which reduced statistical power), our analyses found a significant proportion of sequence cells (80 neurons, or 11.2%; $G(1) = 18.95$, $p < 0.001$).

In order to further characterize their firing properties, additional analyses were performed on the 80 sequence cells identified with these conservative criteria. First, these additional analyses showed that a greater proportion of sequence cells fired preferentially to OutSeq items (58/80; 72.5%; e.g., Fig 3A) compared to InSeq items (22/80; 27.5%; e.g., Fig 3B), proportions significantly different than expected from a uniform distribution ($G(1) = 8.63$, $p < 0.01$). Second, sequence cells included both putative principal neurons (61.3%; 49/80) and interneurons (38.9%; 31/80). Interestingly, this principal-to-interneuron ratio of 1.58:1 is significantly lower than that of the full dataset (5.25:1; $G(1) = 7.67$, $p < 0.01$), though this increased engagement of interneurons may in part be due to an increase in statistical power associated with their higher, more consistent firing rates. Finally, to quantify the amount of sequence information provided by individual cells, we adapted previous measures of information content used in spatial (Skaggs et al. 1993) and temporal processing (MacDonald et al., 2013). According to this sequential information content measure, a value of 0 bits indicates that the cell's activity provides no information about the InSeq/OutSeq status of trials, while a value of 1 bit provides full information. Analyzed over all trials, sequence cells had a mean information content of 0.16 ± 0.03 bits/spike (n = 80), significantly greater than non-sequence cells (0.07 ± 0.01 bits/spike, n = 633; $t(711) = 3.62$, $p < 0.001$). Separating sequence cells by their putative cell type revealed that principal neurons showed a significant trend toward more information per spike (0.21 ± 0.06 bits/spike) than interneurons (0.07 ± 0.01 bits/spike; $t(78)=1.193$, $p = 0.057$), but both cell types exhibited information content values above zero ($t_{Principal(48)} = 3.83$, $p < 0.001$; $t_{Interneurons(30)} = 4.42$, $p < 0.001$). Note that

while interneurons had lower bit/spike values, they have higher firing rates and thus can reach a level of sequence information comparable to that of principal cells over short periods of time. Although information content values cannot be directly compared across studies due to dissimilarities in task demands (which determine the possible range of bit values), this analysis shows that the activity of individual hippocampal cells contains sufficient information to determine the InSeq/OutSeq status of odor presentations.

It should be noted that the above analyses aligned all trials to the port withdrawal response to ensure overt motor dynamics (i.e., behavior) were identical on InSeq and OutSeq trials. As such, this approach did not control for the possibility that InSeq/OutSeq differences in activity were due to potential differences in internal motor dynamics that may have occurred before the withdrawal response. To address this possible confound, we performed additional analyses that focus on time windows during which such internal dynamics or states should be equivalent. First, we expanded the conservative analysis mentioned above to show that the proportion of sequence cells was similar across the sampling period, that is whether we focused our analysis on the time window immediately preceding the withdrawal response (250-0 ms; 10.7%), the window before that (500-250 ms; 7.4%), or the earliest window we could examine (750-500 ms; 9.3%). Had the effect been primarily driven by differences in internal motor dynamics, a different pattern would have been expected: a high proportion immediately before the withdrawal response (when differences in internal state should be the largest) and a low proportion in the earliest time period (when such differences should be smaller). Second, we performed a new analysis in which we specifically controlled for time spent in the

port (which aligned internal motor dynamics across InSeq and OutSeq trials) and obtained a proportion of sequence cells comparable to that reported in our previous analyses (10.0% compared to 11.2%). More precisely, this analysis aligned trials to when the rats' nose entered the port (this can be visualized by aligning trials in our raster plots to the beginning of the shaded areas) and focused the 500 ms analysis window on the time period when animals are expected to be identifying the odor and its InSeq/OutSeq status (i.e., 250-750 ms). Notably, this effect cannot be attributed to withdrawal responses during this sampling window, as those trials were not included in the analysis. Combined with evidence of conjunctive subtypes of sequence cells (see below), these results strongly suggest that differential activity to InSeq and OutSeq items cannot simply be accounted for by potential differences in internal motor dynamics or state.

Neural ensembles accurately distinguished the temporal context (InSeq/OutSeq) of individual trials

Following up on the above finding that many individual neurons fired differentially to InSeq and OutSeq trials (i.e., 26% of neurons were sequence cells), we then examined whether the activity of simultaneously recorded neuronal ensembles (raw firing rates) accurately represented the InSeq/OutSeq status of items on a trial-by-trial basis. Again, this analysis was initially collapsed across recording sessions to maximize sample sizes (N = 13 ensembles). As our initial approach to quantify ensemble activity, we used a population vector correlation method similar to that previously used in spatial (e.g., Mankin et al., 2012) and temporal processing (MacDonald et al., 2013). Briefly, for each session we calculated the correlation between population activity vectors across trial

conditions (each vector representing the firing rate over a 500 ms bin preceding port withdrawal for each neuron on that specific trial). As expected, InSeq trial vectors were highly correlated to each other (correlations between odd and even trials; mean r2 across ensembles = 0.99 ± 0.001 SEM, P's < 0.001) and so were OutSeq trial vectors (odd/even correlations; mean r2 = 0.97 ± 0.004, P's < 0.001). Importantly, correlations between InSeq and OutSeq trial vectors were lower (mean r2 = 0.83 ± 0.049, P's < 0.001) and significantly different from odd/even correlations on InSeq trials ($t(12) = 3.22$, $p < 0.01$) and OutSeq trials ($t(12) = 2.92$, $p < 0.05$) across ensembles. The same pattern (significantly lower correlations between InSeq and OutSeq trials than between odd and even trials) was observed using z-score normalized firing rates (all P's < 0.05). These results indicate that population activity vectors were significantly different depending on the temporal context of the item presented.

To determine whether the InSeq/OutSeq status of a presented item could be decoded from the ensemble activity, we then analyzed the data using a hierarchical clustering algorithm similar to that used in McKenzie et al. (2014) to differentiate categorical representations in hippocampal ensembles. Briefly, the population activity vector of each trial was fed to a classifier (raw firing rates), which assigned each vector to binary clusters by minimizing variance using Ward's method. Each vector was iteratively combined into larger clusters to form a hierarchical tree (see Fig 3E). Classification accuracy was calculated by comparing the overlap (percent) between the two main clusters of population vectors at the top of the tree (clustered according to their similarity) and the actual InSeq/OutSeq status of the trials. This analysis showed that these two

clusters of population vectors strongly matched the actual distributions of InSeq and OutSeq trials (Fig 3E). In fact, overall InSeq/OutSeq trial classification accuracy was 80.01 ± 3.83%, and 9/13 individual ensembles successfully classified the temporal context of trials (permutation P's < 0.01). Note that only the InSeq/OutSeq cluster (top cluster) reached statistical significance, indicating that clusters at lower levels did not account for a meaningful proportion of the cluster variances. We then used a standard k-means and a k-1 validation approach to perform the same classification (k = 2). This approach produced similar results (k-means accuracy: 84.66 ± 1.90%; k-1 accuracy 80.08 ± 3.38%; tk vs. k-1(12) = 0.0824, p = 0.936), and 11/13 individual ensembles successfully classified the InSeq/OutSeq status of trials (permutation P's < 0.01). The same pattern of classification accuracy was observed using z-score normalized firing rates (mean difference in accuracy between raw and normalized activity: 1% for k-means, 3% for hierarchical). Collectively, these different approaches confirm that CA1 ensemble activity coded for the temporal context of presented items on a trial-by-trial basis.

Finally, to examine whether certain types of trials were preferentially represented in misclassified trials, we further examined the results of the hierarchical cluster analysis to quantify the proportion of misclassifications across InSeq/OutSeq status, odors, or ordinal positions. We found that InSeq trials were misclassified less often than OutSeq trials (proportion misclassified: InSeq = 0.16, and OutSeq = 0.49, t(12) = -5.364, p < 0.001). As expected, the proportion of misclassified trials across ensembles was negatively correlated with behavioral performance (InSeq and OutSeq trials combined; r = -0.566, p = 0.003, n = 26). A similar pattern was observed when InSeq and OutSeq

misclassifications were examined separately but the correlations did not reach significance (InSeq: r = -0.398, $p = 0.18$, n = 13; OutSeq: r = -0.402, $p = 0.18$, n = 13). In addition, we found that odors BCDE were misclassified in similar proportions (mean proportion misclassified across odors: ~0.2; FBCDE(3,12) = 1.372, $p = 0.298$; FWXYZ (3,21) = 1.276, $p = 0.309$). Note that odors A and V (when presented OutSeq) were more likely to be misclassified than the other odors (A = 0.52, V = 0.49; FABCDE(4,16) = 3.498, $p < 0.05$, and FVWXYZ(4,28) = 5.021, $p < 0.01$), but this effect was not associated with performance (r = -0.255, $p = 0.401$, n = 13) and likely reflects the fact that the first items of the sequences were not included in the cluster analysis. Interestingly, our results also suggest a gradual increase in misclassifications from sequence position 2 to 5 (significant linear contrast: F(1,12) = 6.528, $p < 0.05$; non-significant main effect: F2345(3,36) = 2.205, $p = 0.104$).

Sequence coding was linked to sequence memory performance

To examine the relationship between sequence coding and sequence memory, we performed separate analyses for each of the three sessions of interest (Well-Trained, Novel1 and Novel2). Our single-cell analyses revealed that the proportion of sequence cells (the proportion identified by our most conservative criteria) paralleled sequence memory performance across the three sessions (Fig 3C): it was highest in the Well-Trained session (15.3%; 42/274 cells), lowest in the Novel1 session (4.3%; 10/234 cells) and high again in the Novel2 session (13.7%; 28/205 cells). This parallel was confirmed by a significant quadratic fit in the magnitude of temporal context coding (absolute values of t ratios of all cells on InSeq vs OutSeq comparison; n = 713) across the three

sessions (FQUAD(2,712) = 6.307, $p < 0.01$). This relationship was examined in more detail by correlating the proportion of sequence cells within a given ensemble with performance across rats and sessions. These analyses showed that the proportion of sequence cells was associated with SMI values (significant trend, r = 0.443, $p = 0.075$, n = 13) and significantly correlated with accuracy on OutSeq trials (r = 0.526, $p < 0.05$, n = 13).

Our ensemble analyses showed a similar pattern across the three sessions (Fig 3F). As reported above, the proportion of ensembles showing above-chance accuracy in classifying trials as InSeq/OutSeq was high across sessions (k-1: 11/13 in total; Hierarchical: 9/13), which is not surprising given the prevalence of sequence cells and the fact that behavioral performance is above chance in all three sessions (at least at the group level in the case of Novel1). More importantly, mean classification accuracy values paralleled performance across sessions: they were highest in the Well-Trained session (k-1: 85.5%; Hierarchical: 83.3%), lowest in the Novel1 session (k-1: 79.4%; Hierarchical: 77.7%) and second highest in the Novel2 session (k-1: 84.7%; Hierarchical: 78.5%), but in neither case did classification accuracy reach a significant quadratic fit across sessions (k-1: FQUAD(2,12) = 0.083, $p = 0.921$; Hierarchical: FQUAD(2,12) = 0.055, $p = 0.947$). However, classification accuracy values were associated with SMI values (significant trends; k-1: r = 0.46, $p = 0.055$, n = 13; Hierarchical: r = 0.443, $p = 0.075$, n = 13) and significantly correlated with accuracy on OutSeq trials (k-1: r = 0.716, $p < 0.01$, n = 13; Hierarchical: r = 0.526, $p < 0.05$, n = 13). Collectively, these findings indicate that this

form of sequence coding is associated with sequence memory performance at the single-cell and ensemble level.

General, conjunctive and probe-specific sequence cells

Sequence cells were identified as cells that fired differentially on InSeq and OutSeq trials. Since this analysis collapses across odors and sequence positions, it may have masked more specific types of sequence coding. To explore this possibility, we examined each sequence cell's activity across four different contrasts: InSeq vs. OutSeq trials (C1), InSeq trials sorted by odor (C2), OutSeq trials sorted by Odor (C3), and OutSeq trials sorted by ordinal position in the sequence (C4). This qualitative approach provided evidence for two primary categories of sequence cells, which were then confirmed using resampling statistics (see Fig 4 and methods). We refer to the first category as "general sequence cells" as they fired differentially to the overall InSeq/OutSeq status of items, regardless of the specific odor presented or the sequence position in which it occurred (p for C1 < 0.05; P's for C2-C4 > 0.05; 60% or 48/80 of sequence cells). General sequence cells could be further divided into cells that fired preferentially to InSeq items (InSeq cells; 29.2% or 14/48 of general sequence cells; e.g., Fig 4, Column 1) or to OutSeq items (OutSeq cells; 70.8% or 34/48 of general sequence cells; e.g., Fig 4, Column 2).

We refer to the second category as "conjunctive sequence cells" as they showed selectivity for specific conjunctions of item and sequence position information (40.0% or 32/80 of sequence cells). Subtypes of conjunctive cells were identified according to which contrast (in addition to C1) yielded a statistically significant ANOVA. The first

subtype exhibited differential activity when specific odors were presented InSeq (*p* for C2 < 0.05; 25.0% or 8/32 of conjunctive cells). For instance, a given cell may show peak firing to odor B when it is (correctly) presented in the second sequence position (e.g., Fig 4, Column 3). Conversely, other conjunctive cells primarily coded for specific mismatches between item and position information. In fact, the second subtype exhibited differential activity when specific odors were presented OutSeq (e.g., peak firing to odor V when OutSeq as in Fig 4, Column 4; *p* for C3 < 0.05; 46.9% or 15/32 of conjunctive cells) and, the third subtype, when specific ordinal positions in the sequence included OutSeq items (e.g., peak firing to third position when an OutSeq odor was presented; P's for C4 < 0.05; 37.5% or 12/32 of conjunctive cells). This evidence of odor selectivity in hippocampal neurons is consistent with previous work (e.g., Wood et al., 1999) but, to our knowledge, ordinal selectivity has not been previously demonstrated and will need to be characterized in further detail in future experiments. A few cells (3/32) showed significant selectivity for more than one contrast (excluding C1) indicating that these subtypes were largely non-overlapping. Finally, additional analyses have confirmed that conjunctive sequence cells were observed in similar proportions after controlling for potential differences in internal motor dynamics (43.6% compared to 40.0% in the original analysis) and that they were found in both putative principal neurons (18/32) and interneurons (14/32). Overall, this evidence of generality and specificity in sequence cell coding suggests that the hippocampal network can represent both general information about the temporal context of items and detailed information about specific items in specific sequence positions.

It is important to note that the occasional underrepresentation of a specific trial type is unlikely to significantly bias these analyses because the ANOVAs examined differential activity across all odors/positions (omnibus tests) and because resampling statistics are generally robust in cases of small or unequal n's (the critical *p* value was determined by permuting the actual trials 1000 times). In fact, this sampling issue is more likely to bias the analyses toward underestimating the actual proportion of conjunctive cells. That being said, we did not have sufficient power to perform all posthoc pairwise comparisons (while properly controlling for the family-wise error rate) and thus are not in a position to specifically compare activity between individual odors or positions. Instead, we examined selectivity across odors or sequence positions using a rank-order analysis, an approach that allowed us to maximize power by quantifying selectivity in a single test. First, for each conjunctive cell, we rank-ordered the odors according to the cell's mean response rate (1: odor with highest mean firing rate; 5: odor with lowest mean firing rate); then, we determined whether the mean rank-orders (one per cell) differed across odors. This analysis revealed no significant difference across odors (ABCDE: $F(4,20) = 2.083$, $p = 0.536$; VWXYZ: $F(4,32) = 1.915$, $p = 0.132$), suggesting that odor selectivity was well distributed across odors. In contrast, the corresponding analysis revealed a graded effect across sequence positions (linear contrast: $F(1,11) = 30.264$, $p < 0.001$; main effect of position: $F(3,33) = 10.809$, $p < 0.001$), with higher firing rates for earlier sequence positions (mean rank order: pos2 = 1.5, pos3 = 2.2, pos4 = 3.0, pos5 = 3.5).

Finally, general and conjunctive sequence cells that displayed preferential firing to OutSeq items were further examined by plotting their activity across the two types of

OutSeq probe trials (Repeats and Skips; see methods). Interestingly, we found many that showed selectivity to one of the two probe types (34.5% or 20/58; Fig 5). These probe-specific sequence cells either fired more to Repeats (35.0% or 7/20 of probe-specific sequence cells) or to Skips (65.0% or 13/20 of probe-specific sequence cells), suggesting hippocampal representations also include specific types of sequence memory violations.

Theta and slow gamma/beta oscillatory dynamics exhibited consistent shifts during task performance, but only slow gamma/beta was modulated by the temporal context of items

We next explored the oscillatory dynamics of CA1 during task performance. To do so, we produced mean perievent spectrograms (PESGs; averaging across all completed sequences in a session) for each rat, as well as for the whole group. These spectrograms showed two clear oscillatory bands with high power, one in the theta range (4-12 Hz) and the other in the slow gamma/beta range (20-40 Hz; see Igarashi et al., 2014), which were apparent at the level of individual trials, individual rats and group. We therefore focused our analyses on those frequency bands. As expected, theta power was high during running (dark red band in 4-12 Hz range preceding first item of the sequence; Fig 6A). However, upon initiation of odor sampling, theta decreased (in both power and center frequency) and slow gamma/beta power increased (yellow clouds during odor sampling windows; Fig6A). Similar increases in slow gamma/beta power during odor sampling have been described previously (Igarashi et al., 2014). Lastly, both theta and slow gamma/beta showed a large decrease in power after port withdrawal. It should be noted that while Figure 6A only shows the average PESG (across sequences and rats), the same overall pattern of theta and slow gamma/beta dynamics was observed within

individual rats and individual sequence presentations (data not shown). Overall, these findings suggest a consistent pattern of theta and slow gamma/beta power dynamics during task performance.

Next, we examined whether these oscillations were influenced by the temporal context of odor presentations. To test this possibility, we produced separate PESGs for InSeq and OutSeq item presentations (Fig 6B, Panels 1 & 2) and computed their z-scored difference to produce a difference spectrogram (Fig 6B, Panel 3). This approach showed that InSeq odors were associated with stronger slow gamma/beta power compared to OutSeq odors, but differences in theta power were not evident. Differences in the delta band were also observed (0-4 Hz; similar to MacDonald et al., 2013), but were not explored further here.

In order to quantify task-related effects on theta and slow gamma/beta bands, an analysis of theta and slow gamma/beta waveforms (averaged across trials and animals) was performed (e.g., Csicsvari et al., 1999; Patel et al., 2012). This approach allowed us to use simple statistical tests to compare waveform amplitudes across sampling windows (PreSeq vs. Odors) or temporal context (InSeq vs. OutSeq). Mean theta and slow gamma/beta waveforms were calculated from band-pass filtered LFP recordings sampled from the same time window used in single-cell and ensemble analyses (500 ms preceding port withdrawal; Fig 6C, E). First, we tested differences between PreSeq (before the first odor) and odor sampling periods (combining both InSeq and OutSeq odors). Consistent with the spectrograms, mean theta waveform amplitude was significantly higher during the PreSeq period compared to the odor sampling periods in the Well-Trained session

(DiffPreSeq-Odors = 0.20 ± 0.06; t(4) = 3.484, $p < 0.05$), but there were no significant differences in the Novel1 (DiffPreSeq-Odors= -0.06 ± 0.13; t(3) = -0.516, $p = 0.642$) or Novel2 sessions (DiffPreSeq-Odors= -0.05 ± 0.03; t(3) = 0.231, $p = 0.832$). In contrast, slow gamma/beta showed consistently larger amplitudes during odor sampling periods compared to PreSeq periods including the Well-Trained (DiffPreSeq-Odors = -0.84 ± 0.17; t(4) = -4.984, $p < 0.01$), Novel1 (DiffPreSeq-Odors = -0.85 ± 0.23; t(3) = -3.686, $p < 0.05$) and Novel2 sessions (DiffPreSeq-Odors = -0.56 ± 0.15; t(3) = -3.928, $p < 0.05$; Fig 6E). Overall, these analyses confirm that theta is stronger before odor sampling begins while slow gamma/beta is stronger during odor sampling.

We then examined differences in waveform amplitude based on the temporal context of items (InSeq vs. OutSeq). There were no significant effects on theta waveform amplitudes in the Well-Trained (DiffInSeq-OutSeq = 0.10 ± 0.13; t(4) = 0.736, $p = 0.503$), Novel1 (DiffInSeq-OutSeq = 0.22 ± 0.16; t(3) = 1.40, $p = 0.255$) or Novel2 session (DiffInSeq-OutSeq = 0.18 ± 0.06; t(3) = 3.09, $p = 0.059$; Fig 6C,D). In contrast, effects of temporal context were observed on slow gamma/beta waveform amplitude. In fact, slow gamma/beta waveforms were of larger amplitude for InSeq odors in the Well-Trained session (DiffInSeq-OutSeq = 0.60 ± 0.16; t(4) = 3.802, $p < 0.05$) but this difference was not present in the Novel1 session (DiffInSeq-OutSeq = 0.04 ± 0.07; t(3) = 0.568, $p = 0.610$; Fig 6E,F). Although slow gamma/beta amplitude on InSeq items increased again in the Novel2 session, it did not reach significance (DiffInSeq-OutSeq = 0.29 ± 0.15; t(3) = 1.956, $p = 0.145$). To follow up on this analysis, we showed that this effect of temporal context on slow gamma/beta amplitude paralleled behavioral performance across sessions,

as demonstrated by a significant quadratic fit (FQUAD(2,12) = 4.282, $p < 0.05$). Furthermore, the size of this effect of temporal context on slow gamma/beta amplitude was correlated with SMI scores (r = 0.680, $p < 0.01$; n = 13) and OutSeq accuracy (r = 0.783, $p < 0.001$; n = 13). No significant relationship was observed between theta amplitude and performance across sessions (quadratic fit: FQUAD(2,12) = 0.274, p = 0.766; correlation with SMI: r = 0.021, p = 0.946; Fig 6D). Collectively, these findings suggest that changes in slow gamma/beta oscillations are associated with the processing of the temporal context of items.

Spike-phase relationships did not strongly differentiate the temporal context of items, but the magnitude of slow gamma/beta modulation was associated with sequence memory performance

We next explored the relationship between spike times and the phase of theta and slow gamma/beta oscillations. Six spike-phase plots (3 sampling periods: PreSeq, InSeq, OutSeq; 2 bands: theta and slow gamma/beta; e.g., Fig 7A, B) were constructed for each of the 713 isolated neurons. Spike-phase relationships were determined by modeling sine waves to each plot and testing for the statistical significance of the fit. We report that the proportion of neurons showing significant slow gamma/beta modulation was relatively consistent across the PreSeq and odor sampling periods (~10%) and that the magnitude of slow gamma/beta modulation during odor sampling periods (InSeq and OutSeq) significantly paralleled sequence memory performance across sessions (tested with a quadratic regression on the F ratios of the sine wave fit for all cells across the 3 sessions; PreSeq: FQUAD(2, 712) = 0.333, p = 0.717; InSeq: FQUAD(2, 712) = 8.603, $p < 0.001$;

OutSeq: FQUAD(2, 712) = 6.960, $p < 0.001$; Fig 7C, bottom row). Additionally, slow gamma/beta modulations showed a small but significant difference between InSeq and OutSeq trials (F ratios difference = 0.16, t(712) = 2.182, $p < 0.05$). In contrast, the proportion of neurons with significant theta modulation was considerably higher during the PreSeq period (~30%) than during the odor sampling period (~12%) and the parallels between the magnitude of theta modulation and performance across sessions were not significant (PreSeq: FQUAD(2, 712) = 0.495, $p = 0.610$; InSeq: FQUAD(2, 712) = 2.048, $p = 0.130$; OutSeq: FQUAD(2, 712) = 1.601, $p = 0.202$; Fig 7C, top row). Note that while theta and slow gamma/beta means showed a comparable pattern across sessions, the variability was considerably higher in theta (note large SEM despite n's of 713).

Subsequently, we examined the preferred phase of spiking activity for only those cells with significant theta or slow gamma/beta modulation (including both principal neurons and interneurons). This analysis shows that spiking activity tended to occur at different phases for theta (mean preferred phase of theta-modulated cells: 305.04 deg) and slow gamma/beta (mean preferred phase of slow-gamma-modulated cells: 181.45 deg; Watson-Williams F(1,570) = 143.584, $p < 0.001$). However, the preferred phases did not significantly vary across PreSeq, InSeq or OutSeq sampling periods (Watson-Williams F tests p's > 0.10). We followed up on this negative finding by examining a sub-sample of cells that showed significant spike-phase relationships in all three sampling periods and analyzed the absolute circular distance between the PreSeq and odor sampling periods (InSeq and OutSeq). Only modest preferred phase shifts were observed across cells (theta: +19.5 degree shift from PreSeq to odor period; slow

gamma/beta: -12.0 degree shift) and none reached significance across sampling periods (Watson-Williams F-test P's > 0.10). In addition, we examined the distribution of phase differences across these cells and saw no evidence of a bimodal distribution, arguing against the possibility that a subset of the population showed a strong and consistent phase difference that was being masked by the rest of the population.

Combined with the above evidence that slow gamma/beta amplitude is modulated by InSeq/OutSeq status and performance across sessions, the finding that the magnitude of slow gamma/beta modulation significantly parallels performance strongly suggests that this oscillation is important for sequence memory performance. Our findings also suggest that theta oscillations and the spike-phase relationships we examined (proportions of modulated cells, the magnitude of the modulation, or the preferred phase of their spiking activity) do not play a key role in identifying the temporal context of items.

Discussion

We have demonstrated that the hippocampus represents repeated sequences of events that take place in the same location. Hippocampal cells in our experiment strongly encoded information about whether a presented odor was located in the correct temporal position of the learned sequence. Some cells represented whether any odor was InSeq or OutSeq, while other cells conjunctively represented both a specific odor and whether the odor was correctly in or out of sequence. A subset of cells that fired preferentially for OutSeq trials also conjunctly fired for odors that had been repeated or skipped in the sequence. We also showed this cellular coding of the sequence is connected to good performance on the task.

In order to avoid any confounds of behavior or spatial location the rats in our task were rewarded equally for InSeq and OutSeq trials and were overtrained until they developed highly stereotyped behavior while always receiving odor from the same location. Thus, OutSeq and InSeq trials of the same odor were initially identical except for whether the odor was in the correct sequential position or not. There is a difference in the response at the end of an odor delivery between OutSeq and InSeq trials, but we controlled for this difference in behavior by controlling for time spent in the odor port in some of our analyses and found the same result. We believe that the cellular coding in hippocampus during this task is reflecting the comparison of the current stimulus event to the expected sequence which might contribute to the hippocampus's ability to learn episodic sequences and help to disambiguate those sequences of events from other similar sequences. This is consistent with previous studies that showed the hippocampus is integral to remembering the order of a sequence of events (Fortin et al., 2002; Kesner, Gilbert, & Barua, 2002). Although the cells we recorded that encode selectively for odor are similar to those reported previously (Wood, Dudchenko, & Eichenbaum, 1999), we believe our findings related to the representation of ordinal sequence of nonspatial events in the hippocampus are unique.

Previous studies have found differences in task related oscillations in the hippocampus. We found an increase in power of 20-40hz oscillations during odor sampling. This finding is in agreement with (Rangel, Chiba, & Quinn, 2015) who similarly found a decrease in theta and an increase in oscillations of 15-30hz during task relevant odor sampling in the dentate gyrus. This phenomenon likely signals a change in

the networks processing state. A very similar network state was found in CA1 in another study during odor sampling (Igarashi, Lu, Colgin, Moser, & Moser, 2014). Igarashi found that CA1 20-40hz oscillations gained power during odor sampling and were coherent with lateral entorhinal cortex, a region known to have olfactory inputs. In light of both of these papers we believe our results supports the view that oscillations within the 20-40hz frequency band are mediating the processing of odor information from LEC through the hippocampus. Once in CA1, this information could be compared to the expected sequence of odors resulting in the task relevant sequence coding described in this study.

This study provides more evidence that the hippocampus is particularly important for temporal processing. There is a theory that hippocampus's main function is to map out sequences of events across time. In this view, place cells are initially encoded when a rat encounters a sequence of places encountered over time, and time cells are encoding regular sequences of events across time (MacDonald et al., 2011). There is also evidence for a gradual changing in the hippocampus representation over time. The rate of this change is driven by the amount and type of intervening experiences, but was shown to still be behaviorally relevant for remembering the order of trial unique sequences on shorter timescales (Mankin et al., 2012; Manns et al., 2007). Our results are consistent with a mathematical model that describes how a neural system might keep track of a sequence of events over a long period of time (Howard et al., 2014). Our rats received an identical odor sequence sampling history in each trial, which could produce a sequence of inputs that leave the hippocampus in a similar network state driven by this

history of input. The input of a new odor from LEC (lateral entorhinal cortex) could arrive in hippocampus with this similar network state and the resulting pattern of firing might be the types of conjunctive coding we found in this task depending on how the input interacted with the network during expected odor (InSeq), skipped odor or repeated odor conditions (OutSeq). These firing characteristics would help disambiguate events that are otherwise identical in stimulus and location based on the history of the network.

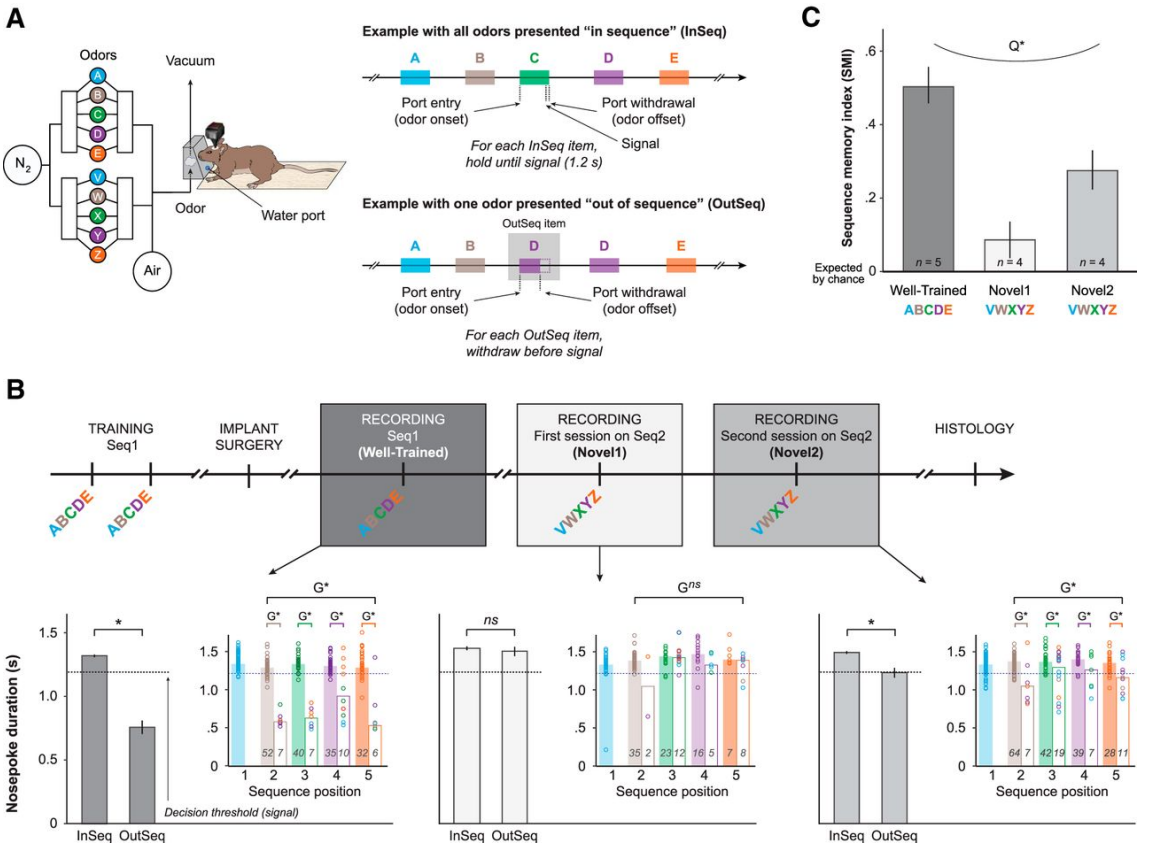

Chapter 2 Figure 1. Sequence memory task design and performance.

Neural activity was recorded as rats performed the cross-species sequence memory task we recently developed, which shows strong behavioral parallels in rats and humans (Allen et al., 2014). Briefly, this hippocampus-dependent task involves repeated presentations of sequences of nonspatial items (odors) and requires subjects to determine whether each item is presented InSeq or OutSeq. Importantly, this nonspatial approach allows us to specifically focus on the temporal demands of the task (by holding spatial location and motor behavior constant) and use different types of probe trials to shed light on underlying sequence representations and cognitive processes. *A*, Apparatus and behavioral design. Using an automated odor delivery system (left), rats were presented with series of five odors delivered in the same odor port. In each session, the same sequence was presented multiple times (right), with approximately half the presentations including all items InSeq (ABCDE) and the other half including one item OutSeq (e.g., ABDDE). Each odor presentation was initiated by a nose-poke and rats were required to correctly identify the odor as either InSeq (by holding their nose-poke response until the signal at 1.2 s) or OutSeq (by withdrawing their nose-poke before the signal; <1.2 s) to receive a water reward.*B*, Experimental timeline (top). Rats were trained preoperatively on Sequence 1 (Seq1; ABCDE) until they reached asymptotic performance. Subsequently, neural activity in region CA1 was recorded while rats continued to be tested on Seq1 for a few sessions, followed by sessions testing a novel sequence (Seq2: VWXYZ). We focused our analyses on three recording sessions per animal: the session with the strongest (Well-Trained; Seq1) and weakest (Novel1; first session on Seq2) levels of sequence memory performance, as well as a session exhibiting intermediate levels of performance (Novel2; second session on Seq2). Example performance from a representative rat on each of the three recording sessions of interest (bottom). Main bar graphs show the mean nose-poke duration on InSeq and OutSeq items, whereas inset plots show the same data sorted by ordinal position in the sequence (x-axis) and by item (color). The color of individual circles represents the correct sequence position for each odor presentation: first sequence position in light blue (A or V), second in brown (B or W), third in green (C or X), fourth in purple (D or Y), and fifth in orange (E or Z). Bars represent the median nose-poke duration for each sequence position (filled bar, InSeq; open bar, OutSeq; n's indicated by values on bars). These data indicate that the rat reliably differentiated between InSeq and OutSeq items in the Well-

Trained session but not in Novel1, with moderate levels of performance in Novel2 (performance levels approximating group means shown in C). Note that only InSeq items (A or V) were presented on the first sequence position.C, Group performance on the three recording sessions of interest (Well-Trained, Novel1, and Novel2). We used a sequence memory index (SMI; Allen et al., 2014; see Materials and Methods) to collapse the behavioral data of each session into a single normalized measure of sequence memory performance. An SMI value of 1 represents perfect performance (correctly holding on all InSeq items and correctly withdrawing on all OutSeq items), while 0 represents chance performance (identical ratio of hold and withdraw responses for InSeq and OutSeq items). Rats exhibited strong, weak, and intermediate levels of sequence memory performance across the three sessions. *, Significant t test; ns, nonsignificant t test; G*, significant G test; Gns, nonsignificant G test; Q*, significant quadratic fit across sessions.

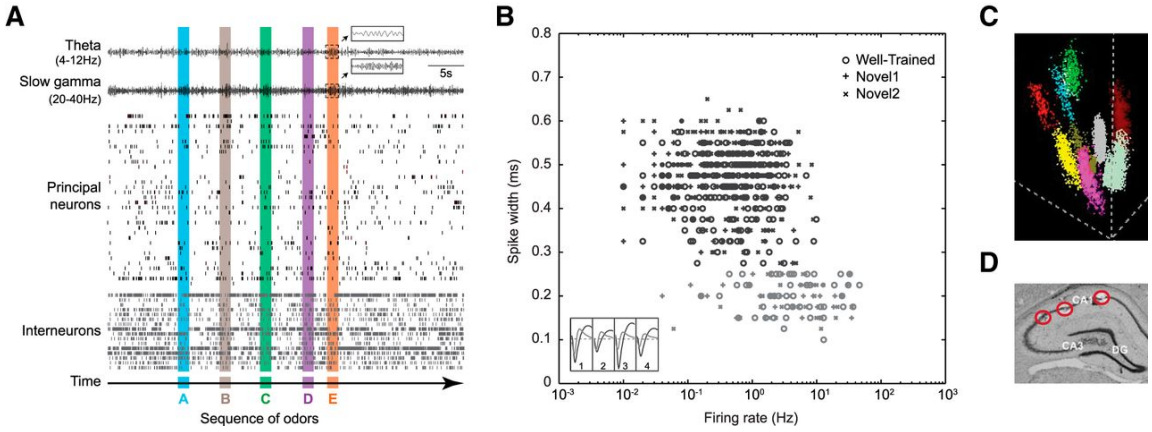

Chapter 2 Figure 2. Electrophysiological recordings.

Spiking activity and local field potentials (LFP) were recorded from the dorsal CA1 region of the hippocampus during task performance. All well-isolated neurons (713 neurons from 13 sessions) were included in the analyses. Raw LFP traces were filtered for 4–12 Hz band (theta) and 20–40 Hz band [beta or low gamma range; labeled slow-gamma here according to Colgin et al. (2009)]. *A*, Example activity from simultaneously recorded neurons (putative principal neurons and interneurons) and LFPs (theta and slow-gamma bands) during one sequence presentation. Inset plots show expanded snapshots of theta and slow-gamma oscillations during an odor presentation. *B*, Scatterplot showing the distribution of putative principal neurons and interneurons across the three sessions of interest (Well-Trained, Novel1, Novel2). The majority (84%) of isolated neurons were classified as putative principal neurons (599 principal neurons, 114 interneurons; see Materials and Methods). Importantly, the principal-to-interneuron ratio and the size of simultaneously recorded neuronal ensembles were consistent across sessions. Inset plot shows representative mean waveforms recorded from the same tetrode (dark gray, pyramidal neurons; light gray, interneurons). *C*, Example 3-D cluster plot of spike amplitude across wires showing nine simultaneously recorded neurons on a single tetrode. *D*, Sample histology slice showing the range of tetrode tip locations (3 tip locations shown; red circles). Tetrodes were targeted at the location denoted by the CA1 label (anteroposterior, −4.0 mm; mediolateral, 3.5 mm). Less than 10% of the tetrodes were located near or in the CA2 region.

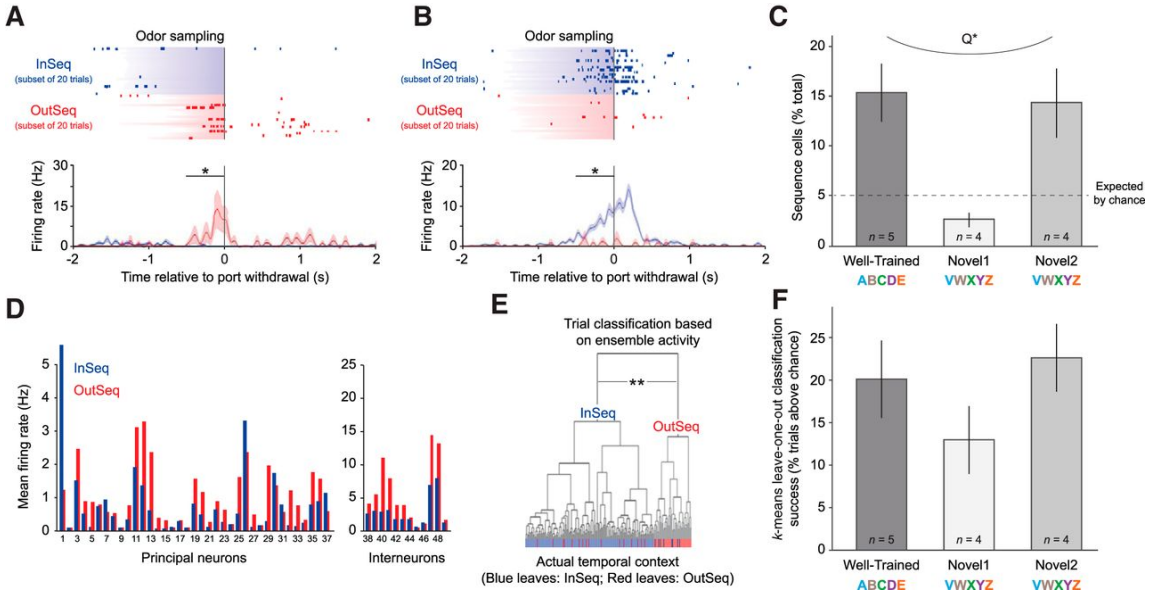

Chapter 2 Figure 3. Nonspatial sequence coding in hippocampal neurons was linked to sequence memory performance.

***A–C*, Single-unit analyses revealed that, while the animals' nose remained in the port, many individual hippocampal neurons fired differentially, depending on the temporal context of the odor presented (whether it was presented InSeq or OutSeq). The majority (73.8%) of these cells ("sequence cells") exhibited significantly higher firing rates on odors presented OutSeq compared with InSeq (*A*, example cell), while the others showed the opposite pattern of activity (26.2%; *B*, example cell). Rasters (top) display spikes (ticks) and odor-sampling periods (shading) on individual trials. Perievent time histograms (bottom) show mean firing rates across all trials (±SEM), binned over 50 ms with minimal smoothing. Note that rasters display equivalent numbers of InSeq and OutSeq trials for clarity but that histograms and statistical analyses (permutation tests; see Materials and Methods) included all trials with odor-sampling periods of ≥500 ms. *C*, The prevalence of sequence cells was positively associated with performance levels. Many sequence cells were observed when animals performed well in the task (3× the proportion expected by chance on Well-Trained and Novel2 sessions), but the proportion of such cells was no greater than expected by chance when animals showed poor memory for the sequence (Novel1). This parallel with performance was confirmed by a significant quadratic fit of the magnitude of sequence-cell coding (*t* ratios of all cells on InSeq vs OutSeq test) across the three sessions. *D–F*, Activity from ensembles of simultaneously recorded neurons strongly differentiated between InSeq and OutSeq items (*D*, example ensemble). *E*, Hierarchical clustering analyses revealed that the top two clusters of ensemble activity vectors in multidimensional space (and only clustering to reach statistical significance) reflected the InSeq/OutSeq status of trials. *F*, *k*-means leave-one-out clustering analyses showed that the proportion of trials accurately decoded as InSeq or OutSeq was also positively associated with performance. More specifically, *k*-means leave-one-out classification accuracy was higher on sessions with strong sequence memory performance (Well-Trained and Novel2) than on sessions with weak sequence memory (Novel1) and was correlated with behavioral performance (data not shown). Error bars indicate ±1 SEM. *, Significant *t* test within 500 ms window indicated by bar (Bonferroni corrected for two 250 ms bins). **, Significant clusters. Q*, Significant quadratic fit across sessions.**

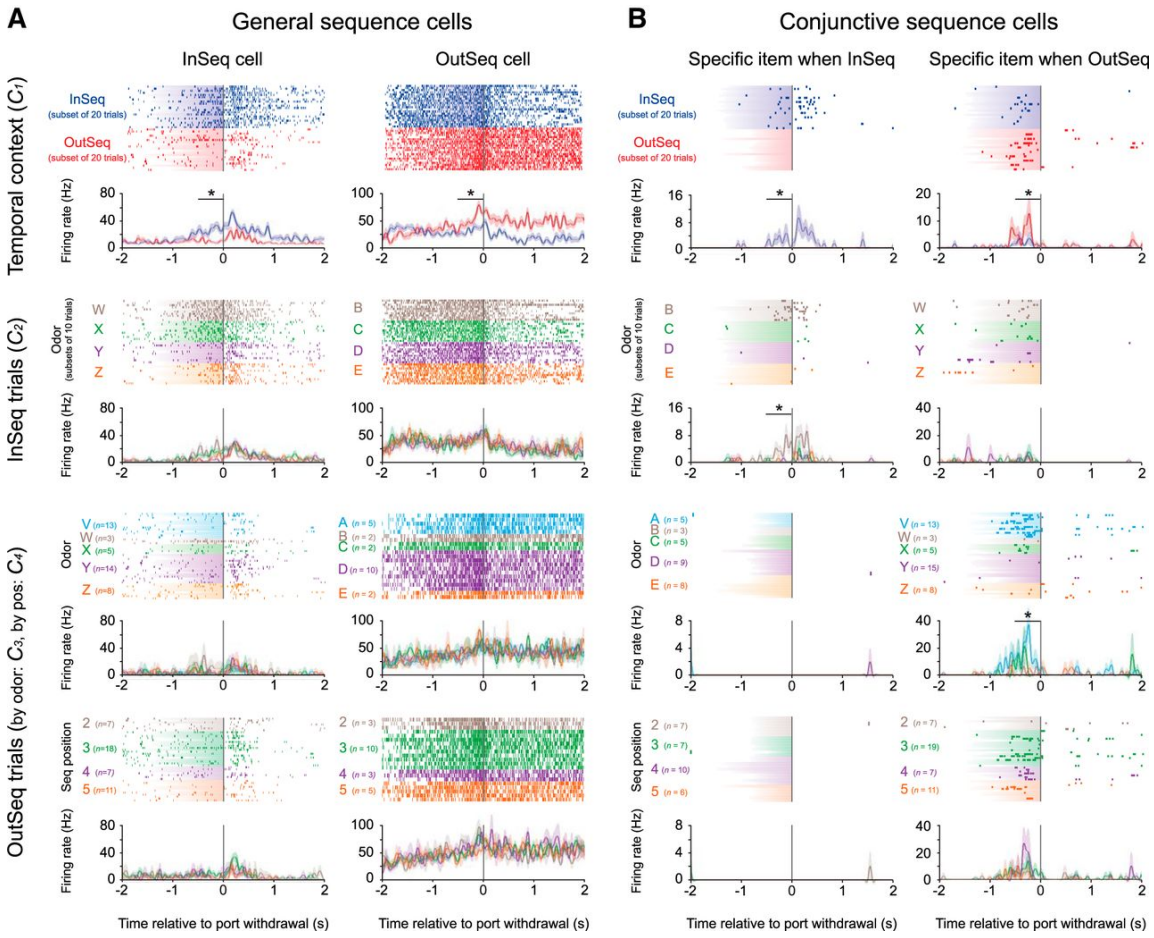

Chapter 2 Figure 4. General and conjunctive sequence coding.

To identify potential subtypes, the activity of each sequence cell was examined across four different contrasts: InSeq versus OutSeq trials (C_1), InSeq trials sorted by odor (C_2), OutSeq trials sorted by Odor (C_3), and OutSeq trials sorted by ordinal position in the sequence (C_4). The activity of four example neurons (one per column) is shown here across the four contrasts (rows) to illustrate some of the observed subtypes. Shaded area in rasters represents odor-sampling durations on individual trials. Perievent time histograms show mean firing rates across all trials (±1 SEM), binned over 50 ms with minimal smoothing. Note that activity to the first odor of each sequence (A or V when presented InSeq) is not shown because it would introduce running-related activity before the nose-poke, making the plots more difficult to interpret. *A*, General sequence cells (60% of sequence cells) fired differentially to the overall InSeq/OutSeq status of items without apparent selectivity for the specific odors presented or the sequence positions in which they occurred (significant *t* test on C_1, but nonsignificant ANOVAs on C_2–C_4). For instance, the left column shows an example of a neuron that significantly increased its firing rate on InSeq trials without clear selectivity across odors presented (compare rows 1, 2; InSeq cell). The right column shows a different neuron, in this case a putative interneuron, which significantly increased its firing rate on OutSeq trials but showed little selectivity for the odor presented or the sequence position in which it occurred (compare rows 1, 3, 4; OutSeq cell). *B*, Conjunctive sequence cells (40% of sequence cells) showed selectivity for specific conjunctions of item and sequence position information. Subtypes of conjunctive cells were identified according to which contrast (in addition to C_1) yielded a statistically significant ANOVA. The first subtype (25% of conjunctive cells) exhibited differential activity when specific odors were presented InSeq (significant ANOVA on C_2, but not on C_3 or C_4). For instance, the left column displays an example neuron for which the increased firing rate to InSeq items (Row 1) was primarily driven by a specificity to Odor B when presented InSeq (Row 2). The same neuron was virtually silent on OutSeq trials (Rows 3 and 4). Conversely, other conjunctive cells primarily coded for specific mismatches between item and sequence position information. In

fact, the second subtype (46.9% of conjunctive cells) exhibited differential activity when specific odors were presented OutSeq (significant ANOVA on C_3, but not on C_2 or C_1). For instance, the right column displays an example for which the higher activity on OutSeq trials (Row 1) was primarily driven by selectivity to Odor V when presented OutSeq (Row 3), with a nonsignificant influence of the sequence position in which it was presented (Row 4). The third subtype (37.5% of conjunctive cells) fired differentially when specific ordinal positions in the sequence included OutSeq items (significant ANOVA on C_4, but not on C_2 or C_3; data not shown). *, Significant *t* test or ANOVA within 500 ms window indicated by bar (Bonferroni corrected for two 250 ms bins).

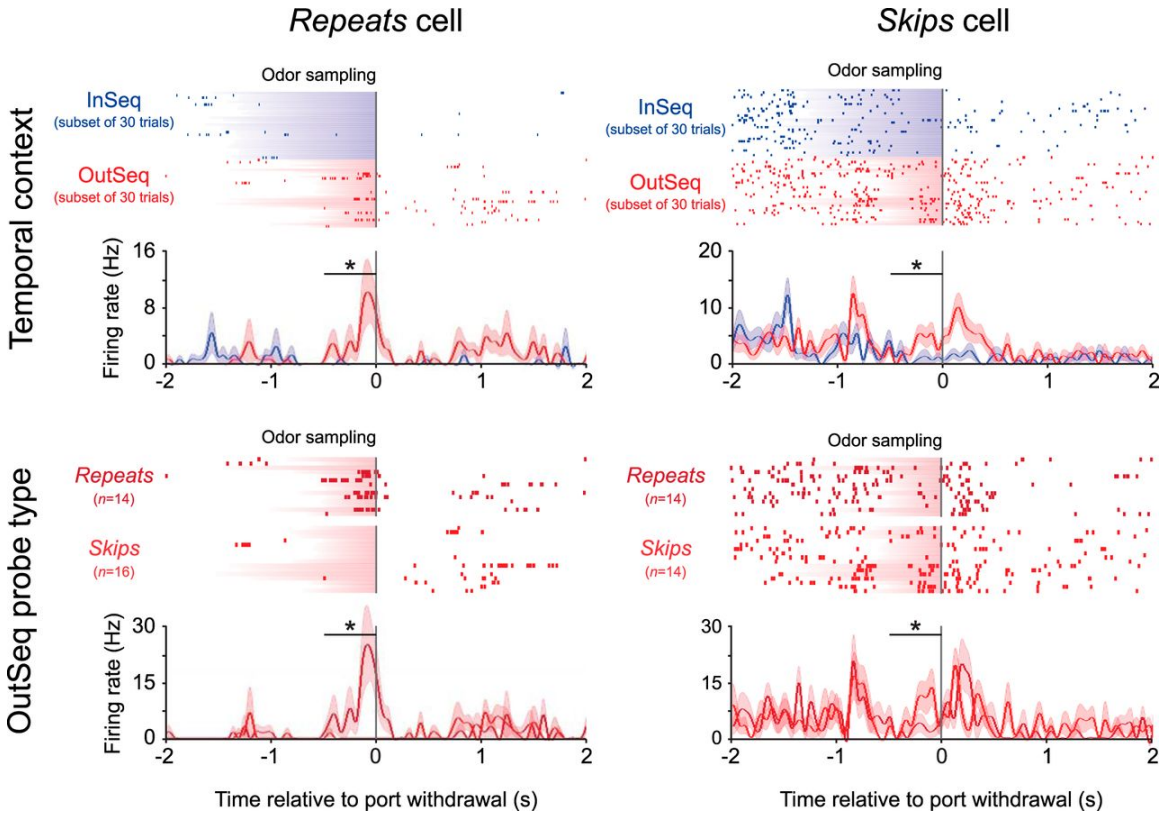

Chapter 2 Figure 5. Probe-type-specific activity.

Statistical analyses revealed that a proportion of sequence cells (34.5%) fired differentially across the two types of OutSeq probe trials (repeats and skips; Allen et al., 2014). Briefly, repeats consist of OutSeq trials in which an earlier item is presented a second time in the sequence (e.g., ABA), whereas skips are OutSeq trials in which an item is presented too early in the sequence (e.g., ABD, which skips over item C). The left column shows an example OutSeq cell selective for repeats (35% of probe-specific sequence cells) and the right column shows an example OutSeq cell exhibiting preferential firing to skips (65% of probe-specific sequence cells). As in Figure 3 and 4, rasters display neural activity for a subset of InSeq trials but perievent histograms (mean firing rate ± SEM) and statistical analyses include all trials. *, Significant *t* test within 500 ms window indicated by bar (Bonferroni corrected for two 250 ms bins).

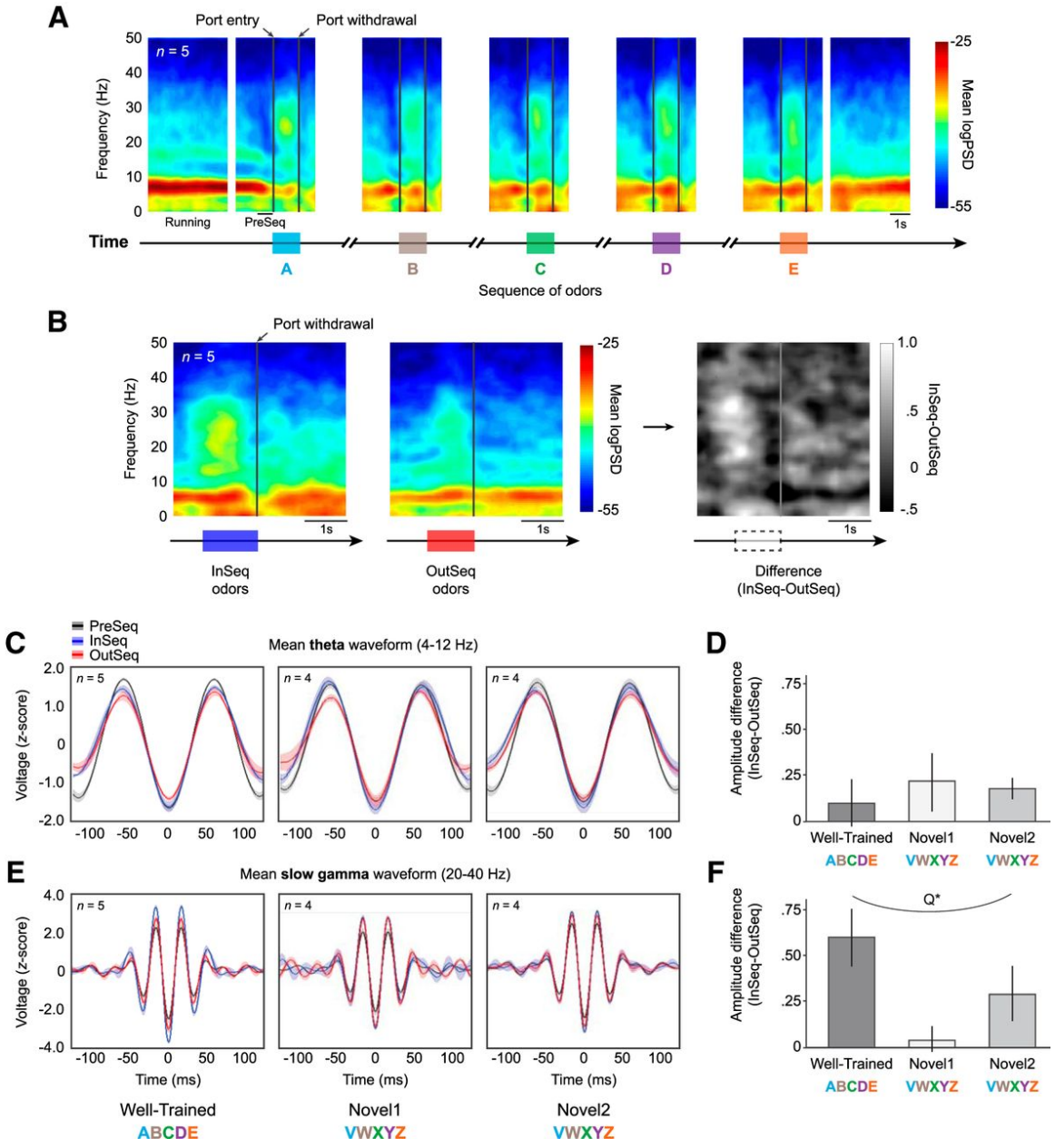

Chapter 2 Figure 6. Slow-gamma, but not theta, oscillations were modulated by the temporal context (InSeq/OutSeq) of items.

***A*, Group PESG for all completed sequences, displayed in successive 4 s blocks aligned across trials and animals. The PESG shows a reliable shift between theta (4–12 Hz) and slow-gamma (20–40 Hz) oscillations during task performance. Although clear theta oscillations were observed during odor sampling, theta power was strongest during the running bouts between sequences. Conversely, slow-gamma oscillations were strongest during odor-sampling periods. The same pattern was also apparent at the level of individual rats or sequence presentations (data not shown). *B*, Group PESGs for InSeq odors (left), OutSeq odors (middle), and InSeq–OutSeq difference (right). Slow-gamma power was higher on InSeq than OutSeq trials, but theta power showed no clear modulation by the temporal context of odors. *C*, *D*, Theta amplitude was similar between InSeq and OutSeq trials across sessions. *C*, Mean theta waveforms (*z*-score normalized amplitude ±SEM) during InSeq and OutSeq trials (500 ms preceding port withdrawal), with PreSeq period shown for comparison (500 ms preceding**

presentation of first odor). *D*, Mean differences in *z*-score normalized theta ampitude (±SEM) between InSeq and OutSeq trials. *E*, *F*, Significant differences in slow-gamma amplitude were observed between InSeq and OutSeq trials across sessions. *E*, Mean slow-gamma waveforms (*z*-score normalized amplitude ± SEM) during InSeq and OutSeq trials, with PreSeq period showed for comparison. *F*, Mean differences in *z*-score normalized slow-gamma ampitude (±SEM) between InSeq and OutSeq trials were associated with performance levels across sessions (significant quadratic fit). *Q, Significant quadratic fit.

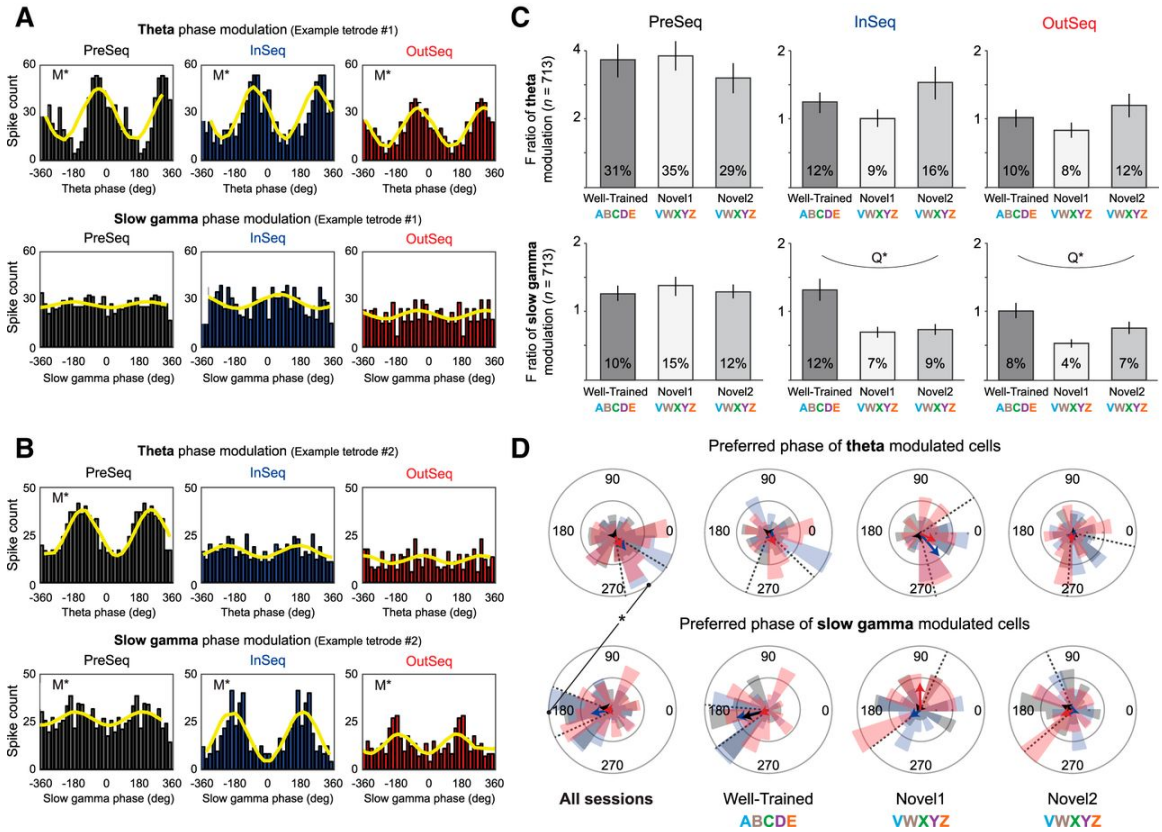

Chapter 2 Figure 7. Spike–phase relationships did not strongly differentiate the temporal context of items, but the magnitude of slow-gamma modulation showed a robust association with sequence memory performance.

A, Spiking activity from example tetrode showing significant theta modulation across PreSeq and odor-sampling periods (InSeq or OutSeq; top) but no significant slow-gamma modulation (bottom). All spike–phase relationships were determined using the local LFP for each cell and tetrode (x-axis: 0° represents the trough of theta or slow gamma, and 180° the peak). Yellow waveforms represent the sine waves fitted to the spike–phase distributions. B, Example from another tetrode showing significant theta modulation during the PreSeq period (but not during odor sampling; top) and significant slow-gamma modulation across time periods (bottom). C, Magnitude of theta (top) or slow-gamma (bottom) modulation across sampling periods and sessions (mean F ratio across all cells ± SEM; n = 713). The magnitude of the phase modulation during odor sampling (InSeq or OutSeq) significantly paralleled performance across sessions for slow gamma (significant quadratic fit). The same pattern did not reach significance for theta, as the variability was considerably higher (note large SEM despite n's of 713). Theta and slow-gamma modulations showed a small but significant difference between InSeq and OutSeq trials (small effect sizes according to Cohen's d). Percentages on bars indicate proportions of significantly modulated cells. D, Preferred phase of spiking activity for cells with significant theta (top) or slow-gamma (bottom) modulation. Circular histograms show the proportion of cells with significant preferred phases across 18° bins (inner circles indicate a proportion of 0.05; outer circles, 0.15). Arrows show the resultant vector length (inner circles indicate r = 0.05; outer circles, r = 0.15) and direction (circular mean). No significant differences were observed across sampling periods (PreSeq, InSeq, or OutSeq) for any of the plots. All sessions combined (left): the mean preferred phase (collapsed across sampling periods) was significantly different between theta and slow gamma (theta: 305.04°; slow gamma: 181.45°; dotted lines indicate 95% confidence

intervals of means). A qualitatively similar pattern was observed in each session (Well-Trained, Novel1, Novel2) but the resulting reduction in sampling increased error variance and the effects did not reach significance. M*, Significant modulation (theta or slow gamma); Q*, significant quadratic fit; *, significant difference in preferred phase.

CHAPTER THREE

Studies on time cells in the hippocampus prior to this work (published in 2016) focused on area CA1. To determine whether time cells are restricted to CA1, we recorded from hippocampal pyramidal neurons in CA3, as well as CA1, in rats running in place on a treadmill while performing a spatial alternation task in a T-maze. CA3 cells exhibited robust temporal modulation similar to the pattern of time cell activity in CA1, and the same populations of CA1 and CA3 cells also had similar spatial coding patterns as rats traversed the maze outside the treadmill. Furthermore, the temporal and spatial coding patterns were largely equivalent when animals performed a simplified version of the task that made no demands on memory. This finding that temporal coding does not require memory load is contrary to previous published results. These findings support the view that the hippocampus performs the same computations on temporal and spatial information when processing experiences across space and time.

This is an earlier manuscript version that was published in a different form in Salz et al., 2016. In chapter four we perform analyses on cells defined in the current form of this chapter, as well as cells defined using a different method in the published version of this paper. We thought including this version of the manuscript would make chapter 4 clearer as well as be informative in its differences and similarities to the published work using different methodologies to define time cells.

Salz, D. M., Tiganj, Z., Khasnabish, S., Kohley, A., Sheehan, D., Howard, M. W., & Eichenbaum, H. (2016). Time Cells in Hippocampal Area CA3. The Journal of Neuroscience, 36(28), 7476‑7484

Introduction

The hippocampus plays a critical role in the temporal organization of memories (Eichenbaum et al., 2014), and a potential mechanism for this temporal organization are hippocampal "time cells", neurons in hippocampal area CA1 that fire at specific moments in temporally structured experiences (Kraus et al., 2013; MacDonald, Carrow, Place, & Eichenbaum, 2013; MacDonald et al., 2011; Modi et al., 2014; Pastalkova et al., 2008; Wang, Romani, Lustig, Leonardo, & Pastalkova, 2015). So far, time cells have been examined only in CA1 and it is currently unknown whether other areas of the hippocampus have time cells or where the temporal properties of CA1 time cells originate. One intriguing possibility is that CA1 receives temporal information directly from the medial entorhinal cortex (MEC) and is specialized for the temporal organization of memories within the hippocampus. Consistent with this possibility is that time cells are also found in MEC (Kraus et al., 2015), MEC lesions disrupt fine timing of CA1 neuronal activity (Schlesiger et al., 2015), and MEC cells that project directly to the CA1 are critical for memory requiring an association across time (Kitamura et al., 2014). Also, other studies have distinguished a selective role for CA1 and not CA3 in making associations across time (e.g., Farovik et al., 2010; Kesner et al., 2005), and in the reorganization of spatial representations over long periods (Mankin et al., 2012). On the other hand, within CA1, temporal coding properties parallel those of spatial coding properties including that time and place cells are found in the same population simultaneously and the same cells can encode both place and time, that both can also encode specific events along with place or time, and both respond to a change in the

relevant spatial or temporal cues by a “remapping” or “retiming”, respectively. Place cells are prevalent in CA3, as they are in CA1, so the parallels between time and place cells suggests that the entire hippocampal circuitry is involved in both temporal and spatial processing (Eichenbaum, 2014).

To address whether temporal processing within the hippocampus is limited to area CA1 or instead is a more general processing function of the hippocampus, we compared temporal coding properties of CA1 and CA3 neurons in rats running in place on a treadmill in between alternating paths in a delayed alternation T-maze task. During treadmill running, the behavior of rats is typically stereotyped and the head is located narrowly above the water delivery port, thus clamping both behavior and location. In previous studies, we have reported that CA1 pyramidal cells fire robustly associated with both elapsed time and distance run on the treadmill, with little influence of variations in the animal’s head location, indicating that temporal and distance coding is not contaminated with place coding in animals running on the treadmill (Kraus et al., 2013). We also compared the spatial firing properties of these neurons as rats traversed arms of the maze outside the treadmill and we compared the temporal firing properties of CA1 and CA3 neurons as animals performed a simpler version of the task that does not require memory.

Methods

Subjects

Neural activity data was collected from 11 male, 400-550 gm Long-Evans rats. All rats were water deprived but provided with food ad libitum. The weight of the rats was monitored regularly as a means of regulating good health. All animal procedures were approved by the Boston University Institutional Animal Care and Use Committee.

Task

The apparatus was a 122 cm × 92 cm rectangular track with a "stem" in the middle of the long dimension onto which the treadmill was inserted. Water ports were located at the end of the treadmill and on each long arm (see Figure 3c). On the first day of training, rats were allowed to freely explore the maze and forage for scattered water rewards. On the next day, rats were allowed to run only in the forward direction on right-turn trials for water rewards (henceforth called "looping"). Then they were shaped on treadmill running by providing rewards on the treadmill while progressively increasing the treadmill speeds for longer periods until the rat completed a 20 sec run at 20 cm/sec. Subsequently, the rats were trained without the treadmill activated to alternate left and right turns at the choice point in order to receive rewards after each successful alternation. Once the rat consistently performed over 90% correct on alternation, treadmill activation was reinstated and the animals were retrained to alternate with treadmill running. In this final phase of training, rats were given a small 0.05 ml water reward for entering the treadmill and a large reward 0.1 ml following a 20 sec run at 20 cm/s on the treadmill on each trial. They then approached a choice point and were required to turn in the direction

opposite to that where they entered the stem to receive another 0.05 ml reward after correct alternations.

Electrode implants and physiological recording

Once rats performed above 90% correct over a week of testing, electrode drives were implanted. Five rats were trained in alternation before implantation, and neuronal activity was recorded during separate sessions of alternation and looping. Three other rats were implanted after training on looping (right-turn) only, and then subsequently neuronal activity was recorded during the looping task. Then these animals were trained on the alternation task and subsequently recordings were taken as they performed this task. Three additional rats were trained and recordings were taken only during the looping task.

Each tetrode comprised four 12 μm nichrome wires (Sandvik Heating Technology), and was gold-plated until an impedance of 200–250 kΩ at 1, 000 Hz was reached (Komorowski, Manns, & Eichenbaum, 2009). The microdrive was implanted 1 mm into the cortex above the hippocampus unilaterally in 7 rats (AP: - 3.3 ML: + 2.8) and bilaterally in 4 rats (AP: - 3.4 ML: $\pm$ 3.0). After at least one week of surgical recovery, tetrodes were gradually lowered into CA1 and later into CA3. Electrical recordings were made using a 96 channel Multichannel Acquisition Processor (MAP) (Plexon Inc.) where spike channels were referenced to another ipsilateral electrode to remove movement-related artifacts. Action potentials were detected by threshold crossing and digitized at 40 kHz . Preliminary identification of CA1 and CA3 recordings was made by a combination of tracking the electrode depth and observation of spike bursting

at the theta rhythm, strong theta power, and the presence of sharp wave ripples during sleep. Position data was captured using light-emitting diodes situated on the rat's head stage that were monitored at 30 Hz by a Cineplex Digital Capture System (Plexon) and synchronized to neural data.

After completion of the experiments, rats were anesthetized with 2.5% isoflurane and small lesions were made at the end of the tetrodes by passing 40 μA of direct current through each wire. Animals were then injected with an overdose of pentobarbital sodium/phenytoin sodium (Euthasol, Virbac Animal Health) and transcardially perfused with 0.05 M phosphate-buffered saline (PBS) followed by 4% paraformaldehyde in 0.05 M PBS. The brain was removed and post-fixed in 4% paraformaldehyde and then cryoprotected using a 30% sucrose solution in 0.05 M KPBS. Slices were then stained with cresyl violet in order to perform histological confirmation of tetrode locations in CA1 and CA3 (Figure 1).

Analysis of temporal and spatial firing patterns

Individual neurons were isolated by manually sorting clusters of waveforms using Offline Sorter (Plexon). Sorting was performed using the relative amplitudes across each wire, the waveform width, and the peak to valley distance. The sorted clusters were screened for inter-spike intervals shorter than the neuronal refractory period, indicating that there could be multiple units. Spiking and tracking data were imported into MATLAB for further analysis with custom scripts.

Temporal tuning curves for each neuron were created by comparing firing rate as a function of elapsed time on the treadmill in 100 ms time (= 2 cm distance) bins. Spatial

tuning curves for each neuron were created for periods where the rat was moving at a speed of 4 cm/s or greater by comparing firing rate as function of linearized spatial position on the maze in 2 cm spatial bins. The spike counts and occupancy times in each bin were independently smoothed for time or space by convolving with a Gaussian smoothing kernel of 400 ms time or 8 cm distance, respectively. Session average tuning curves where compiled in an identical way, but by averaging bins across trials before smoothing.

We also analyzed spatial firing patterns as animals traversed the maze outside the treadmill. For the analysis of spatial firing the maze path was linearized by transforming the tracking signals into polar coordinates, and maze segments were binned using the angle of the tracking and a 2 cm binned polar angle definition of the maze. Spatial activity patterns were assessed for periods when the rat was on the arms of the maze excluding the stem and areas where rats slowed before entering or leaving the stem. The total linearized distance during alternation trials was 400 cm, the same distance rats ran on the treadmill. For looping sessions, we linearized the entire maze traversed, except the treadmill, for a total linearized distance of 330 cm.

Using a methodology our lab previously developed (MacDonald et al. 2013), a cell was considered a “time cell” or “place cell” if all five of the following criteria were met:

1. Generalized linear model. A generalized linear model of firing rate during the delay period was constructed using a Poisson canonical link function. The firing rates in each bin of the delay or maze were modeled distributed as X ~Poisson (lambda;

McCullagh & Nelder, 1989). The model was formulated as shown in Equation 1 and fit to data from each neuron separately. On the right hand side of the expression, the alpha term is a constant. The first summation operates on bin (distance or time) related predictors (d) and their coefficients Beta, with d being a dummy variable to indicate the *i*th bin (for a similar implementation, see also Stapleton et al., 2006).

$$ln\lambda_d = \alpha + \sum_{i=1}^{I} \beta_i d_i \quad (1)$$

The generalized linear model was fit to the data using MATLAB (version R2014b, MathWorks; generalizedlinearmodel.fit). To test whether a neuron was temporally modulated under this framework, we compared the deviance of a model with bin-dependent predictors (Eq. 1) and a constant (a bin-independent predictor) to the deviance of a model that included only a constant. A model with more parameters than an alternative model will always have a smaller deviance (i.e., when the latter is nested in the former and both are compared with the saturated model) but is preferred only if the reduction in deviance is greater than what one would expect based upon expanding the number of parameters in the model. Thus, an analysis of deviance tested whether the reduction in deviance was greater than the .95 quantile of a χ^2 random variable with degrees of freedom equal to the number of additional bin-dependent predictors ($p < 0.05$) (McCullagh & Nelder, 1989).

2. ANOVA. A one-way ANOVA was used to test whether firing rates varied across bins. A neuron was considered temporally or spatially modulated if there was a main effect of bin ($p < 0.05$).

3. Random-shift test. This test assessed whether the trial averaged firing rates were greater than expected if the spike trains were randomly shifted in time or space. The neuron's spike train was shifted on each trial by a random number of bins, and the spike train was wrapped around to the beginning of the array when the shift brought it past the end of the array. A session average of the shifted spike trains for each bin was calculated using this surrogate dataset to create a control tuning curve smoothed in the same way as the real data. This process was repeated 999 more times to generate a null distribution of firing rates for each bin. If the actual trial-averaged firing rate during at least one bin was > 95% of the firing rates in the same bin's null distribution, the cell was considered to be temporally or spatially modulated. This procedure largely preserves the structure of the spike train on each trial but decouples it from the consistent timing or position of the putative firing field.

4. Correlation between subsets of trials. To assess reliability across trials, the Pearson-product moment correlation between binned trial averaged activity from even-numbered and odd-numbered trials was computed. A firing field was considered reliable if this correlation was significantly different from 0 ($p < 0.05$).

5. *Identification of a firing field.* To define a single time or place field, bins for which activity exceeded three standard deviations above the mean firing rate were located. If this field had a drop in firing rate below the mean firing rate of the cell before the start

or end of the array it was considered a firing field. The length of a single firing field was equal to the number of bins of which it was that composed.

When comparing the firing fields of time cells and place cells between different distributions we used a two-sample *t* test along with Hedges' *g* effect size and its 95% confidence interval. This effect size is a variation on Cohen's *D* that corrects for biases due to small sample sizes (Hedges, 1981) and is calculated using the following formula:

$$g = \frac{\overline{x}_1 - \overline{x}_2}{s^\star} \tag{2}$$

$$s^\star = \sqrt{\frac{(n_1-1)s_1^2+(n_2-1)s_2^2}{n_1+n_2-2}} \tag{3}$$

These controlled effect sizes may be conservatively interpreted with Cohen's (1988) convention of small (0.2), medium (0.5), and large (0.8) (Hedges, 1985). Exact analytical confidence intervals for Hedges' *g* were calculated by iteratively calculating how far the centrality of the distribution deviates from the null hypothesis. Hedges' *g* and the confidence interval were calculated using the 'Measures of Effect Size toolbox for matlab v1.4. In case these measures were biased from non-normal distributions, we also tested for differences between these distributions by running a two-sample Kolmogorov-Smirnov test.

Power Analysis was performed with the goal to achieve a power of 0.8, given an alpha value of 0.05 with our smallest sample size of (73,53) to differentiate an effect size of $g = 0.51$.

When comparing two nominal variables for independence we performed Fisher's exact test to calculate the two-tailed *p* value.

Descriptive statistics are listed with $\pm$ SE.

Information Scores were calculated in bits/spike using equation 4.

$$I = \sum_{i=1}^{n} P_i \frac{Z_i}{\overline{Z}} log_2 \frac{Z_i}{\overline{Z}} \tag{4}$$

where P_i is the probability of occupying the *i*th spatial or temporal bin, Z_i is the firing Rate in the *i*th spatial bin and $\overline{Z}$ is the mean firing rate across all bins (Skaggs & McNaughton, 1998).

Results

Analyses were performed on data from 11 rats in 74 recording sessions that yielded a total of 463 CA1 cells and 481 CA3 cells. The recording sites are shown in Figure 1b. Neurons with an average firing rate over the entire session greater than 5 Hz were considered putative interneurons and excluded from further analysis, leaving 386 putative CA1 pyramidal cells and 379 putative CA3 pyramidal cells. In the following analyses, we first consider temporal and spatial modulation of the firing patterns of these cells in the combination of alternation and looping sessions; additional analyses showed there were only minor differences in firing patterns between the session types, as described later.

Time cells

Of all putative pyramidal cells, 199 CA1 cells and 222 CA3 cells that had an average firing rate of at least 0.2 Hz and a peak firing rate of at least 1 Hz during treadmill running were included analyses aimed to determine whether their activity was temporally modulated. As in MacDonald et al. (2013), we identified time cells as neurons with temporally modulated firing patterns confirmed by each of five statistical tests (Table 1). Using this operational definition, 53/222 (23.9%) of CA3 cells qualified as time cells. The proportion of CA3 time cells was somewhat smaller than that of CA1 time cells (73/199 (36.7%); Fisher's exact test $p = 0.006$, two-tailed). Examples of CA3 time cells that fired at different moments are shown in Figures 2a-d.

In both CA1 and CA3 ensembles, time cells span the entire treadmill run. However, there was an overrepresentation of the beginning of the treadmill run, although relatively fewer cells fired at times in the middle of the run (Figure 2e). In CA1, 59 (80.8%) cells exhibit peak firing in the first third of the run, 4 (5.5%) cells peaked in the second third, and 10 (13.7%) cells peaked in the final third of the treadmill run. In CA3, the proportions are similar with 42 (79.2%) cells exhibiting peak firing in the first third of the run, 4 (7.5%) cells peaked during the middle third, and 7 (13.2%) cells peaked during the last third of the treadmill run. The distributions of peak firing times in CA1 and CA3 did not differ (Fisher's exact test $p = 0.90$, two-tailed).

We also compared CA1 and CA3 time cells on additional conventional measures of firing patterns. There was no significant difference in the peak firing rate of time cells between the two populations (CA1 5.7 $\pm$ 0.5 Hz, CA3 5.2 $\pm$ 0.5 Hz, two-sample t-test $t = 0.75$, $p = 0.45$, Hedges $g = 0.14$, with 95% CI [-0.22, 0.50], KS test D (73, 53) = 0.10, $p = 0.89$). There was also no significant difference in the size of time fields between the two populations (CA1 4.5 $\pm$ 0.3 sec, CA3 4.5 $\pm$ 0.3 sec, t-test $t = 0.05$, $p = 0.96$, Hedges $g = 0.01$, with 95% CI [-0.34, 0.35], KS test D (73, 53) = .11, $p = 0.82$). Additionally, there was no significant difference in the mean number of time fields per cell between these populations (CA1 1.0 $\pm$ 0.01 fields, CA3 1.0 $\pm$ 0.03 fields, two sample t-test $t = -1.85$, $p = 0.07$, Hedges $g = -0.34$, with 95% CI [-0.69, 0.03], KS test D (74, 50) = 0.07, $p = 0.99$). Finally, there was no significant difference in temporal information between CA1 and CA3 (CA1 1.8 $\pm$ 0.1 bits/spike, CA3 1.8 $\pm$ 0.1 bits/spike, two-sample t-test $t = -0.12$, $p = 0.91$, Hedges $g = -0.02$, with 95% CI [-0.38, 0.34], KS test D (73, 53) = 0.10, p

= 0.90). The absence of population differences was unlikely due to low statistical power in our analyses, because, using our smallest sample size, we had the statistical power to measure medium to large differences of down to 0.51 standard deviations between CA1 and CA3 time fields.

Place cells

In addition, 242 CA1 cells and 317 CA3 cells that had an average firing rate of at least 0.2 Hz and peak firing rate of at least 1 Hz on the linearized portions of the maze were included in further spatial analysis. The prevalence of place cells in CA3 was similar to that in CA1 place cells, such that 122/317 (38.5%) CA3 cells and 84/242 (34.7%) CA1 cells passed all five criteria for reliable spatial modulation (Table 2) and these proportions were not statistically different (Fisher's exact test $p = 0.37$, two-tailed)

Many neurons that were time cells on the treadmill were also place cells on the maze. We compared the proportions of cells that had a firing rate average of at least 0.2 Hz and a peak firing above 1 Hz on both the treadmill and the maze, resulting in 152 cells (152/386 = 39.4%) in CA1 and 174 cells (174/379 = 45.9%) in CA3 that fired under both conditions. In CA3, 14 (8.0%) cells had both a time field and a place field. By comparison, in CA1, 16 (10.5%) cells had a reliable firing field both during the treadmill run and on the maze. These proportions did not significantly differ (Fisher's exact test $p = 0.57$, two-tailed) and these proportions did not differ from the expectation of random conjoint coincidence of time and place coding by the same neuron in CA1 (Fisher's exact test $p = 0.18$, two-tailed) or CA3 (Fisher's exact test $p = 0.12$, two-tailed). It is notable that, in cells that did not pass all the criteria for time and place, a greater proportion of

cells passed the criterion for time in the distinct fields test (Fisher's exact test $p < 0.1x10^{-10}$, two-tailed) and a greater proportion of cells passed the criterion for place in the GLM (Fisher's exact test $p < 0.1x10^{-10}$, two-tailed) and ANOVA tests (Fisher's exact test $p < 0.1x10^{-10}$, two-tailed).

We also compared multiple conventional measures of spatial firing properties of CA1 and CA3 cells. There was no significant difference between the peak firing rates of place cells in CA1 and CA3 (CA1 6.0 $\pm$ 0.6 Hz, CA3 7.1 $\pm$ 0.6 Hz, two-sample t-test t = -1.33, p = 0.19, Hedges g = -0.18, with 95% CI [-0.45, 0.09], KS test D (84, 122) = .12, p = 0.33). There was also no difference in the mean size of place fields in the two areas (CA1 61.6 $\pm$ 2.5 cm, CA3 60.0 $\pm$ 1.8 cm, two-sample t-test t = 0.58, p = 0.56, Hedges g = 0.08, with 95% CI [-0.19, 0.35], KS test D (84, 122) = 0.07, p = 0.96). CA1 and CA3 did not differ in place fields per cell (both averaged 1.0 $\pm$ 0.1 place fields per cell, two sample t-test t = 0.39, p = 0.70, Hedges g = 0.05, with 95% CI [-0.22, 0.32], KS test D (88, 124) = 0.06, p = 0.99). There was a small significant difference in the spatial information of CA1 and CA3 place cells (CA1 0.7 $\pm$ 0.07 bits/spike, CA3 1.0 $\pm$ 0.07 bits/spike, two-sample t-test t = -2.96, p = 0.003, Hedges g = -0.41, with 95% CI [-0.68, -0.13], KS test D (84, 122) = 0.20, p = 0.03).

Time and place cells are equally prevalent and robust with and without memory load

We also examined whether differences in the properties of CA3 and CA1 time cells might emerge depending on the memory demands of the task. In this assessment we compared properties of time cells in animals performing the alternation task, which required remembering the immediately preceding path during treadmill running, and the

"looping" task, which did not require memory. Even though the looping task makes no memory demands, robust time cell patterns were apparent throughout the delay in both CA1 and CA3 neurons (Figure 3). Time cells were equally prevalent in both areas during looping and alternation sessions (CA1: looping 46/115 (40.0%), alternation 27/84 (32.1%), Fisher's exact test $p = 0.50$, two-tailed, CA3: looping 24/126 (19.0%), alternation 29/96 (30.2%), Fisher's exact test $p = 0.09$, two-tailed). The proportion of CA3 time cells was smaller than that of CA1 time cells in looping sessions (CA1 46/115 (40.0%), CA3 24/126 (19.0%), Fisher's exact test $p = 0.0003$, two-tailed), but the proportion was similar in alternation sessions (CA1 27/84 (32.1%), CA3 29/96 (30.2%), Fisher's exact test $p = 0.76$, two-tailed). Comparing the distributions of peak activity in looping and alternation sessions when dividing the treadmill run into thirds, there were no significant differences in CA1 (looping [38, 3, 5], alternation [21,1,5], Fisher's exact test $p = 0.52$, two-tailed) or in CA3 (looping [16, 3, 5], alternation [26,1,2], Fisher's exact test $p = 0.11$, two-tailed). Additionally there was no significant difference in the distributions of CA1 and CA3 peak activity during looping and alternation sessions (looping: CA1 [38, 3, 5], CA3 [16,3,5], Fisher's exact test $p = 0.32$, two-tailed; alternation: CA1 [21,1,5], CA3 [26,1,2], Fisher's exact test $p = 0.46$, two-tailed).

We also compared time cells in alternation and looping sessions on other conventional measures of firing field properties. There were no significant differences in peak firing rate between CA1 or CA3 cells in alternation and looping sessions (CA1: looping 5.5 $\pm$ 0.5 Hz, alternation 6.3 $\pm$ 1.0 Hz, two-sample t-test $t = -0.76$, $p = 0.45$, Hedges $g = -0.18$ with 95% CI [-0.66, 0.30], KS test D (47, 27) = 0.13, $p = 0.93$; CA3:

looping 5.0 ± 0.5 Hz, alternation 6.3 ± 1.0 Hz, two-sample t-test $t = 0.41$, $p = 0.69$, Hedges $g = 0.11$ with 95% CI [-0.45, 0.67], KS test D (23, 27) = 0.21, $p = 0.57$). The mean time field size in looping sessions was not significantly different from alternation sessions in CA1 or CA3 (CA1: looping 4.6 ± 0.3 sec, alternation 4.5 ± 0.4 sec, two-sample t-test t =0.18, p =0.86, Hedges g =0.04 with 95% CI [-0.43, 0.51], KS test D (47, 28) = 0.13, p =0.92; CA3: looping 4.8 ± 0.5 sec, alternation 4.5 ± 0.5 sec, two-sample t-test t = -0.73, p = 0.47, Hedges g = -0.20 with 95% CI [-0.73, 0.35], KS test D (25, 29) = 0.2, p = 0.45). There were also no differences in the number of time fields between looping and alternating sessions in CA1 or CA3 (CA1: looping 1.0 fields, alternation 1.0 ± 0.04 fields, two-sample t-test t = -1.33, p = 0.19, Hedges g = -0.32 with 95% CI [-0.79, 0.17], KS test D (47, 27) = 0.04, p = 1; CA3: looping 1.1 ± 0.06 fields, alternation 1.0 ± 0.04 fields, two-sample t-test t = -0.16, p = 0.87, Hedges g = -0.05 with 95% CI [-0.61, 0.52], KS test D (23, 27) = 0.01, p = 1). There were also no differences in temporal information between looping and alternation sessions in CA3 cells (looping 1.8 ± 0.2 bits/spike, alternation 1.5 ± 0.1 bits/spike, two-sample t-test t = -0.12, p = 0.90, Hedges g =-0.03 with 95% CI [-0.59, 0.53], KS test D (23, 27) = 0.15, p =0.92), but there was a modest difference in temporal information between session types in CA1 (looping 1.9 ± 0.1 bits/spike, alternation 1.5 ± 0.1 bits/spike, two-sample t-test t = 2.03, p = 0.046, Hedges g = 0.48 with 95% CI [-0.003, 0.96], KS test D (47, 27) =0.38, p =0.008).

With regard to spatial firing characteristics of place cells, there were differences between the prevalence of place cells in looping versus alternation sessions in CA1 (looping 58/127 (45.7%), alternation 26/93 (28.0%), Fisher's exact test two-tailed p =

0.008) but no significant differences between looping versus alternation sessions in CA3 (looping 76/179 (42.5%), alternation 46/138 (33.3%), Fisher's exact test two-tailed p = 0.10). There were no differences in place field peak firing rate between looping and alternation in either CA1 or CA3 (CA1: looping 5.8 $\pm$ 0.7 Hz, alternation 6.4 $\pm$ 1.2 Hz, two-sample t-test t = -0.43, p = 0.67, Hedges g = -0.10 with 95% CI [-0.55, 0.36], KS test D (61, 27) = 0.13, p = 0.89; CA3: looping 7.2 $\pm$ 0.7 Hz, alternation 6.4 $\pm$ 1.2 Hz, two-sample t-test t = -0.33, p = 0.74, Hedges g = -0.07 with 95% CI [-0.46, 0.32], KS test D (94,35) = 0.09, p = 0.97). There was also no difference in spatial information between looping and alternating sessions in CA1 or CA3 (CA1: looping 0.7 $\pm$ 0.08 bits/spike, alternation 0.7 $\pm$ 0.1 bits/spike, two-sample t-test: t = -0.38, p = 0.71, Hedges g =-0.09 with 95% CI [-0.54, 0.37], KS test D (61, 27) = 0.25, p = 0.18; CA3: looping 1.0 $\pm$ 0.08 bits/spike, alternation 0.7 $\pm$ 0.1 bits/spike, two-sample t-test: t = 0.69, p = 0.49, Hedges g = 0.14 with 95% CI [-0.25, 0.53], KS test D (94, 35) = 0.19, p = 0.24). Place fields were significantly smaller on the looping maze than on the alternation maze in CA1 and CA3 (CA1: looping 58.5 $\pm$ 2.4 cm, alternation 68.2 $\pm$ 5.8 cm, two-sample t-test t = -1.81, p = 0.07, Hedges g = -0.40 with 95% CI [-0.85, 0.05], KS test D (61, 29) = 0.32, p = 0.02; CA3: looping 56.6 $\pm$ 1.8 cm, alternation 68.2 $\pm$ 5.8 cm, two-sample t-test t = 2.87, p =0.005, Hedges g =0.55 with 95% CI [0.16, 0.93], KS test D (94, 37) = 0.32, p = 0.005). There was a small but significant difference between the number of place fields between looping and alternation in CA1 and CA3 assessed via t-test, but not KS test (CA1: looping 1.0 fields, alternation 1.1 $\pm$ 0.05 fields, two-sample t-test t = -2.18, p = 0.03, Hedges g = -0.50 with 95% CI [-0.96,-0.03], KS test D (61, 27) = 0.07, p = 1; CA3:

looping 1.0 fields, alternation 1.07 $\pm$ 0.05 fields, two-sample t-test $t = 2.37$, $p = 0.02$, Hedges $g = 0.47$ with 95% CI [0.07, 0.86], KS test D (94, 35) = 0.06, $p = 1$).

Discussion

The present findings provide evidence that CA3 neurons fire at specific, successive moments during a fixed interval, indicating that temporal coding within the hippocampus is not exclusively supported by the temporoammonic pathway from MEC directly to CA1. Rather, the source of temporal information to CA1 could originate in CA3 or MEC, both of which process temporal information and project to CA1, or in as yet unidentified areas.

The firing properties of time cells in CA3 were quite similar to those in CA1. The similarities in temporal firing patterns were not entirely matched by equivalent spatial firing characteristics of the same cell populations, in that spatial information was higher in CA3 than CA1, a finding that is in agreement with previous studies (Barnes, McNaughton, Mizumori, Leonard, & Lin, 1990; Mizuseki, Royer, Diba, & Buzsáki, 2012). The regional differences in spatial information were small, and the distinction between regional differences in place and time coding could be due to the fundamental difference in ever-present external information about location versus external information about time only at the beginning of a temporal interval. By this view, CA3 may take advantage of continuous spatial information to outperform CA1 in spatial pattern completion but not in temporal pattern completion for lack of continuous information.

There was an overrepresentation of time cells in the beginning of the treadmill run and an underrepresentation in the middle of that period. The early overrepresentation has been reported previously for CA1 time cells (Kraus et al., 2013; MacDonald et al., 2011). The sparsity of time cells in the middle of the treadmill run might be related to the long running period of 20 sec used in this experiment as compared to earlier studies, which might have exposed a limit of temporal representation of the hippocampus, with the late firing cells driven by a categorically different anticipation of the end of the treadmill run. Alternatively, time cells might be distributed across time in a logarithmic fashion, such that time fields are wider later in the period (Howard et al., 2014). By this view, more time cells may be detected at the end of the run than in the middle because their much wider fields are being cut off when the delay ends.

The observation of time cells in both CA1 and CA3 when the memory load had been eliminated differs from a previous report where it was observed that time cells appear only when a memory demand is imposed (Pastalkova et al., 2008). Pastalkova's task involved a rat running on a running wheel for a set period of time for reward. A possible explanation for the discrepancy of these results may lie in the nature of the control task of the previous study, which lacked a structured timing of the full set of events within trials that our looping sessions contained.

Mankin et al. (Mankin et al., 2015, 2012) reported that place cell patterns in CA1 as well as CA2, but not CA3, evolve over periods of several hours and days and have suggested that a temporal signal for long periods might be selectively represented in the final stages of intrinsic hippocampal processing. In contrast, the current findings indicate

similar temporal processing in CA1 and CA3, in addition to MEC (Kraus et al., 2015), suggesting that mechanisms for temporal organization of specific experiences and identification of separate temporal contexts may involve distinct coding mechanisms.

Taken together, the present results are consistent with the view that the properties of time cells parallel those of place cells, such that, like spatial processing, temporal processing is prevalent throughout the hippocampus regardless of memory demands. These observations are consistent with the view that the hippocampus performs the same computations on spatial and temporal information to construct an organization of experience, and both dimensions require only consistency of temporal and spatial input (Eichenbaum, 2014).

Task	Region	Total Cells	GLM	ANOVA	Shift Test	Even/odd Correlation	Distinct Fields	All Tests
Alternation	CA1	84	80 (95.2)	36 (42.9)	79 (94.0)	33 (39.3)	73 (86.9)	27 (32.1)
Looping	CA1	115	111 (96.5)	73 (63.5)	104 (90.4)	59 (51.3)	99 (86.1)	46 (40.0)
Combined	CA1	199	191 (95.9)	109 (54.8)	183 (91.9)	92 (46.2)	172 (86.4)	73 (36.7)
Alternation	CA3	91	84 (92.3)	42 (46.2)	87 (95.6)	33 (36.3)	83 (91.2)	29 (31.9)
Looping	CA3	131	119 (90.8)	44 (33.6)	115 (87.8)	37 (28.2)	111 (84.7)	24 (18.3)
Combined	CA3	222	203 (91.4)	86 (38.7)	202 (91.0)	70 (31.5)	194 (87.4)	53 (23.9)

Chapter 3 Table 1. Number (and percentage in parentheses) of cells that passed specific tests for time cell criteria during the treadmill run.

Task	Region	Total Cells	GLM	ANOVA	Shift Test	Even/odd Correlation	Distinct Fields	All Tests
Alternation	CA1	104	102 (98.1)	104 (100)	104 (100)	96 (92.3)	32 (30.8)	26 (25.0)
Looping	CA1	138	138 (100)	134 (97.1)	138 (100)	130 (94.2)	62 (45.0)	58 (42.0)
Combined	CA1	242	240 (99.1)	238 (98.3)	242 (100)	226 (93.3)	94 (38.8)	84 (34.7)
Alternation	CA3	127	125 (98.4)	117 (92.1)	127 (100)	108 (85.0)	83 (65.3)	46 (36.2)
Looping	CA3	190	186 (97.9)	180 (94.7)	190 (100)	180 (94.7)	112 (58.9)	76 (40.0)
Combined	CA3	317	311 (98.1)	297 (93.7)	317 (100)	288 (90.9)	195 (61.5)	122 (38.5)

Chapter 3 Table 2. Number (and percentage in parentheses) of cells that passed specific tests for place cell criteria when traversing the maze.

Figure 1

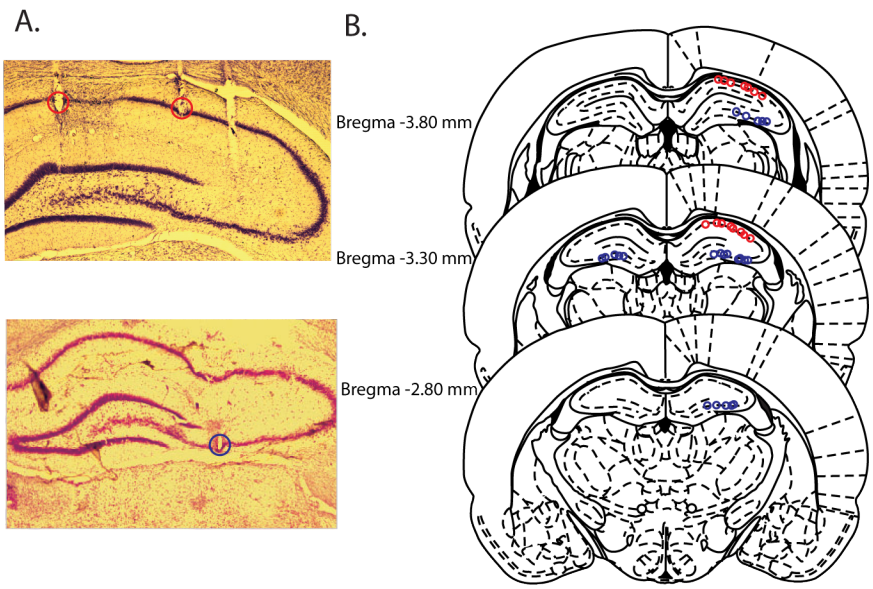

Chapter 3 Figure 1. Tetrode locations in CA3 and CA1.

A. Representative coronal slices of CA1 (red circles) and CA3 (blue circle) recording lesion sites. B. Reconstruction of all recording sites in CA1 (red circles) and CA3 (blue) with sections taken from Paxinos and Watso (2007).

Figure 2

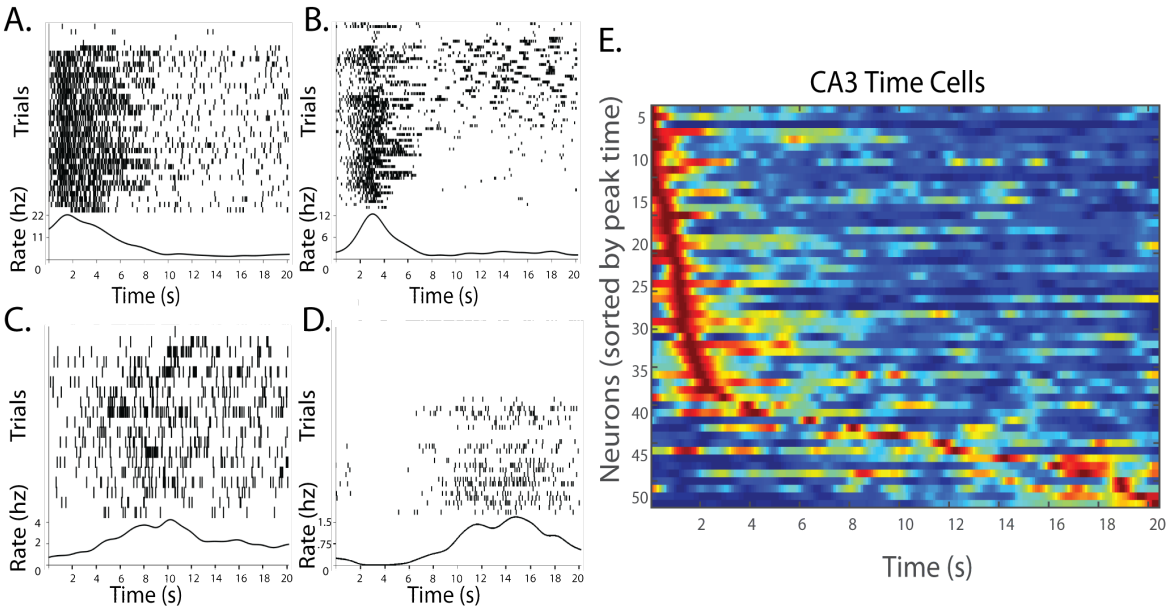

Chapter 3 Figure 2. Time cell firing patterns of CA3 neurons.

A-D. Raster plots showing temporally modulated spiking during individual trials in four CA3 neurons. In each panel, average firing rate (Hz) across the treadmill run. E. The firing patterns of all identified CA3 time cells, including both alternation and looping sessions. Each row represents the normalized firing rate of one neuron over the duration of the treadmill run, and the order of neurons presented is determined by the peak firing times. In each row red correlates to the highest firing rate observed while blue correlates to the lowest firing rate observed.

Figure 3

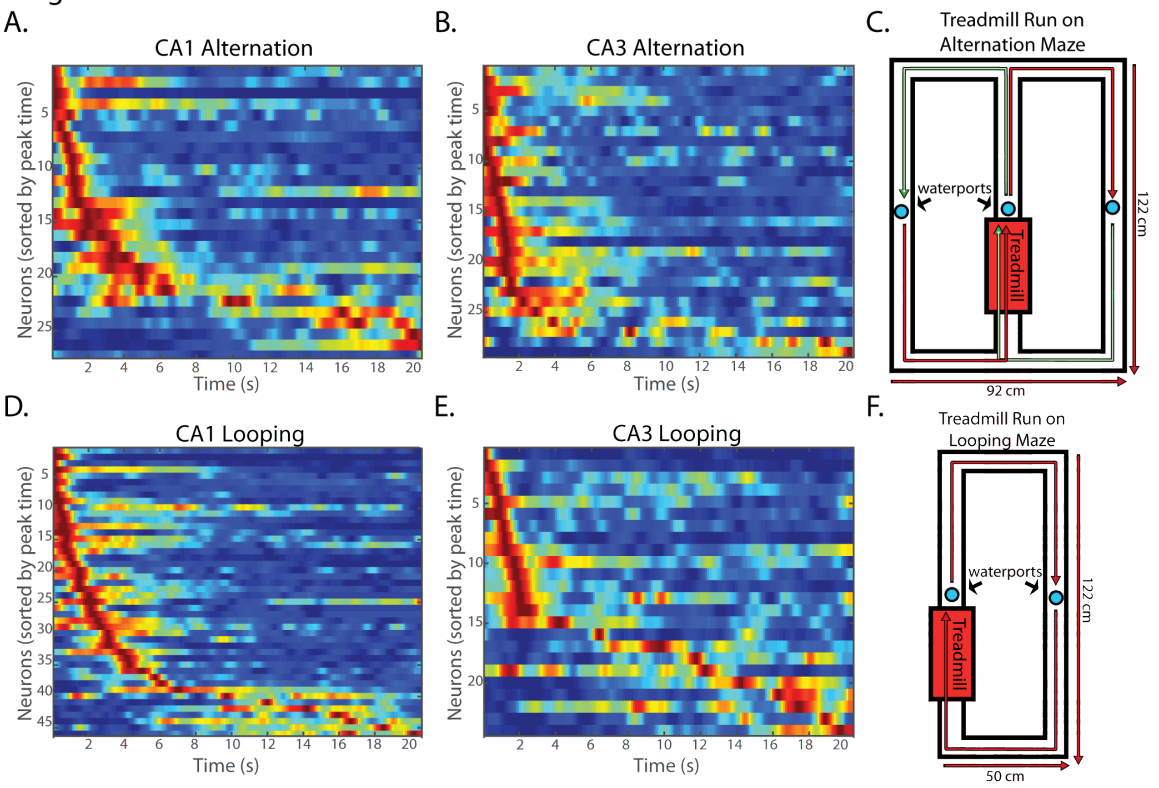

Chapter 3 Figure 3. Time cell firing patterns and maze representations.

Time cell firing patterns in CA1 and CA3 during treadmill running in alternation (A, B) and looping (D, E) sessions. C and F. Representations of the alternation and looping mazes.

Figure 4

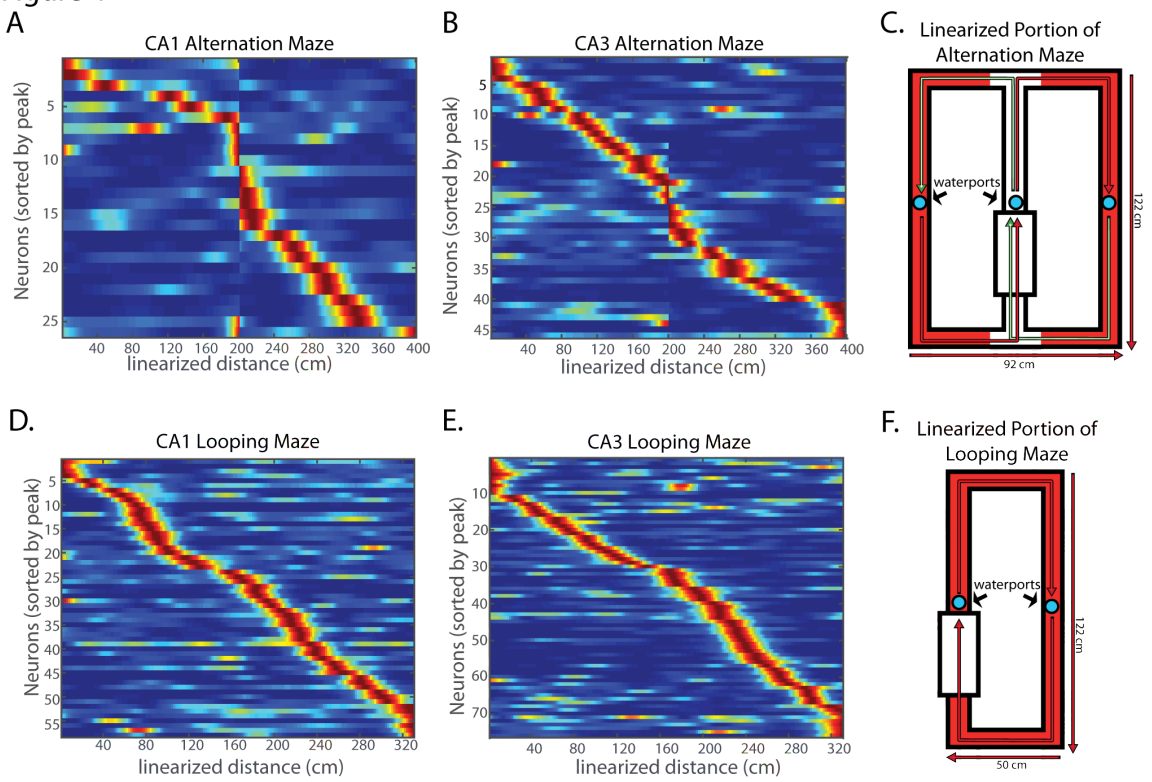

Chapter 3 Figure 4. Place cell firing patterns and maze representations.

Place cell firing patterns in CA1 and CA3 during alternation (A, B) and looping (D, E) sessions. C and F. Diagram of the alternation and looping mazes with red areas indicating parts of the mazes where spatial firing patterns were analyzed.

CHAPTER FOUR

Prior work has shown that time cells increase in field size and decrease in number across a delay. This pattern is consistent with the Weber Fechner law which describes many other neural and behavioral phenomena. In this chapter we performed exploratory analyses on a previously collected dataset to attempt to explicitly test if time cells follow the Weber Fechner law using several quantitative predictions. Because we were concerned that biases introduced from the selection criteria might skew our results, we applied two distinct methodologies for identifying time cells. Cells with time fields that follow the Weber Fechner law should have symmetric fields in log time. We therefore applied a 2x2 design when testing the predictions of the Weber Fechner law, testing time cells using both methodologies defined in both regular and log time. Results from our analyses were inconclusive with different results for the different time cell defining methods. Our current approach was limited in part due to inherent issues within the behavioral paradigm used to collect the data. Further experiments designed to test this theory will need to be devised to draw firmer conclusions.

Introduction

Since time cells were first discovered, several different models have been considered to describe what type of processing time cells are participating. Previously we argued that time cells firing throughout a delay are likely to be involved in the hippocampus's ability to learn associations between events across time. We have also seen evidence that time cells and place cells are drawn from the same population of cells,

and have very similar firing characteristics in time and space in the hippocampus. Because of this, it is parsimonious to imagine that these cells are performing a similar computation whether an animal is moving through an environment or running in place on a treadmill. One of the main functions of the hippocampus is to build associations across time and space. My roommate's cat has learned that one room has a litter box and a room ten feet away is off limits. The cat has also learned that if he is in the off limits room when someone starts walking up the stairs he has 30 seconds to run out of the room and hide or he might get sprayed with water. In both of these cases it is plausible that place and time cells might be involved in these associations across time and space.

One family of models based on the Weber Fechner law could account for the similarity of spatial and temporal processing and many other aspects of hippocampal firing and will be more closely examined here. Originally the Weber Fechner law was developed to describe the perception of just noticeable differences of the sensory system. Weber initially had subjects weigh objects while blindfolded and found that their ability to judge whether two weights were different didn't depend on the difference in the object weights but in the ratio of this difference between the weights to the overall weight of an object. Fechner formalized and derived this relationship, showing that the perception of change of a stimulus increases at a constant ratio with the strength of the stimulus increase (Hoagland, 1930).

Since the Weber Fechner law's inception, it has been demonstrated in many cognitive and perception paradigms. One example is the perception of time, in which a wide variety of timing tasks in human and animal models demonstrate scalar properties

(Lejeune & Wearden, 2006; Wearden & Lejeune, 2008). One type of task that measures a person's ability to distinguish two time intervals depends on how long those time intervals were. Longer intervals need to have two time intervals that are proportionally more different in order for the subject to notice that they are different lengths of time. This was demonstrated when people were less precise in their temporal judgements that occurred at longer intervals (Buhusi & Meck, 2005; Lewis & Miall, 2009; Treisman, 1963). There are a wide variety of timing models using very different mechanisms, but a common feature of all these models is that they account for this consistent timescale invariance in interval timing (Gallistel & Gibbon, 2000; Meck et al., 2008). Scalar invariance is so common in the cognitive literature, that it has been argued that it should be considered a universal principle (Chater & Brown, 2008; Howard & Shankar, 2018).

In addition to being demonstrated in many cognitive and perception paradigms, the Weber Fechner law has also been observed in neural circuitry and processing. One example is in the topographic representation of visual space. When examining the topographic representation of two points on the striatal cortex, the distance that those points represent in the visual receptive field is logarithmically related to the distance between the points. (Hubel & Wiesel, 1974; Van Essen, Newsome, & Maunsell, 1984). Schwartz described evidence for logarithmic conformal mapping in secondary visual cortex, inferior pulvinar, somatosensory cortex and the LGN that all together point towards logarithmic mapping as a 'ubiquitous structure in the brain (Schwartz, 1977). This anatomical logarithmic architecture could easily develop during development and could be the mechanism for size, shift, and rotation invariance in the visual system

enabling pattern recognition of objects at different distances, locations, and orientations (Schwartz, 1980). Additionally logarithmic mapping is more efficient and less sensitive to image manipulation than other models of visual coding. (Messner & Szu, 1985; Schwartz, 1980).

Because of the Weber law's prevalence in neural systems and cognition particularly in cognitive tasks involving time, it is reasonable to explore if similar principles apply to hippocampal circuitry and temporal processing. Time cells could provide a temporal contextual scaffolding for association memories similar to theories of place cells and the cognitive map (Eichenbaum et al., 2014; Smith & Mizumori, 2006; Wood et al., 1999). If time cells are representing time and distance between stimulus events as previously reported (Kraus et al., 2013) the hippocampal system will be faced with a similar computational problem of needing to represent small and large things as other neural systems such as the visual cortex. In order to separately represent stimuli that happen close in time, cells would need to have firing fields with a fine temporal resolution. If the system were to represent all time with equal precision, a fine temporal resolution would be very inefficient requiring a huge number of cells for events that occur much farther apart in time. The number of cells required would increase linearly with time. A more efficient method would be to have the temporal resolution of cells align with the time between events, but since there is so much variability in the time between events it would be safest to approximate representing all possible time intervals between events. Temporal memories organized in a scale invariant way would lose temporal precision across long time scales but would gain impressive amounts of

efficiency compared to using only fields of a similar size (Shankar & Howard, 2012). In fact the optimal representation that accounts for all possible time intervals has cells represent the time or distance from a stimulus in a scale invariant manner following the Weber Fechner law (Figure 1)(Howard & Shankar, 2018). We designed our recent experiment outlined in the previous chapter with an alternating T-maze task with a delay of twenty seconds. This increased our ability to measure the distribution of time cells and their widths across the delay to see if they follow the same scalar invariant principles found throughout the literature.

Historically different methods have been used to define time cells. We were concerned that the different methodologies might contain different biases, and therefore performed our analyses on time cells defined using multiple classifications in a 2x2 design. We used two methods of time cell classification, the first defined in Chapter 3, and the other in a paper published from the same originating dataset (Salz et al., 2016). Additionally we defined cells using both these methodologies in regular and log time because cells with time fields following the Weber Fechner law could have symmetric fields and be more accurately labeled in log time.

In our previous experiment it was reported that the time cells increased their width and decreased their prevalence over the delay (Salz et al., 2016). This finding has also been replicated in many other papers and multiple brain systems (Kraus et al., 2015, 2013; MacDonald et al., 2011; Tiganj, Jung, Kim, & Howard, 2016). In order to quantitatively test whether time cells follow the Weber Fechner law we did an exploratory study reexamining the data from our previous experiment. There are four

different tests that we will use to examine if the data fits with the Weber Fechner law. A distribution of field centers that follow the Weber Fechner law would be distributed according to the power law with an exponent of minus one in regular time. In log time Weber Fechner cells would have a uniform distribution of field centers. Additionally we will examine how the field widths change across the delay. If time cells are following the Weber Fechner law, their fields will linearly increase in size with the delay with a y-intercept of zero, when the stimulus that set off the time cells occurred. Alternatively, if measured in log time the Weber Fechner field widths would stay constant across the delay.

Methods

Analyses were performed on data from 11 rats in 74 recording sessions that yielded a total of 944 cells. Neurons with an average firing rate over the entire session greater than 5 Hz were considered interneurons and excluded from further analysis, leaving 765 putative pyramidal cells. Of all putative pyramidal cells, 433 cells that had an average firing rate of at least 0.2 Hz during treadmill running were considered in analyses aimed to determine whether their activity was temporally modulated.

Five test method of identifying time cells

We used the time cells defined in Chapter 3. Temporal tuning curves for each neuron were created by comparing firing rate as a function of elapsed time on the treadmill in 100 ms time (= 2 cm distance) bins. The spike counts and occupancy times in

each bin were independently smoothed by convolving with a Gaussian smoothing kernel of 400 ms time. Session average tuning curves where compiled in an identical way, but by averaging bins across trials before smoothing.

A cell was considered a "time cell" if all five of the following criteria were met:

1. Generalized linear model. A generalized linear model of firing rate during the delay period was constructed using a Poisson canonical link function. The firing rates in each bin of the delay or maze were modeled distributed as X~Poisson (lambda; McCullagh and Nelder, 1989). The model was formulated as shown in Equation 1 and fit to data from each neuron separately. On the right hand side of the expression, the alpha term is a constant. The first summation operates on bin (time) related predictors (d) and their coefficients Beta, with d being a dummy variable to indicate the *i*th bin (for a similar implementation, see also Stapleton, Lavine, Wolpert, Nicolelis, & Simon, 2006).

$$ln\lambda_d = \alpha + \sum_{i=1}^{I} \beta_i d_i \quad (1)$$

The generalized linear model was fit to the data using MATLAB (version R2014b, MathWorks; generalizedlinearmodel.fit). To test whether a neuron was temporally modulated under this framework, we compared the deviance of a model with bin-dependent predictors (Eq. 1) and a constant (a bin-independent predictor) to the deviance of a model that included only a constant. A model with more parameters than an alternative model will always have a smaller deviance (i.e., when the latter is nested in the former and both are compared with the saturated model) but is preferred only if the

reduction in deviance is greater than what one would expect based upon expanding the number of parameters in the model. Thus, an analysis of deviance tested whether the reduction in deviance was greater than the .95 quantile of a χ^2 random variable with degrees of freedom equal to the number of number of additional bin-dependent predictors ($p < 0.05$) (McCullagh & Nelder, 1989).

2. ANOVA. A one-way ANOVA was used to test whether firing rates varied across bins. A neuron was considered temporally modulated if there was a main effect of bin ($p < 0.05$).

3. Random-shift test. This test assessed whether the trial averaged firing rates were greater than expected if the spike trains were randomly shifted in time. The neuron's spike train was shifted on each trial by a random number of bins, and the spike train was wrapped around to the beginning of the array when the shift brought it past the end of the array. A session average of the shifted spike trains for each bin was calculated using this surrogate dataset to create a control tuning curve smoothed in the same way as the real data. This process was repeated 999 more times to generate a null distribution of firing rates for each bin. If the actual trial-averaged firing rate during at least one bin was > 95% of the firing rates in the same bin's null distribution, the cell was considered to be temporally modulated. This procedure largely preserves the structure of the spike train on each trial but decouples it from the consistent timing of the putative firing field.

4. Correlation between subsets of trials. To assess reliability across trials, the Pearson-product moment correlation between binned trial averaged activity from even-

numbered and odd-numbered trials was computed. A firing field was considered reliable if this correlation was significantly different from 0 ($p < 0.05$).

5. *Identification of a firing field.* To define a single time field, bins for which activity exceeded three standard deviations above the mean firing rate were located. If this field had a drop in firing rate below the mean firing rate of the cell before the start or end of the array it was considered a firing field. The length of a single firing field was equal to the number of bins of which it was that composed.

Nested maximum likelihood estimation models of temporally-modulated firing

Methods for the estimation of temporally modulated firing were described in (Salz et al., 2016). We classified time cells by comparing nested maximum likelihood models of a cell's spike train, with models that included or didn't include time. For each model we performed the maximum likelihood fit across all the treadmill runs. Nested models were compared using a likelihood ratio test to assess the probability that adding parameters significantly ($p < 0.02$ Bonferroni corrected for the number of cells) improved the fit.

We compared the following four models to find the model that best fit the spiking data. First, we calculated the maximum likelihood estimation (MLE) of a spike train assuming constant firing across the whole treadmill run. This model $p_1(t; \Theta_1)$ gives the probability of a spike at any given time point t, but did not include any temporal terms, so the set of parameters Θ_1 only includes a constant term (a_1):

$$\boldsymbol{p_1(t; \Theta_1) = a_1} \quad (2)$$

This model was compared to a nested four-parameter model $p_2(t;\Theta_2)$ (Equation 3), that includes a temporally modulated term T, which modeled a Gaussian time field with two parameters:

$$\boldsymbol{p_2(t;\Theta_2) = a_2 + a_3 T} \quad (3)$$

where T is just a Gaussian field controlled by μ and σ:

$$\boldsymbol{T(t;\ \sigma,\mu) = e^{\frac{-(t-\mu)^2}{2\sigma^2}}} \quad (4)$$

In order to be classified as a time cell, we required that model $\boldsymbol{p_2}$, which included a term for temporal modulation, provided a better fit than the constant model $\boldsymbol{p_1}$. In addition, we evaluated another set of models. The three-parameter $\boldsymbol{p_3}$ included a temporal term but did not include a constant background firing rate:

$$\boldsymbol{p_3(t;\Theta_3) = a_4 T} \quad (5)$$

and a seven-parameter model $p_4(t;\Theta_4)$ (Equation 6) includes a constant term with amplitude a_1 along with two Gaussian time fields, T_1 and T_2 defined using the function $T(t;\ \sigma,\mu)$ defined in equation 4. Each time field is defined with separate parameters for the amplitude of the two time fields (a_6, a_7), the temporal shift of the peak of each of the time fields (μ_1, μ_2) and the standard deviation for each of the time fields (σ_1, σ_2):

$$\boldsymbol{p_4(t;\Theta_4) = a_5 + a_6 T_1 + a_7 T_2} \quad (6)$$

Cells that significantly improved their fit with a model that included temporal parameters were considered time cells if they passed a reliability test. Reliability of a time cell's firing field was tested by separating even and odd trials and performing the analysis separately using the above procedures. Cells that were significantly fit by models with temporal parameters in both even and odd trials had a Pearson's correlation taken

between the curves of their even and odd fits. Cells which had a Pearson's correlation coefficient r > 0.4 were considered to have reliable firing and labeled time cells. We did not find any cells for which p_4 fit better than p_2 so we will not consider multiple time fields further. 61 cells were fit better by p_3 than p_2. For these cells, we used the estimates of μ and σ taken from p_3.

Implementation of MLE for nested model methodology

We allowed μ to vary between -20 s and 40 s and required σ to be less than 40 s. Given that the duration of each treadmill run was 20 seconds and the temporal resolution was 1 ms for each trial there are $20{,}000$ points per trial. If a spike was observed in a particular 1 ms time bin $f(t)$ was set to 1, otherwise it was set to 0. For each time bin, the model gives us probability that a spike occurs. We then computed the log-likelihood (LL), a sum of the log probabilities:

$$\underset{\boldsymbol{\theta}}{\boldsymbol{arg\,max}}\,\boldsymbol{LL} = \sum_{\boldsymbol{trials}} \sum_{\boldsymbol{t}} \left(\boldsymbol{f(t)} \times \left(-\boldsymbol{log}\left(\boldsymbol{p(t;\Theta)} \right) \right) + (\boldsymbol{1} - \boldsymbol{f(t)}) \times \left(-\boldsymbol{log}\left(\boldsymbol{p(t;\Theta)} \right) \right) \right) \qquad (7)$$

To find the best fitting model in a maximum likelihood sense in an automated and efficient way we searched the parameter space using a combination of particle swarming and the Quasi-Newton method. Particle swarming (Poli et al., 2007) was performed first (with the swarm size equal to 50) and its output was used to initialize the Quasi-Newton method which was performed second (the number of maximum function evaluations was set to 10000).

To ensure that a model had an accurate assessment of the center and width of a time field, we only considered cells that clearly peaked during the treadmill run. For the beginning of the treadmill run only cells with a model parameter μ that was greater than σ were included for further analysis. Because fields at the end of the treadmill run are much wider than cells in the beginning of the run, the largest σ that was used to remove a cell at the beginning of the treadmill, σ_{max}, was used as the cut off for μ for all cells at the end of the treadmill run (20 seconds - σ_{max}). For a model with two time fields to be considered, both fields had to have their centers during the treadmill run as above. Additionally, the two fields had to be nonoverlapping such that μ_1 and μ_2 were separated by at least $\sigma_1 + \sigma_2$.

Identifying cells in log time using the same methods

The Weber Fechner law makes specific predictions about the growth of field width and location of time cells. It has been argued that tuning curves of scale invariant cells might be skewed in regular time but symmetrical in log time, a pattern demonstrated in figure 1. To account for this possibility, cells were relabeled using the 5 test and nested models methods outlined above, but in a log time scale (all equations t =>ln(t)).

Results

Time cell selection methods

Which cells were labeled as time cells from the dataset varied based on which selection criteria were used. As we considered the various types of biases and how to

correct for them, we ended up with four different overlapping groups of labeled cells (Figure 2). We performed the same analyses on all four groups in order to see if the scalar property occurs robustly despite the variability of our selection criteria.

Initially, we performed analyses on time cells identified in Chapter 3 that passed all five criteria tests but whose peak firing rate was not in the first 200 ms leaving a total of 102 time cells. This methodology was modeled after previous papers from our lab (MacDonald et al., 2013, 2011). However, if a cell's firing field exists on a logarithmic time scale, the tuning curve will not be symmetric in linear time but in log time, and might not be accurately captured by our five criteria tests. To combat any biases this possible asymmetry might introduce, the earlier analysis using five tests to categorize time cells was repeated but this time using a logarithmic time scale that would better capture logarithmic firing fields. We again removed cells whose peak firing rate was before the first 200 ms of the delay and labeled 94 log time cells that passed all five criteria tests in log time. Of these 94 time cells, 65 were also classified as time cells using the linear time criteria tests

Time cells are equally prevalent using Nested Models methodology

The time cells above were identified based on passing five different criteria tests in log or standard time. The problem with this methodology is that the tests involve many parameters that are set manually by eye and guesswork. Each of these parameters when tweaked up or down can vary whether a particular cell is classified as time cells. Because of this, these criteria tests are likely biasing in unknown ways the group of cells that are being classified as time cells. To attempt to characterize the population of time cells in a

less biased way, we developed a new method of identifying neurons with temporally modulated firing patterns by comparing nested maximum likelihood estimation models (see Methods for details) (Salz et al., 2016; Tiganj et al., 2016). The other benefit of using this method was the ability to accurately estimate in an unbiased way the width of a cell's tuning curve even when there is sporadic out of field firing and other noise. According to the model, cells fire at different times after a specific stimulus event. We therefore removed cells using our unbiased field width measure, that started firing before the salient stimulus of the treadmill turning on. Starting the delay from the water reward was considered, but measurements of field width and distribution would be biased by other sequences of cells firing to another salient stimuli during the delay.

Using our nested model MLE operational definition, 128 of 433 cells qualified as time cells. When compared to the previous five test method of identifying time cells (Chapter 3), only 68 cells were considered time cells using both methodologies. 58 cells were labeled time cells using the previous five test method that were not labeled time cells using the nested model method (Figure 2). This difference is mostly due to the more stringent rules throwing out any cells which have firing fields that start before the treadmill run onset. Many of these cells may have been triggered by the water reward before the treadmill run, the sound of the water valve, or even arrival at the water port. These cells were removed in order to ensure that comparisons of the density of time cell representations across the delay were not biased by any possible stimulus or reward responsive cells. 81 cells were labeled time cells using the nested model method that were not labeled using the five test method (Figure 2). Many of these cells were captured

because of an increased sensitivity to temporal tuning curves despite out of field firing and noise during the delay.

If time cells are scale invariant and have fields on a logarithmic time scale, the tuning curves will not be symmetric in linear time but in log time, and might not be accurately captured by the nested model's Gaussian fields. To combat any biases this possible asymmetry might introduce we used a similar approach to that used for the 5 test labeled time cells. We performed a new nested model categorization of time cells using a logarithmic time scale and identified 114 cells that qualified as time cells. Of these 92 cells were identified using the nested model categorization with both log and standard time (figure 2).

Distribution of time cells across time

Distribution of time cells identified using 5 criteria tests in linear time

If time cells are efficiently organized to perform temporal associations in a manner that is scale invariant, we would expect a distribution of field centers that follow a power law distribution. We therefore looked to see how time fields were distributed across the delay in our task. As discussed in the previous chapter, there is an overrepresentation early in the delay and an underrepresentation in the middle of the delay. The temporal firing fields of cells plotted in linear time are strongly skewed to earlier in the delay (Figure 3A). This can be seen clearly in Figure 4A where the cumulative density function of the field peak times starts above the uniform distribution and then falls below the uniform distribution in the middle of the delay. We used a curve fitting procedure to estimate the best fit of the distribution of time field firing peaks. The

power law maximum log likelihood fit (LL) was better than the exponential maximum log likelihood fit (Figure 4A, power law: $x^{-0.83}$ LL = -962.2 exponential: $e^{-.0002x}$ $LL = -973.3$), and using the log likelihood ratio test, both the power law and exponential fits were significantly better than the uniform fits (LL = -1008.9, $p \approx 0$). This suggests that time cells might be distributed according to the power law, which would be scale invariant. However, if the time cells distribution followed the Weber Fechner law the exponent on the power law would be 1. We compared the best fitting exponent of 0.83 to the fit with an exponent of 1 using the log likelihood ratio and found a significant difference ($p < .01$). This can be interpreted that the distribution of time fields is close to scale invariant but does not precisely follow the Weber Fechner law.

Distribution of time cells identified using five criteria tests in log time

The distribution of time cells labeled using the five criteria tests in log time would be scale invariant if they follow a uniform distribution in log time. Using a Kolmogorov–Smirnov (KS) test we compared the distribution of log defined time cells to the uniform distribution in log time and found a significant difference (KS test: $D(94)=0.15$, $p = 0.01$). Nonuniform distribution of time fields on a log time scale suggests that despite the log time cells being overrepresented earlier in the delay, they are not distributed as expected from a Weber Fechner distribution.

Distribution of time cells identified using nested models method in linear time

Despite the removal of so many early firing cells, nested model identified time cell coding still shows an overabundance of time cells early in the treadmill run. The non-uniformity of the distribution of time cells centers is evident when compared to the

uniform distribution (dashed line in Figure 3C). This difference in the distribution of time cells from uniform was significant (KS test D (128) = 0.17, p = 0.001). Another visualization of this relationship can readily be seen in the cumulative distributions of time field centers (Figure 4C), when the cumulative distribution rises faster than the uniform distribution (diagonal line) early in the delay interval. This overrepresentation early in the delay occurs despite the large number of cells we didn't consider that had firing peaks during the delay, but whose firing field identified using the width from the nested model MLE started before the treadmill run began.

In order to approximate the distribution of time cells across the delay defined using the nested model approach, we performed the curve fitting procedure that was used earlier on cells identified with the five test method. The ML power law fit and ML exponential fit both were significantly better fits for the data than the uniform distribution according to the log likelihood ratio test (Figure 4D, power law: $x^{-0.3}, LL = -1209.9, p = 0.002$; exponential: $e^{-4e^{-5}}, LL = -1211.5,\ p = 0.01$; uniform: $LL = -1214.6$). Similar to the finding using this analysis on the 5 test time cells, the power law curve fit the data better than the exponential curve suggesting that these time cells may be scale invariant. If the time cells distribution followed the Weber Fechner law the exponent on the power law would be 1. We compared a fit with exponent of 1 to the best fitting power law exponent of 0.3 using the log likelihood test and found a significant difference ($p < .001$) implying that although scale invariant this distribution of time fields are not following the Weber Fechner law.

Distribution of time cells identified using nested models method in log time

The time cells defined using the nested models approach in log time could better capture time cells whose fields had tuning curves symmetric in log time. Whether the distribution of the centers of log time nested model cells follows the uniform distribution was examined by viewing them on a log scale (Figure 3D), and in the cumulative density function (Figure 4D). In both cases the distribution does not closely follow the uniform distribution. We explicitly tested if the distribution differs from the Weber Fechner law with a nonuniform distribution by performing a KS test. The distribution of time cells was significantly different from uniform (KS test: $D(114) = 0.25$, $p < .001$). This implies that this log nested model defined distribution of time cells does not follow the Weber Fechner law in their spacing.

How time cell field widths vary across time

Five test method defined cells do not follow Weber Fechner law as their width increases across time

If time cells are scale invariant and follow the Weber Fechner law, time cell field widths will linearly increase as the delay increases. This relationship can be visualized with a scatter plot of time field widths over the period of the treadmill run. For the time cells defined using the five test method in regular time we see that most cells with small firing fields fire early in the delay (Figure 5A). A linear regression confirmed a linear relationship between field width and when the time cell fired on the treadmill ($F(1,154) = 114$, $p < .001$; $R^2 = 0.43$). For every second of the treadmill run, field widths grew .3 seconds with a significant intercept of 2.8 seconds field width at the start of the treadmill run. If time cells are initiated by the stimulus of the treadmill starting and follow the

Weber Fechner law, the intercept of this linear relationship would be at zero when the treadmill starts. This might result from time cells that were initiated by a stimulus before the treadmill started. We next performed a regression of a quadratic fit of the data and found that it fit the data better than a linear fit $F(1,154) = 84.7$, $p< 0.001$; $R^2=0.52$). This implies that the distribution isn't linear and Weber Fechner does not accurately describe the growth of field widths across the treadmill run.

Five test method in log time defined cells do not follow Weber Fechner law as their width increases across time

The time cells defined in log time might better capture the possibility of logarithmic growth of time field widths across time. If these cells are scale invariant we would expect their field width in log time to be a constant across the treadmill run. This relationship can be visualized with a scatter plot of time field widths over the period of the treadmill run in log time. For the time cells defined using the five test method in log time we see that cells have a fairly consistent field width in log time across the treadmill run. (Figure 5B). A linear regression to test this found a barely significant linear relationship between the field size and time on the treadmill ($F(1,109) = 7.0$, $p < .01$; $R^2= 0.06$). For every second of the treadmill run the width of time fields decreased .07 seconds with an intercept of .97. This is further evidence that field width is growing as time on the treadmill increases, but this significant result implies that our sample of cells are close to but not exactly scale invariant.

Nested model defined cells follow Weber Fechner law as their width increases across time

With our original defined time cells using the five test method our heuristic for defining field width was susceptible to noise and bias based on which parameters we used to define the field cutoffs. Using MLE defined time cells we have more confidence in the unbiased field width estimate inherent to the technique. When viewing the relation of the width of time fields across the treadmill run the width of cells still clearly increases across time (Figure 5C). A linear regression of field widths along with times of the field centers confirmed a strong linear relationship ($F(1,124) = 108$, $p < .001$; $r^2 = 0.47$) such that width of a time field increased 0.45 ± 0.04 seconds for every second of treadmill running. The intercept of the regression was not significant. A significant slope and nonsignificant intercept aligns with expectations from the Weber Fechner law.

Nested model in log time defined cells do not clearly follow Weber Fechner law as their width increases across time

A scatter plot of time fields of our log defined time cells in log time shows a much weaker relationship between width and field time. If these log time cells were scale invariant, the field widths should not change across time in log scale. We repeated the linear regression analysis of field widths and times of field centers on the log defined time cells in log time (figure 5D) $F(1,114) = 15.6$, $p < 0.001$; $r^2 = 0.10$) such that the width of a time field increased 0.34 ± 0.09 log seconds for every log second running on the treadmill with a significant intercept of 1.5 log seconds, $p < 6e^{-25}$. A quadratic curve also fit the data better than the constant and linear models ($F(1,114) = 35.6$, $p < .001$; $r2 = 0.33$). These results show nested model log time cell field widths increased in log time

across the treadmill run, suggesting that these cells may not be organized in a scale invariant manner.

Discussion

It is notable that despite working on the same data set our cell-selection methodologies labeled different cell populations and produced different results. When performing analyses, it is important to recognize the bias cell selection methodologies might have on the results. The seemingly innocuous decisions made in choosing tests and parameters to use when classifying time or place cells can have potential downstream biases. In this chapter, several reasonable methodologies based on previous work were presented. The five test method involved setting a large number of parameters within a range of realistic bounds. Changing the parameters within those reasonable bounds had an impact on what cells were ultimately selected as time cells and the final parameters were selected in part based on a subjective validation. Some of these parameters might also bias the cell selection in a way that would affect our measures. The new nested model method defined here avoids many of these pitfalls by significantly reducing the number of parameters necessary for defining time cells and allowing a more neutral unbiased criterion for labeling these cells. The reliability measure is the only remaining step in the algorithm that still required manual parameter setting. An important future direction when using this nested model method to define place and time cells will be to improve upon this part of the methodology.

Using the nested model defined time cells, we replicated the findings of the previous chapter using the five test method defined time cells. In all cases the distribution of time cells and their firing field widths resulted in a temporal representation that decreased in resolution with the passage of time on the treadmill. Time cell sequences initially represent time with high resolution from many cells with short temporal tuning curves and decrease their resolution across time with less cells firing with increased field widths. The size of a time cell's field width increased and the prevalence of time fields decreased across the treadmill run in cells defined in standard and log time. If the Weber Fechner law applies to time cells their field widths will increase in size in a scale invariant way. To test this, we checked if the distribution of fields increased linearly in standard time and was flat in log time. Of all four sets of cells, only the cells defined using the nested model method in standard time had time field widths that were scale invariant along the time of the treadmill run.

Despite the Weber Fechner law having precise predictions to compare our results to, it will not be possible to draw definitive conclusions with data collected using the current behavioral paradigm. Many of the cells had firing fields early on in the treadmill run but actually started firing before the treadmill started. Some of these cells started firing during the water reward before the start of the treadmill run. Other cells initiated firing when the rat arrived at the treadmill shortly before the water reward. The reward before the treadmill run was necessary to get rats onto the treadmill and ready to run. Even with the reward the rats would often pause before getting onto the treadmill. If time cells were to follow the Weber Fechner law each salient stimulus could produce a

sequence of time cells. There is evidence for firing fields starting after these three potential stimuli; getting onto the treadmill, receiving water reward, and initiating the treadmill run. Any of our time cells could have been triggered by any one of these stimuli making estimation of the distribution of cells after a stimulus event difficult. An additional complication results from the varying amount of time between when the rats first get onto the treadmill and when the rats trigger the water reward, which ranged from a tenth to several seconds. This variation in stimulus intervals makes it impossible to establish an exact estimate of the distribution of time cells in a model which assumes Weber Fechner distribution responses to stimuli in our particular experiment.

Any model of hippocampal networks will need to account for the decrease in temporal resolution of time cells in both the distribution and width of time fields discussed in these results. Many of the findings reported here are loosely consistent with Weber Fechner, but better data will be needed to test this claim. If time cells precisely align with the predictions of Weber Fechner, it will be strong evidence that that model is describing fundamental aspects of hippocampal processing. Data from a different task would be necessary to draw firmer conclusions.

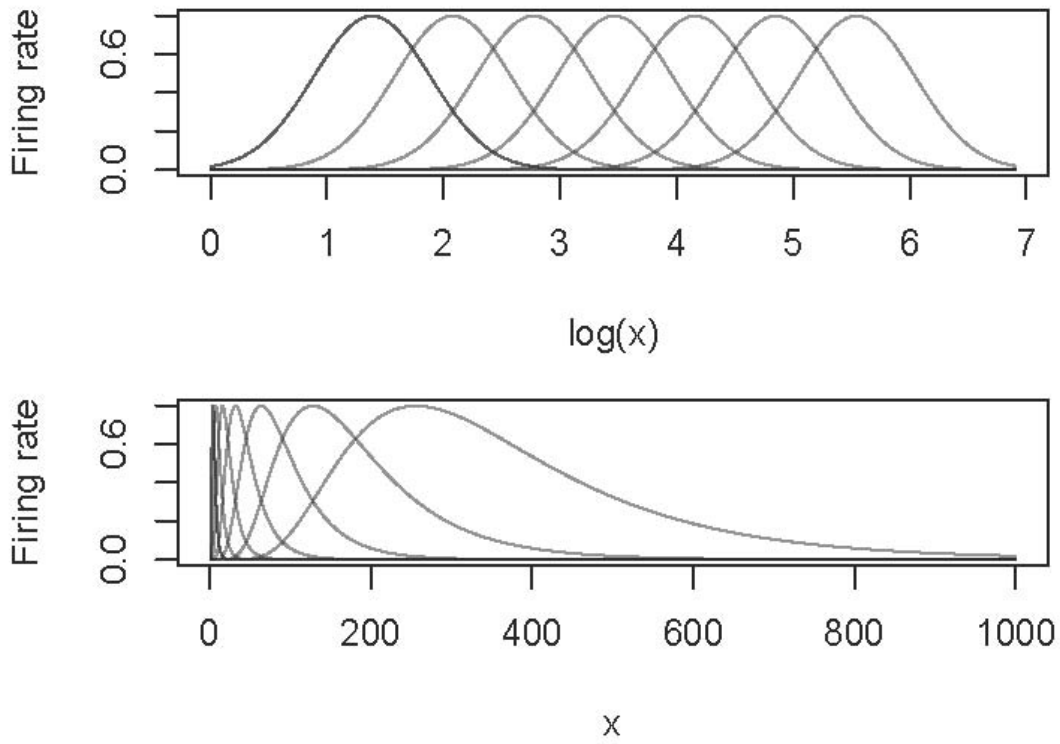

Chapter 4 Figure 1. Representation of Weber Fechner scale invariant tuning curves.

The top graph shows equally spaced symetric tuning curves on a log scale. The bottom graph shows these same tuning curves in regular time demonstrating increased tuning curve width and spacing between tuning curves.

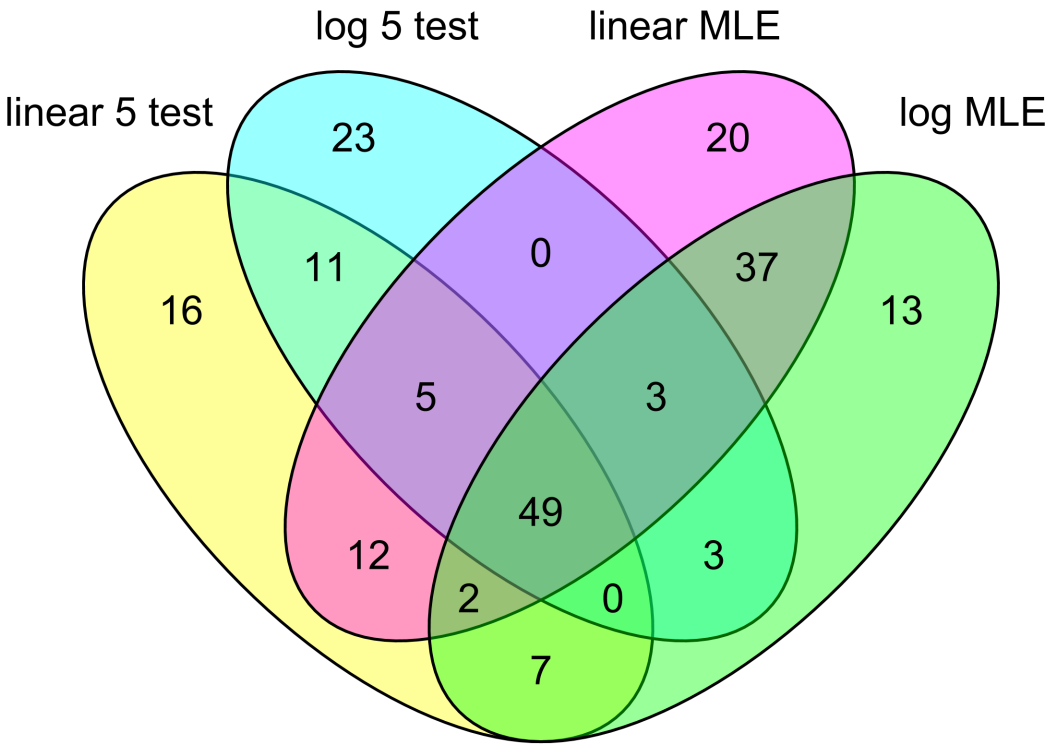

Chapter 4 Figure 2. Venn diagram containing the cells identified using the four different methodologies.

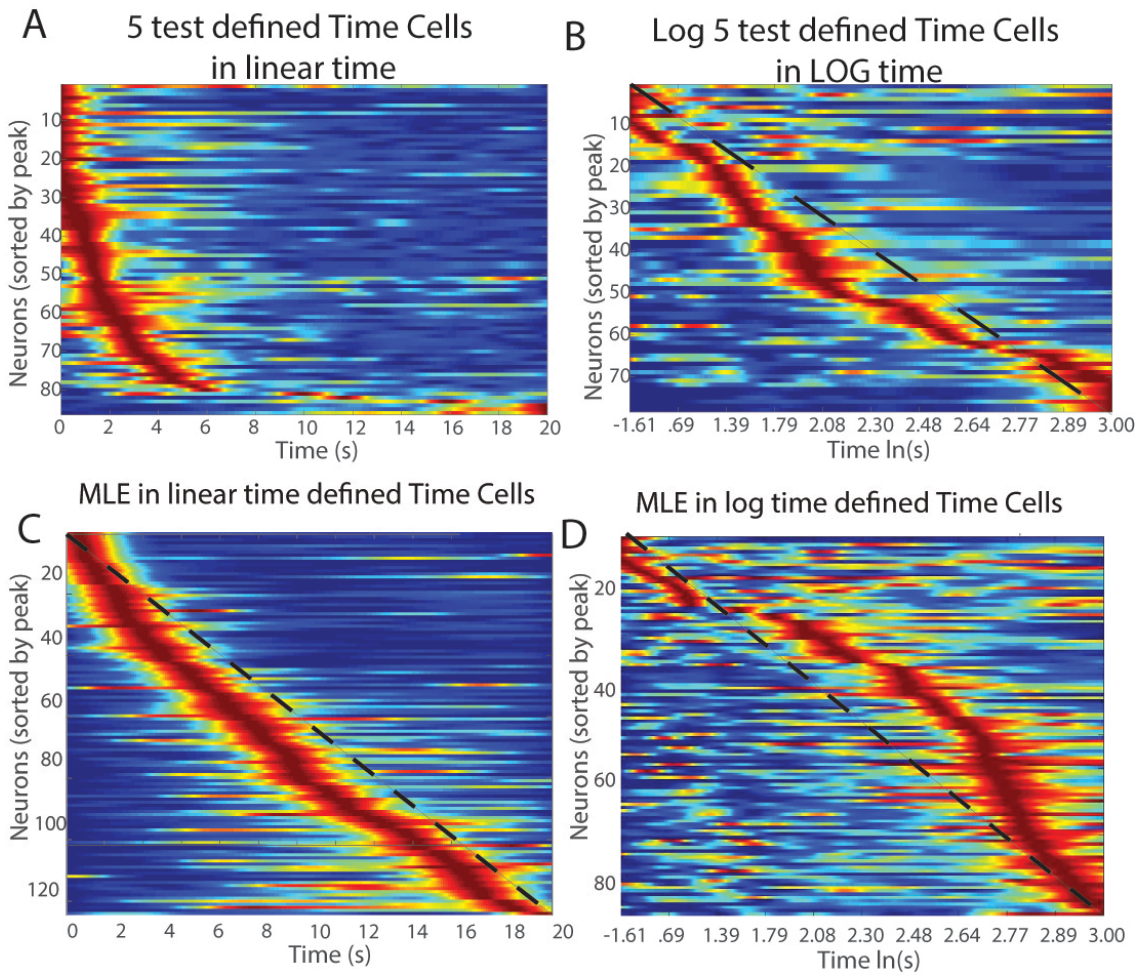

Chapter 4 Figure 3. The firing patterns of five test defined time cells.

Each row represents the normalized firing rate of one neuron over the duration of the treadmill run, and the order of neurons presented is determined by the peak firing times. Standard time defined time cells displayed with A) standard time axis B) log time axis, and Log time defined time cells displayed with C) standard time axis D) log time axis.

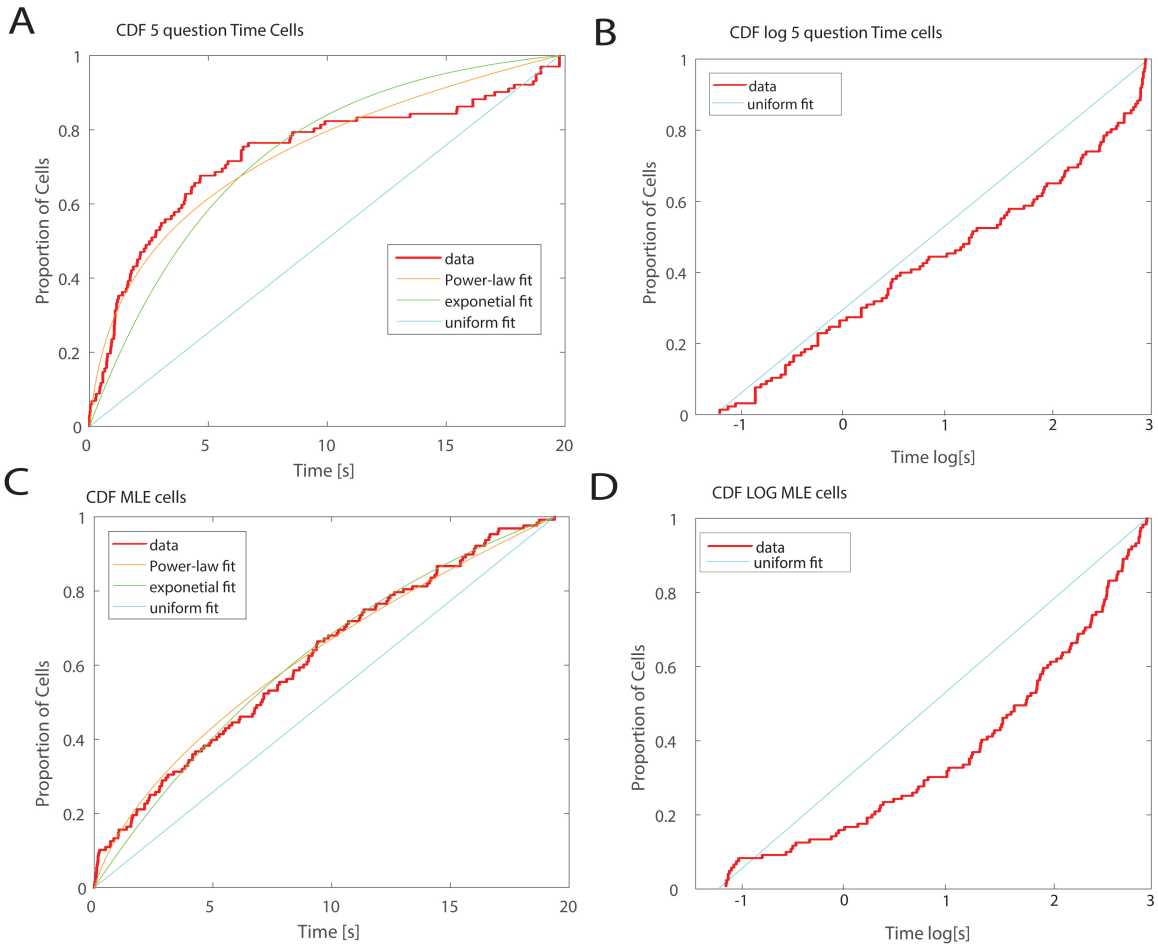

Chapter 4 Figure 4. Cumulative distribution functions with best fitting curves.

A) 5 tests standard time with best fitting parameters were power law: $x^{0.83}$, exponential: $e^{.0002x}$B) 5 tests log time C) Nested model standard time with best fitting parameters power law: $x^{0.3}$ exponential: $e^{4e^{-5}}$ and D) nested model log time defined time cells.

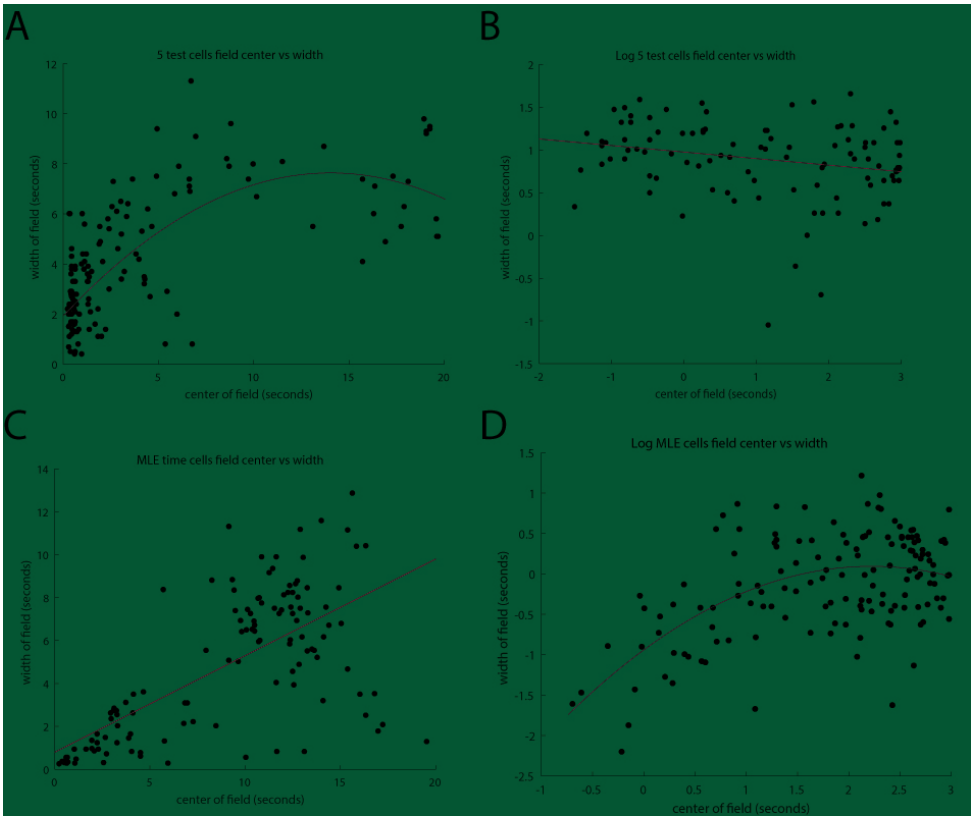

Chapter 4 Figure 5. Scattergram of the center in time of firing fields on the treadmill run and the width of those fields.

In red is the best fitting curve. A. Best fitting curve was quadratic: $-.2x^2+.9x-1$ B. Best fitting curve was linear: -.1x+1 C. Best fitting curve was linear: .45x+1(ns) D. best fitting curve was quadratic: $-.03x^2+.8x+2$

CHAPTER FIVE

There is a variety of evidence that the hippocampus is involved in memory that involves temporal processes (Eichenbaum et al., 2014; Farovik et al., 2010; Fortin et al., 2002; Hattori et al., 2015; Lehn et al., 2009; Mayes et al., 2010; Ross et al., 2009; Spiers et al., 2001). In the preceding experiments we demonstrated two more examples of the hippocampus representing repeated sequences of events across time that take place in the same location. In Chapter 2, we described how hippocampal cells in CA1 may represent the temporal position of an odor in a learned sequence of odors. In Chapter 3, we found cells in CA3 that fire at specific times during a delay in a regular repeated sequence of events that involved running on a treadmill getting rewarded and running around a track to start another treadmill run. The sequence order cells in chapter 2 fired during the stimulus presentation and seem to represent a comparison of the current stimulus to the expected sequence of events. This requires the sequence to be stored within or passed to the hippocampus and is an example of the complex conjunctive encoding of nonspatial information in the hippocampus (Komorowski, Manns, & Eichenbaum, 2009; MacDonald, Lepage, Eden, & Eichenbaum, 2011; McKenzie & Eichenbaum, 2011). In chapter 3, we reproduced the finding of time cells in CA1 and reported for the first time in the literature time cells in CA3. We found time cells from both regions behaving very similarly to place cells from the same regions. This led to the conjecture that the hippocampus is performing the same processing steps when a rat is walking around a familiar environment as it is during a delay in a familiar sequence of events. In this view, place cells are initially encoded when a rat encounters a sequence of places encountered

over time. Time cells meanwhile are encoding regular sequences of events across time (MacDonald et al., 2011). Another way of expressing this is that the hippocampus is performing a general computation for encoding a series of attended stimuli across time which can also happen across space.

In Chapter 3, we found time cells in the hippocampus using a treadmill run delay task. Rats ran a delayed alternation task and a simple loop on a track (Chapter 3 Figure 3). This evidence indicates with the right circumstances (i.e., during the loop task), time cells do not require a memory load to fire during a treadmill run delay period. This work is in contrast to previous findings that indicated time cells could be found when a rat performed delayed alternation, but not when a rat simply ran for set periods of time for reward (Pastalkova et al., 2008). The differences between that task and the loop task we employed were small. In their experiment, the rat could choose to run on the running wheel and take breaks of different durations, which resulted in different behavior between runs. In contrast, our rats sometimes took a break after drinking a reward on the treadmill, but then would run a loop around the maze before getting on the treadmill again. One possibility is the rigid temporal structure of stimuli leading up to the delay in our looping task places the hippocampus in a similar starting state that leads to the regular output of time cells. Another possibility is that a rat choosing to run on a running wheel (as presented in Patalkova et al., 2008) is less salient then running onto a treadmill that starts automatically (as we used). An important direction for future research will be distinguishing which variables are necessary and sufficient to obtain time cells in the hippocampus.

One significant difference between our time cell data and place cell data is the increase in field width over the delay period, and also the increase in spacing of time cells during the delay; observations not found in place cells. An animal's location in space is constantly being updated with visual stimuli that could be used to update its current location. When this visual information is missing, place field spatial selectivity is reduced (Aghajan et al., 2015). During the delayed alternation task, the delay in our treadmill does not include a change in spatial location, so a change in spatial information is not conveyed the hippocampus. Therefore, it is possible that isolating the system from new spatial input is what revealed the underlying pattern of field width growth in the hippocampus. There are models that posit these cells should be present at all times, but would only be measurable within specifically designed testing conditions (Howard et al., 2014).

Even without relevant visual input, kinesthetic inputs have been found to impact the spatial information of place cells within a virtual environment (Chen et al., 2013). Additionally, kinesthetic inputs have been shown to impact time cells during a delayed alternation task (Kraus et al., 2013). It is well established that proprioceptive, somatosensory, and vestibular senses contribute to place cell activity (and likely have at least some influence on time cell activity), but it is unknown whether the time cell attributes we described exist in the absence of these kinesthetic components. To study this researchers have used virtual reality environments to distinguish various inputs into hippocampus. For example, researchers found evidence that visual cues are sufficient for maintaining head direction cell activity, even in the absence of vestibular cues (Acharya,

Aghajan, Vuong, Moore, & Mehta, 2016). Other studies demonstrated that removing local cues through virtual reality significantly impacted spatial information but maintained theta sequences (Aghajan et al., 2015; Chen et al., 2018). Even more relevant to the present treadmill task, visual position and distance traveled have both been shown to influence place cells to varying degrees (Chen et al., 2013; Ravassard et al., 2013). These various vestibular and proprioceptive inputs are still strong drivers of hippocampal cells even in the absence of spatial inputs. The use of a treadmill during the delay in our task therefore muddies the interpretations that can be made from our results. Our lab previously eliminated vestibular and spatial inputs (MacDonald et al., 2013), but the rats still would sometimes move their limbs during the delay. Additionally the paradigm involved very short delays and low cellular firing rates that limit its usefulness for constraining models of hippocampal function. Further distinguishing the neural processing due to movement versus the passage of time during a delay will require a new paradigm that can tease apart these inputs.

There are a variety of models of sequence generation that have been applied to time cells and speculation on how these models can generate memory (Friston & Buzsáki, 2016; Itskov et al., 2011; Rajan, Harvey, & Tank, 2016). These models allow for plasticity between cells that fire across longer time intervals of seconds as opposed to the typical neural time scale measured in tens of milliseconds. In these models sequences are represented across long time scales as replay events and as theta sequences. For replay, the binding across time is accomplished by a reconstruction of previously experienced events during rest periods (Karlsson & Frank, 2009; Skaggs & McNaughton, 1996).

Regarding theta sequences, neural activity binds experienced events to a series of cell assemblies during a theta cycle (Gupta et al., 2012; Skaggs & McNaughton, 1996). Theta sequences and replay events can be interpreted multiple ways depending on the model. There may be pre-existing sequences that are then linked, through experience, to a series of events. Dragoi & Tonegawa (2011) have suggested that this occurs through a phenomenon they call preplay. They observed brain activity resembling replay before an environment was experienced, which they describe then being mapped onto the subsequent events. Others have supported a contrasting interpretation of these replay and theta sequences, which suggests that experienced events directly create new neural sequences in the hippocampus (Foster & Wilson, 2006; Nádasdy, Hirase, Czurkó, Csicsvari, & Buzsáki, 1999). Both models were initially developed to describe place cells, but are easily adapted to time cells. When new spatial memories are formed navigating a new context, it can be described as learning a sequence of spatial events across time. This sequence of spatiotemporal events is what is being represented in theta sequences and replay events. In this understanding there is not much difference between the processing occurring in place and time cells, just the difference in inputs from the experimental context in which they are measured.

Neither of these models explain the increase in field width over time, nor the increase in spacing of time cells that we observed. These models are missing elements that would produce predictions regarding cell spacing and field width. This may be related to a predominant assumption in the literature stemming from the work described in Pastalkova et al., (2008). Because that work did not find changing field widths nor

changes in distribution of fields, other researchers have built simple models that don't incorporate field width or cell spacing predictions, even though these activity measures have been reported elsewhere (Kraus et al., 2015, 2013; MacDonald et al., 2011; Mau et al., 2018; Salz et al., 2016). Further, it may be possible that the selection criteria and field width measures used by Pastalkova et al., (2008) biased the cells selected, which in turn biased the results. Both field width and distribution increases might be present for some tasks but not others. In the present work, we explored modeling changes in field width and distribution, but found the precise curves difficult to determine. One model that closely resembles neural data already has specific predictions for the rate that the width and distribution of time cells would change over the delay (Liu, Tiganj, Hasselmo, & Howard, 2018). A more precise estimate of the curve could be determined from an experimental paradigm with more control over rat behavior (the timing of the elements of the task phases in our paradigm might have precluded obtaining the values necessary to constrain a model).

There is value in seeking parsimony in our models of hippocampal function. Our two experimental findings can be tied together in a model using time cells as a way of bridging between events and tying into an ordinal representation of a sequence. Both of these experiments involved temporal processing. Despite this similarity in firing characteristics of time cells and the InSeq and OutSeq cells involved in processing ordinal information, they are not necessarily part of the same processing stream. There is evidence of parallel processing streams (Soltesz & Losonczy, 2018) that could explain how firing for sequences and firing during a delay might be controlled by different

processes. Further research supports how the integration of parallel processing streams can accomplish a more multifaceted representation. That is, some time cells maintain stable representation of time across days, while other cells change their representations across long time periods in a way that could distinguish experiences across days (Mankin et al., 2012; Mau et al., 2018). With further use of long term in-vivo calcium imaging, examination of activity from large numbers of cells during different temporal processing tasks could help build overarching models. These models could further describe how the hippocampus is involved in the processing of a wide variety of tasks.

There are many avenues of research to pursue to fully elucidate the temporal processing of the hippocampus, but I believe pursuit of these answers will shed light on the full breadth of computations the hippocampus supports.

BIBLIOGRAPHY

Acharya, L., Aghajan, Z. M., Vuong, C., Moore, J. J., & Mehta, M. R. (2016). Causal Influence of Visual Cues on Hippocampal Directional Selectivity. *Cell*, *164*(1), 197–207. https://doi.org/10.1016/j.cell.2015.12.015

Aghajan, Z. M., Acharya, L., Moore, J. J., Cushman, J. D., Vuong, C., & Mehta, M. R. (2015). Impaired spatial selectivity and intact phase precession in two-dimensional virtual reality. *Nature Neuroscience*, *18*(1), 121–128. https://doi.org/10.1038/nn.3884

Allen, T. A., & Fortin, N. J. (2013). The evolution of episodic memory. *Proceedings of the National Academy of Sciences*, *110*(Supplement 2), 10379–10386. https://doi.org/10.1073/pnas.1301199110

Allen, T. A., Salz, D. M., McKenzie, S., & Fortin, N. J. (2016). Nonspatial Sequence Coding in CA1 Neurons. *The Journal of Neuroscience*, *36*(5), 1547–1563. https://doi.org/10.1523/JNEUROSCI.2874-15.2016

Barnes, C. A., McNaughton, B. L., Mizumori, S. J. Y., Leonard, B. W., & Lin, L.-H. (1990). Chapter 21 Chapter Comparison of spatial and temporal characteristics of neuronal activity in sequential stages of hippocampal processing. In J. Z. and O. P. O. J. Storm-Mathisen (Ed.), *Progress in Brain Research* (Vol. 83, pp. 287–300). Amsterdam: Elsevier. Retrieved from http://www.sciencedirect.com/science/article/pii/S0079612308612571

Buhry, L., Azizi, A. H., & Cheng, S. (2011). Reactivation, Replay, and Preplay: How It Might All Fit Together. *Neural Plasticity*, *2011*. https://doi.org/10.1155/2011/203462

Buhusi, C. V., & Meck, W. H. (2005). What makes us tick? Functional and neural mechanisms of interval timing. *Nature Reviews Neuroscience*, *6*(10), 755–765. https://doi.org/10.1038/nrn1764

Burgess, N., Maguire, E. A., & O'Keefe, J. (2002). The Human Hippocampus and Spatial and Episodic Memory. *Neuron*, *35*(4), 625–641. https://doi.org/10.1016/S0896-6273(02)00830-9

Chater, N., & Brown, G. D. A. (2008). From Universal Laws of Cognition to Specific Cognitive Models. *Cognitive Science*, *32*(1), 36–67. https://doi.org/10.1080/03640210701801941

Chen, G., King, J. A., Burgess, N., & O'Keefe, J. (2013). How vision and movement combine in the hippocampal place code. *Proceedings of the National Academy of Sciences*, *110*(1), 378–383. https://doi.org/10.1073/pnas.1215834110

Chen, G., King, J. A., Lu, Y., Cacucci, F., & Burgess, N. (2018). Spatial cell firing during virtual navigation of open arenas by head-restrained mice. *ELife*, *7*. https://doi.org/10.7554/eLife.34789

Davachi, L., & DuBrow, S. (2015). How the hippocampus preserves order: the role of prediction and context. *Trends in Cognitive Sciences*, *19*(2), 92–99. https://doi.org/10.1016/j.tics.2014.12.004

Dragoi, G. (2013). Internal operations in the hippocampus: single cell and ensemble temporal coding. *Frontiers in Systems Neuroscience*, *7*, 46. https://doi.org/10.3389/fnsys.2013.00046

Dragoi, G., & Buzsáki, G. (2006). Temporal Encoding of Place Sequences by Hippocampal Cell Assemblies. *Neuron*, *50*(1), 145–157. https://doi.org/10.1016/j.neuron.2006.02.023

Dragoi, G., & Tonegawa, S. (2011). Preplay of future place cell sequences by hippocampal cellular assemblies. *Nature*, *469*(7330), 397–401. https://doi.org/10.1038/nature09633

Dudchenko, P. A., & Wood, E. R. (2014). Splitter Cells: Hippocampal Place Cells Whose Firing Is Modulated by Where the Animal Is Going or Where It Has Been. In D. Derdikman & J. J. Knierim (Eds.), *Space,Time and Memory in the Hippocampal Formation* (pp. 253–272). Springer Vienna. Retrieved from http://link.springer.com/chapter/10.1007/978-3-7091-1292-2_10

Eichenbaum, H., & Fortin, N. J. (n.d.). Bridging the Gap Between Brain and Behavior: Cognitive and Neural Mechanisms of Episodic Memory. *Journal of the Experimental Analysis of Behavior*, *84*(3), 619–629. https://doi.org/10.1901/jeab.2005.80-04

Eichenbaum, H., MacDonald, C. J., & Kraus, B. J. (2014). Time and the Hippocampus. In D. Derdikman & J. J. Knierim (Eds.), *Space,Time and Memory in the Hippocampal Formation* (pp. 273–301). Springer Vienna. Retrieved from http://link.springer.com/chapter/10.1007/978-3-7091-1292-2_11

Farovik, A., Dupont, L. M., & Eichenbaum, H. (2010). Distinct Roles for Dorsal CA3 and CA1 in Memory for Sequential Nonspatial Events. *Learning & Memory*, *17*(1), 12–17. https://doi.org/10.1101/lm.1616209

Fortin, N. J., Agster, K. L., & Eichenbaum, H. B. (2002). Critical role of the hippocampus in memory for sequences of events. *Nature Neuroscience*, *5*(5), 458–462. https://doi.org/10.1038/nn834

Fortin, N. J., Wright, S. P., & Eichenbaum, H. (2004). Recollection-like memory retrieval in rats is dependent on the hippocampus. *Nature*, *431*(7005), 188–191. https://doi.org/10.1038/nature02853

Foster, D. J., & Wilson, M. A. (2006). Reverse replay of behavioural sequences in hippocampal place cells during the awake state. *Nature*, *440*(7084), 680–683. https://doi.org/10.1038/nature04587

Frank, L. M., Brown, E. N., & Wilson, M. (2000). Trajectory Encoding in the Hippocampus and Entorhinal Cortex. *Neuron*, *27*(1), 169–178. https://doi.org/10.1016/S0896-6273(00)00018-0

Friston, K., & Buzsáki, G. (2016). The Functional Anatomy of Time: What and When in the Brain. *Trends in Cognitive Sciences*, *20*(7), 500–511. https://doi.org/10.1016/j.tics.2016.05.001

Gallistel, C. R., & Gibbon, J. (2000). Time, rate, and conditioning. *Psychological Review*, *107*(2), 289–344. https://doi.org/10.1037/0033-295X.107.2.289

Gibbon, J. (1977). Scalar expectancy theory and Weber's law in animal timing. *Psychological Review*, *84*(3), 279–325. https://doi.org/10.1037/0033-295X.84.3.279

Gill, P. R., Mizumori, S. J. Y., & Smith, D. M. (2011). Hippocampal episode fields develop with learning. *Hippocampus*, *21*(11), 1240–1249. https://doi.org/10.1002/hipo.20832

Gilmartin, M. R., & Helmstetter, F. J. (2010). Trace and contextual fear conditioning require neural activity and NMDA receptor-dependent transmission in the medial prefrontal cortex. *Learning & Memory*, *17*(6), 289–296. https://doi.org/10.1101/lm.1597410

Gupta, A. S., Meer, M. A. A. van der, Touretzky, D. S., & Redish, A. D. (2012). Segmentation of spatial experience by hippocampal theta sequences. *Nature Neuroscience*. https://doi.org/10.1038/nn.3138

Hasselmo, M. E. (2008). Grid cell mechanisms and function: Contributions of entorhinal persistent spiking and phase resetting. *Hippocampus*, *18*(12), 1213–1229. https://doi.org/10.1002/hipo.20512

Hattori, S., Chen, L., Weiss, C., & Disterhoft, J. F. (2015). Robust hippocampal responsivity during retrieval of consolidated associative memory: Hippocampal Involvement After Memory Consolidation. *Hippocampus*, *25*(5), 655–669. https://doi.org/10.1002/hipo.22401

Hedges, L. V. (1981). Distribution Theory for Glass's Estimator of Effect size and Related Estimators ,

Distribution Theory for Glass's Estimator of Effect size and Related Estimators. *Journal of Educational Statistics*, *6*(2), 107–128. https://doi.org/10.3102/10769986006002107

Hoagland, H. (1930). The Weber-Fechner law and the all-or-None Theory. *The Journal of General Psychology*, *3*(3), 351–373. https://doi.org/10.1080/00221309.1930.9918215

Hoge, J., & Kesner, R. P. (2007). Role of CA3 and CA1 subregions of the dorsal hippocampus on temporal processing of objects. *Neurobiology of Learning and Memory*, *88*(2), 225–231. https://doi.org/10.1016/j.nlm.2007.04.013

Howard, M. W., & Eichenbaum, H. (2013). The hippocampus, time, and memory across scales. *Journal of Experimental Psychology: General*, *142*(4), 1211–1230. https://doi.org/10.1037/a0033621

Howard, M. W., MacDonald, C. J., Tiganj, Z., Shankar, K. H., Du, Q., Hasselmo, M. E., & Eichenbaum, H. (2014). A Unified Mathematical Framework for Coding Time, Space, and Sequences in the Hippocampal Region. *The Journal of Neuroscience*, *34*(13), 4692–4707. https://doi.org/10.1523/JNEUROSCI.5808-12.2014

Howard, M. W., & Shankar, K. H. (2018). Neural scaling laws for an uncertain world. *Psychological Review*, *125*(1), 47–58. https://doi.org/10.1037/rev0000081

Hubel, D. H., & Wiesel, T. N. (1974). Uniformity of monkey striate cortex: a parallel relationship between field size, scatter, and magnification factor. *Journal of Comparative Neurology*, *158*(3), 295–305.

Igarashi, K. M., Lu, L., Colgin, L. L., Moser, M.-B., & Moser, E. I. (2014). Coordination of entorhinal-hippocampal ensemble activity during associative learning. *Nature*, *510*(7503), 143–147. https://doi.org/10.1038/nature13162

Itskov, V., Curto, C., Pastalkova, E., & Buzsáki, G. (2011). Cell Assembly Sequences Arising from Spike Threshold Adaptation Keep Track of Time in the Hippocampus. *The Journal of Neuroscience*, *31*(8), 2828–2834. https://doi.org/10.1523/JNEUROSCI.3773-10.2011

Jacobs, N. S., Allen, T. A., Nguyen, N., & Fortin, N. J. (2013). Critical role of the hippocampus in memory for elapsed time. *The Journal of Neuroscience: The Official Journal of the Society for Neuroscience*, *33*(34), 13888–13893. https://doi.org/10.1523/JNEUROSCI.1733-13.2013

Jadhav, S. P., & Frank, L. M. (2014). Memory Replay in the Hippocampus. In D. Derdikman & J. J. Knierim (Eds.), *Space,Time and Memory in the Hippocampal Formation* (pp. 351–371). Springer Vienna. Retrieved from http://link.springer.com/chapter/10.1007/978-3-7091-1292-2_13

Karlsson, M. P., & Frank, L. M. (2009). Awake replay of remote experiences in the hippocampus. *Nature Neuroscience*, *12*(7), 913–918. https://doi.org/10.1038/nn.2344

Kesner, R. P., Gilbert, P. E., & Barua, L. A. (2002). The role of the hippocampus in memory for the temporal order of a sequence of odors. *Behavioral Neuroscience*, *116*(2), 286–290. https://doi.org/10.1037/0735-7044.116.2.286

Kesner, R. P., & Hunsaker, M. R. (2010). The temporal attributes of episodic memory. *Behavioural Brain Research*, *215*(2), 299–309. https://doi.org/10.1016/j.bbr.2009.12.029

Kesner, R. P., Hunsaker, M. R., & Gilbert, P. E. (2005). The Role of CA1 in the Acquisition of an Object-Trace-Odor Paired Associate Task. *Behavioral Neuroscience*, *119*(3), 781–786. https://doi.org/10.1037/0735-7044.119.3.781

Kitamura, T., Pignatelli, M., Suh, J., Kohara, K., Yoshiki, A., Abe, K., & Tonegawa, S. (2014). Island Cells Control Temporal Association Memory. *Science*, *343*(6173), 896–901. https://doi.org/10.1126/science.1244634

Komorowski, R. W., Manns, J. R., & Eichenbaum, H. (2009). Robust Conjunctive Item–Place Coding by Hippocampal Neurons Parallels Learning What Happens Where. *The Journal of Neuroscience*, *29*(31), 9918–9929. https://doi.org/10.1523/JNEUROSCI.1378-09.2009

Kraus, B. J., Brandon, M. P., Robinson II, R. J., Connerney, M. A., Hasselmo, M. E., & Eichenbaum, H. (2015). During Running in Place, Grid Cells Integrate Elapsed Time and Distance Run. *Neuron*, *88*(3), 578–589. https://doi.org/10.1016/j.neuron.2015.09.031

Kraus, B. J., Robinson II, R. J., White, J. A., Eichenbaum, H., & Hasselmo, M. E. (2013). Hippocampal "Time Cells": Time versus Path Integration. *Neuron*, *78*(6), 1090–1101. https://doi.org/10.1016/j.neuron.2013.04.015

Lehn, H., Steffenach, H.-A., Strien, N. M. V., Veltman, D. J., Witter, M. P., & Håberg, A. K. (2009). A Specific Role of the Human Hippocampus in Recall of Temporal

Sequences. *The Journal of Neuroscience*, *29*(11), 3475–3484. https://doi.org/10.1523/JNEUROSCI.5370-08.2009

Lejeune, H., & Wearden, J. H. (2006). Scalar properties in animal timing: Conformity and violations. *The Quarterly Journal of Experimental Psychology*, *59*(11), 1875–1908. https://doi.org/10.1080/17470210600784649

Lewis, P. A., & Miall, R. C. (2009). The precision of temporal judgement: milliseconds, many minutes, and beyond. *Philosophical Transactions of the Royal Society B: Biological Sciences*, *364*(1525), 1897–1905. https://doi.org/10.1098/rstb.2009.0020

Liu, Y., Tiganj, Z., Hasselmo, M., & Howard, M. (2018). A Neural Microcircuit Model for a Scalable Scale-invariant Representation of Time. *BioRxiv*, 327387. https://doi.org/10.1101/327387

MacDonald, C. J., Carrow, S., Place, R., & Eichenbaum, H. (2013). Distinct Hippocampal Time Cell Sequences Represent Odor Memories in Immobilized Rats. *The Journal of Neuroscience*, *33*(36), 14607–14616. https://doi.org/10.1523/JNEUROSCI.1537-13.2013

MacDonald, C. J., Lepage, K. Q., Eden, U. T., & Eichenbaum, H. (2011). Hippocampal Time Cells Bridge the Gap in Memory for Discontiguous Events. *Neuron*, *71*(4), 737–749. https://doi.org/10.1016/j.neuron.2011.07.012

Mankin, E. A., Diehl, G. W., Sparks, F. T., Leutgeb, S., & Leutgeb, J. K. (2015). Hippocampal CA2 Activity Patterns Change over Time to a Larger Extent than

between Spatial Contexts. *Neuron*, *85*(1), 190–201. https://doi.org/10.1016/j.neuron.2014.12.001

Mankin, E. A., Sparks, F. T., Slayyeh, B., Sutherland, R. J., Leutgeb, S., & Leutgeb, J. K. (2012). Neuronal code for extended time in the hippocampus. *Proceedings of the National Academy of Sciences*, *109*(47), 19462–19467. https://doi.org/10.1073/pnas.1214107109

Manns, J. R., Howard, M. W., & Eichenbaum, H. (2007). Gradual Changes in Hippocampal Activity Support Remembering the Order of Events. *Neuron*, *56*(3), 530–540. https://doi.org/10.1016/j.neuron.2007.08.017

Mau, W., Sullivan, D. W., Kinsky, N. R., Hasselmo, M. E., Howard, M. W., & Eichenbaum, H. (2018). The Same Hippocampal CA1 Population Simultaneously Codes Temporal Information over Multiple Timescales. *Current Biology*, *28*(10), 1499-1508.e4. https://doi.org/10.1016/j.cub.2018.03.051

Mayes, A. R., Isaac, C. L., Holdstock, J. S., Hunkin, N. M., Montaldi, D., Downes, J. J., … Roberts, J. N. (2010). Memory for single items, word pairs, and temporal order of different kinds in a patient with selective hippocampal lesions. *Cognitive Neuropsychology*. Retrieved from http://www.tandfonline.com/doi/abs/10.1080/02643290125897

McCullagh, P., & Nelder, J. A. (1989). *Generalized linear models* (Vol. 37). CRC press. Retrieved from https://books.google.com/books?hl=en&lr=&id=h9kFH2_FfBkC&oi=fnd&pg=PR16&dq=McCullagh+P,+Nelder+JA+(1989)+Generalized+linear+models.+Boca

+Raton,+FL:+Chapman+and+Hall/CRC.&ots=JhTXbTJPCM&sig=BxRxTkXBRzAEzy9w_47KGjrA2Dg

McEchron, M. D., Tseng, W., & Disterhoft, J. F. (2003). Single Neurons in CA1 Hippocampus Encode Trace Interval Duration during Trace Heart Rate (Fear) Conditioning in Rabbit. *The Journal of Neuroscience*, *23*(4), 1535–1547.

Meck, W. H., Penney, T. B., & Pouthas, V. (2008). Cortico-striatal representation of time in animals and humans. *Current Opinion in Neurobiology*, *18*(2), 145–152. https://doi.org/10.1016/j.conb.2008.08.002

Mehta, M. R. (2015). From synaptic plasticity to spatial maps and sequence learning. *Hippocampus*, *25*(6), 756–762. https://doi.org/10.1002/hipo.22472

Merchant, H., Harrington, D. L., & Meck, W. H. (2013). Neural Basis of the Perception and Estimation of Time. *Annual Review of Neuroscience*, *36*(1), 313–336. https://doi.org/10.1146/annurev-neuro-062012-170349

Messner, R. A., & Szu, H. H. (1985). An image processing architecture for real time generation of scale and rotation invariant patterns. *Computer Vision, Graphics, and Image Processing*, *31*(1), 50–66. https://doi.org/10.1016/S0734-189X(85)80075-X

Miall, C. (1989). The Storage of Time Intervals Using Oscillating Neurons. *Neural Computation*, *1*(3), 359–371. https://doi.org/10.1162/neco.1989.1.3.359

Mizuseki, K., Royer, S., Diba, K., & Buzsáki, G. (2012). Activity dynamics and behavioral correlates of CA3 and CA1 hippocampal pyramidal neurons. *Hippocampus*, *22*(8), 1659–1680. https://doi.org/10.1002/hipo.22002

Modi, M. N., Dhawale, A. K., & Bhalla, U. S. (2014). CA1 cell activity sequences emerge after reorganization of network correlation structure during associative learning. *ELife*, *3*. https://doi.org/10.7554/eLife.01982

Nádasdy, Z., Hirase, H., Czurkó, A., Csicsvari, J., & Buzsáki, G. (1999). Replay and Time Compression of Recurring Spike Sequences in the Hippocampus. *Journal of Neuroscience*, *19*(21), 9497–9507. https://doi.org/10.1523/JNEUROSCI.19-21-09497.1999

Naya, Y., & Suzuki, W. A. (2011). Integrating What and When Across the Primate Medial Temporal Lobe. *Science*, *333*(6043), 773–776. https://doi.org/10.1126/science.1206773

Palombo, D. j., Keane, M. m., & Verfaellie, M. (2015). Does the hippocampus keep track of time? *Hippocampus*, n/a-n/a. https://doi.org/10.1002/hipo.22528

Pastalkova, E., Itskov, V., Amarasingham, A., & Buzsáki, G. (2008). Internally Generated Cell Assembly Sequences in the Rat Hippocampus. *Science*, *321*(5894), 1322–1327. https://doi.org/10.1126/science.1159775

Paz, R., Gelbard-Sagiv, H., Mukamel, R., Harel, M., Malach, R., & Fried, I. (2010). A neural substrate in the human hippocampus for linking successive events. *Proceedings of the National Academy of Sciences*, *107*(13), 6046–6051. https://doi.org/10.1073/pnas.0910834107

Poli, R., Kennedy, J., & Blackwell, T. (2007). Particle swarm optimization. *Swarm Intelligence*, *1*(1), 33–57. https://doi.org/10.1007/s11721-007-0002-0

Quirk, C. R., Allen, T. A., & Fortin, N. J. (2013). Temporary inactivations of the hippocampus and prefrontal cortex impair memory for sequences of events. In *Society for Neuroscience Abstracts* (Vol. 39).

Rajan, K., Harvey, C. D., & Tank, D. W. (2016). Recurrent Network Models of Sequence Generation and Memory. *Neuron*, *90*(1), 128–142. https://doi.org/10.1016/j.neuron.2016.02.009

Rakitin, B. C., Gibbon, J., Penney, T. B., Malapani, C., Hinton, S. C., & Meck, W. H. (1998). Scalar expectancy theory and peak-interval timing in humans. *Journal of Experimental Psychology: Animal Behavior Processes*, *24*(1), 15–33. https://doi.org/10.1037/0097-7403.24.1.15

Ranganath, C., & Ritchey, M. (2012). Two cortical systems for memory-guided behaviour. *Nature Reviews Neuroscience*, *13*(10), 713–726. https://doi.org/10.1038/nrn3338

Rangel, L. M., Chiba, A. A., & Quinn, L. K. (2015). Theta and beta oscillatory dynamics in the dentate gyrus reveal a shift in network processing state during cue encounters. *Frontiers in Systems Neuroscience*, *9*. https://doi.org/10.3389/fnsys.2015.00096

Ravassard, P., Kees, A., Willers, B., Ho, D., Aharoni, D., Cushman, J., … Mehta, M. R. (2013). Multisensory Control of Hippocampal Spatiotemporal Selectivity. *Science*, *340*(6138), 1342–1346. https://doi.org/10.1126/science.1232655

Ross, R. S., Brown, T. I., & Stern, C. E. (2009). The retrieval of learned sequences engages the hippocampus: Evidence from fMRI. *Hippocampus*, *19*(9), 790–799. https://doi.org/10.1002/hipo.20558

Sakon, J. J., Naya, Y., Wirth, S., & Suzuki, W. A. (2014). Context-dependent incremental timing cells in the primate hippocampus. *Proceedings of the National Academy of Sciences*, 201417827. https://doi.org/10.1073/pnas.1417827111

Salz, D. M., Tiganj, Z., Khasnabish, S., Kohley, A., Sheehan, D., Howard, M. W., & Eichenbaum, H. (2016). Time Cells in Hippocampal Area CA3. *The Journal of Neuroscience*, *36*(28), 7476–7484. https://doi.org/10.1523/JNEUROSCI.0087-16.2016

Schlesiger, M. I., Cannova, C. C., Boublil, B. L., Hales, J. B., Mankin, E. A., Brandon, M. P., … Leutgeb, S. (2015). The medial entorhinal cortex is necessary for temporal organization of hippocampal neuronal activity. *Nature Neuroscience*, *18*(8), 1123–1132. https://doi.org/10.1038/nn.4056

Schwartz, E. L. (1977). Spatial mapping in the primate sensory projection: analytic structure and relevance to perception. *Biological Cybernetics*, *25*(4), 181–194.

Schwartz, E. L. (1980). Computational anatomy and functional architecture of striate cortex: a spatial mapping approach to perceptual coding. *Vision Research*, *20*(8), 645–669.

Sederberg, P. B., Miller, J. F., Howard, M. W., & Kahana, M. J. (2010). The temporal contiguity effect predicts episodic memory performance. *Memory & Cognition*, *38*(6), 689–699.

Shankar, K. H., & Howard, M. W. (2012). Optimally fuzzy temporal memory. *ArXiv:1211.5189 [Cs]*. Retrieved from http://arxiv.org/abs/1211.5189

Skaggs, W. E., & McNaughton, B. L. (1996). Replay of Neuronal Firing Sequences in Rat Hippocampus During Sleep Following Spatial Experience. *Science*, *271*(5257), 1870–1873. https://doi.org/10.1126/science.271.5257.1870

Skaggs, W. E., & McNaughton, B. L. (1998). Spatial firing properties of hippocampal CA1 populations in an environment containing two visually identical regions. *The Journal of Neuroscience*, *18*(20), 8455–8466.

Smith, D. M., & Mizumori, S. J. Y. (2006). Hippocampal place cells, context, and episodic memory. *Hippocampus*, *16*(9), 716–729. https://doi.org/10.1002/hipo.20208

Soltesz, I., & Losonczy, A. (2018). CA1 pyramidal cell diversity enabling parallel information processing in the hippocampus. *Nature Neuroscience*, *21*(4), 484–493. https://doi.org/10.1038/s41593-018-0118-0

Spiers, H. J., Burgess, N., Hartley, T., Vargha-Khadem, F., & O'Keefe, J. (2001). Bilateral hippocampal pathology impairs topographical and episodic memory but not visual pattern matching. *Hippocampus*, *11*(6), 715–725. https://doi.org/10.1002/hipo.1087

Staddon, J. E. R., & Higa, J. J. (1999). Time and Memory: Towards a Pacemaker-Free Theory of Interval Timing. *Journal of the Experimental Analysis of Behavior*, *71*(2), 215–251. https://doi.org/10.1901/jeab.1999.71-215

Stapleton, J. R., Lavine, M. L., Wolpert, R. L., Nicolelis, M. A., & Simon, S. A. (2006). Rapid taste responses in the gustatory cortex during licking. *The Journal of Neuroscience*, *26*(15), 4126–4138.

Staresina, B. P., & Davachi, L. (2009). Mind the Gap: Binding Experiences across Space and Time in the Human Hippocampus. *Neuron*, *63*(2), 267–276. https://doi.org/10.1016/j.neuron.2009.06.024

Tiganj, Z., Jung, M. W., Kim, J., & Howard, M. W. (2016). Sequential Firing Codes for Time in Rodent Medial Prefrontal Cortex. *Cerebral Cortex*, 1–9. https://doi.org/10.1093/cercor/bhw336

Treisman, M. (1963). Temporal discrimination and the indifference interval. Implications for a model of the "internal clock." *Psychological Monographs*, *77*(13), 1–31.

Tulving, E. (2001). Episodic memory and common sense: how far apart? *Philosophical Transactions of the Royal Society of London B: Biological Sciences*, *356*(1413), 1505–1515.

Tulving, E., & Markowitsch, H. J. (1998). Episodic and declarative memory: Role of the hippocampus. *Hippocampus*, *8*(3), 198–204. https://doi.org/10.1002/(SICI)1098-1063(1998)8:3<198::AID-HIPO2>3.0.CO;2-G

Van Essen, D. C., Newsome, W. T., & Maunsell, J. H. (1984). The visual field representation in striate cortex of the macaque monkey: asymmetries, anisotropies, and individual variability. *Vision Research*, *24*(5), 429–448.

Wang, Y., Romani, S., Lustig, B., Leonardo, A., & Pastalkova, E. (2015). Theta sequences are essential for internally generated hippocampal firing fields. *Nature Neuroscience*, *18*(2), 282–288. https://doi.org/10.1038/nn.3904

Wang, Y., Roth, Z., & Pastalkova, E. (2016). Synchronized excitability in a network enables generation of internal neuronal sequences. *ELife*, *5*, e20697. https://doi.org/10.7554/eLife.20697

Wearden, J. H., & Lejeune, H. (2008). Scalar properties in human timing: Conformity and violations. *The Quarterly Journal of Experimental Psychology*, *61*(4), 569–587.

Weiss, C., & Disterhoft, J. F. (2011). Exploring Prefrontal Cortical Memory Mechanisms with Eyeblink Conditioning. *Behavioral Neuroscience*, *125*(3), 318–326. https://doi.org/10.1037/a0023520

Wood, E. R., Dudchenko, P. A., & Eichenbaum, H. (1999). The global record of memory in hippocampal neuronal activity. *Nature*, *397*(6720), 613–616. https://doi.org/10.1038/17605

Woodruff-Pak, D. S., & Disterhoft, J. F. (2008). Where is the trace in trace conditioning? *Trends in Neurosciences*, *31*(2), 105–112. https://doi.org/10.1016/j.tins.2007.11.006

Yang, G., Lai, C. S. W., Cichon, J., Ma, L., Li, W., & Gan, W.-B. (2014). Sleep promotes branch-specific formation of dendritic spines after learning. *Science*, *344*(6188), 1173–1178. https://doi.org/10.1126/science.1249098

CURRICULUM VITAE